Energy Research and Development Division

FINAL PROJECT REPORT

High-Performance Integrated Window and Façade Solutions for California

Gavin Newsom, Governor
January 2020 | CEC-500-2020-001

PREPARED BY:

Primary Authors:
Eleanor S. Lee
D. Charlie Curcija, Ph.D.
Taoning Wang
Christoph Gehbauer
Luís L. Fernandes, Ph.D.
Robert Hart

David Blum, Ph.D.
Howdy Goudey
Anothai Thanachareonkit, Ph.D.
Gregory Ward, Anyhere Software.
David Geisler-Moroder, Ph.D., Bartenbach GMbH
John Breshears, Architectural Applications
Stephen E. Selkowitz
Christian Kohler
Jinqing Peng, Ph.D.

Lawrence Berkeley National Laboratory
1 Cyclotron Road, MS: 90-3111
Berkeley, CA 94720
Phone: 510-486-4997 | Fax: 510-486-4089
LBNL Website: http://facades.lbl.gov

Contract Number: EPC-14-066

DISCLAIMER

ACKNOWLEDGEMENTS

- Mark Perepelitza, SERA
- Mudit Saxena, Vistar Energy Consulting
- Kevin Vilhauer, Milgard
- Daniel Wacek, Viracon
- David Warden, YKK-AP
- Margaret Webb, IGMA
- Peter Yost, BuildingGreen

PREFACE

The California Energy Commission's Energy Research and Development Division supports energy research and development programs to spur innovation in energy efficiency, renewable energy and advanced clean generation, energy-related environmental protection, energy transmission and distribution and transportation.

In 2012, the California Public Utilities Commission established the Electric Program Investment Charge (EPIC) to fund public investments in research to create and advance new energy solutions, foster regional innovation, and bring ideas from the lab to the marketplace. The California Energy Commission and the state's three largest investor-owned utilities—Pacific Gas and Electric Company, San Diego Gas & Electric Company, and Southern California Edison Company—were selected to administer the EPIC funds and advance novel technologies, tools, and strategies that provide benefits to their electric ratepayers.

The Energy Commission is committed to ensuring public participation in its research and development programs that promote greater reliability, lower costs, and increase safety for the California electric ratepayer and include:

- Providing societal benefits.
- Reducing greenhouse gas emission in the electricity sector at the lowest possible cost.
- Supporting California's loading order to meet energy needs first with energy efficiency and demand response, next with renewable energy (distributed generation and utility scale), and finally with clean, conventional electricity supply.
- Supporting low-emission vehicles and transportation.
- Providing economic development.
- Using ratepayer funds efficiently.

High-Performance Integrated Window and Façade Solutions for California is the final report for the High-Performance Integrated Window and Façade Solutions for California project (Grant Number EPC-14-066) conducted by the Lawrence Berkeley National Laboratory. The information from this project contributes to the Energy Research and Development Division's EPIC Program.

For more information about the Energy Research and Development Division, please visit the [Energy Commission's research website](www.energy.ca.gov/research/) (www.energy.ca.gov/research/) or contact the Energy Commission at 916-327-1551.

ABSTRACT

The researchers developed a new generation of high-performance façade systems and supporting design and management tools to support industry in meeting California's greenhouse gas reduction targets, reduce energy consumption, and enable an adaptable response to minimize real-time demands on the electricity grid. The project resulted in five outcomes: (1) The research team developed an R-5, 1-inch thick, triple-pane, insulating glass unit with a novel low-conductance aluminum frame. This technology can help significantly reduce residential cooling and heating loads, particularly during the evening. (2) The team developed a prototype of a window-integrated local ventilation and energy recovery device that provides clean, dry fresh air through the façade with minimal energy requirements. (3) A daylight-redirecting louver system was prototyped to redirect sunlight 15–40 feet from the window. Simulations estimated that lighting energy use could be reduced by 35–54 percent without glare. (4) A control system incorporating physics-based equations and a mathematical solver was prototyped and field tested to demonstrate feasibility. Simulations estimated that total electricity costs could be reduced by 9-28 percent on sunny summer days through adaptive control of operable shading and daylighting components and the thermostat compared to state-of-the-art automatic façade controls in commercial building perimeter zones. (5) Supporting models and tools needed by industry for technology R&D and market transformation activities were validated. Attaining California's clean energy goals require making a fundamental shift from today's ad-hoc assemblages of static components to turnkey, intelligent, responsive, integrated building façade systems. These systems offered significant reductions in energy use, peak demand, and operating cost in California.

Keywords: Highly insulating windows, ventilative façades, daylighting, dynamic façades, switchable glazing, model predictive controls, bidirectional scattering distribution functions, high-performance buildings, energy efficiency

TABLE OF CONTENTS

LIST OF FIGURES

LIST OF TABLES

EXECUTIVE SUMMARY

Introduction

Window and façade systems affect heating, ventilation, air-conditioning, and lighting energy use in buildings. Together, these constitute the largest electricity end uses in buildings in California. In addition to window technologies, the façade and window systems include features of roofs, walls, overhangs, and window attachments. To meet California's goal to double energy savings in new and existing buildings by 2030, innovative window and façade technologies must be developed and disseminated broadly and quickly.

Windows are unique building components. All owners want views, daylight, and connection with the outdoors. This makes windows key design features that affect the market value of every building. However, windows are typically much less insulating than wall systems. In addition to reducing heat transfer by improving insulation properties, innovations in dynamic control of reflectance and emissivity across different wavelengths of light show promise, as do innovative applications and designs for mechanical shading. By reducing heat transfer, windows affect the operational efficiency of HVAC systems and can support low-energy heating and cooling strategies. Despite the energy savings potential; however, high-performance window and façade systems have often been slow or unsuccessful in gaining market share, due to cost and complexity.

Cost-effectiveness is a key factor for building owners in deciding whether to invest in a new technology. Payback based on energy cost savings defines cost-effectiveness when consumers purchase new technologies. However, the basis for determining cost-effectiveness has shifted, due to intermittent renewable energy generation. Renewable energy accounted for 27 percent of California's electricity supply in 2016, and that percentage continues to climb to meet California's 2030 goal of 50 percent. The growth of renewable energy has dramatically changed the time-dependent value of electricity. In the past, energy-efficient windows that provided peak electricity demand savings during midday were most cost-effective. However, because of peak generation times of renewable energy, savings during the midafternoon to evening hours are becoming more important. Uncertainty in the market and lack of knowledge on how best to provide energy-responsive solutions make it more difficult to achieve California's clean energy goals.

Purpose

This project sought to develop a new generation of high-performance façade systems, along with supporting design and management tools, so that industry, including suppliers, designers, contractors, and owners, could help California reach its greenhouse gas reduction targets. The technology research and development focused on two objectives:

1. reducing overall energy consumption in buildings, particularly for end-uses that cause the most strain on the power grid, and

2. enabling an adaptable response to minimize real-time demands on the electricity grid.

Process

The first strategy focused on reducing HVAC energy use through improved window and building façade performance, particularly in the single-family and high-density residential markets. The most attractive alternatives increase energy efficiency and provide peak demand reductions during critical late afternoon and evening hours, when electricity costs and demand are higher. The second strategy focused on adaptable, predictive, self-learning control of dynamic façade technologies such as solar control, daylighting, ventilation. These technologies can also provide load reductions that respond to real-time energy and demand costs. The intent of the research was to develop and verify performance of prototype technologies, and to help industry bring them towards commercialization. The research addressed energy, electric demand, comfort, indoor environmental quality, maintenance, operation, and other practical requirements that drive market acceptance.

Supporting research focused on developing and promoting open source mathematical tools. The industry needs these tools for design analysis, codes and standards, and rating and certification programs. The work included developing a control system platform for adaptive façade systems, to develop and analyze grid-responsive strategies.

Results

This project advanced knowledge and technologies in five areas (Figure ES-1):

1. Highly insulating windows,
2. Energy recovery façade systems which include ventilation,
3. Window systems which direct sunlight deep into the building,
4. Simulation models for light-scattering technologies to optimize daylight and heat gains.
5. Adaptive control tools for operable daylighting and shading systems.

Highly Insulating Windows

State-of-the-art, dual-pane windows have an insulation level of about R-3. This project developed a lightweight, triple-pane window, resulting in an R-5 insulation level. The 1-inch-thick insulating glass unit was designed with a nonstructural 1/36-inch glass center layer placed between two conventional 1/4-inch glass layers and assembled with a warm edge spacer and krypton gas fill. The project team combined this "thin" insulating glass unit with a novel thermally broken frame. The frame utilizes a non-continuous design that minimizes conductive heat transfer between the outdoors and indoors.

Figure ES-1: Schematic of Integrated Façade System
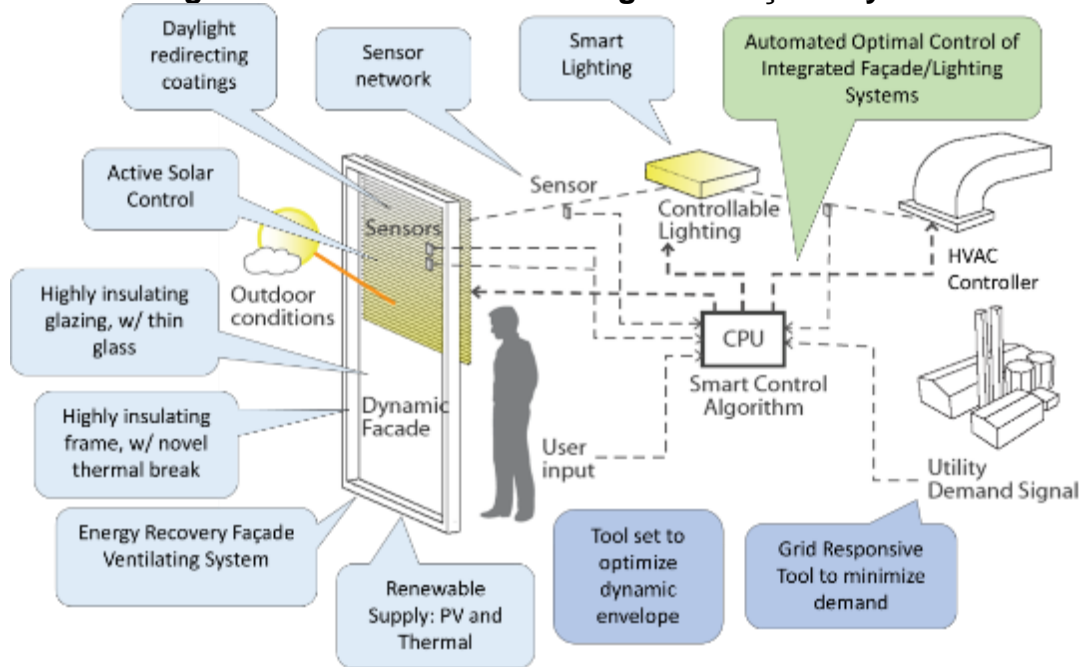
Thermal performance of the prototype frame was measured in Lawrence Berkeley National Laboratory's (LBNL) infrared thermography facility and simulated with industry standard LBNL WINDOW software. The prototype frame achieved a 20 to 90 percent improvement over the traditional thermal break frame and an 80 to 170 percent improvement over an aluminum frame. Overall, the low-solar-gain window shows potential to reduce HVAC energy use roughly 5 to 7 percent across all California climate zones, with a payback of 10 years, given a mature market incremental cost of $1 per square foot of window.

Energy Recovery-Based Façade Ventilation Systems

A novel window-integrated local ventilation and energy recovery device was developed to provide fresh air through the façade to the indoors with minimal energy requirements. To avoid issues associated with ventilation air that might be at a different temperature or humidity levels than the indoor air, an energy recovery core was incorporated that conditioned incoming air for temperature and moisture content with a heat exchanger to save energy when possible. The system was designed for compatibility with automated controls.

The design of the local ventilation and energy recovery device consists of a membrane heat exchanger, an airflow distribution header, fans, air inlet and outlet louvers, bypass ducts, a small photovoltaic (PV) array, and an associated maximum power point tracking controller and battery. The project team designed the prototype to use as many off-the-shelf components as possible.

To confirm product performance, the team tested the local ventilation and energy recovery prototype in the LBNL infrared thermography lab environmental chamber, which provided controlled temperatures and scheduled temperature changes on the interior and exterior of the device. The team also tested the device at LBNL's Mobile Window Thermal Test facility to measure the energy required to make up for heating in direct vent and energy recovery modes. The energy recovery and direct vent cases showed close agreement.

The research team simulated the performance of the unit on a single-zone building model for three California climates. The energy simulation showed heating and cooling savings of 17 to 39 percent, with a payback of six years, given a mature market cost of $20 per window lineal foot.

Daylight Redirecting Systems

Daylight can offset electric lighting requirements, as well as reduce lighting energy use and heat gains from electric lighting. Daylight also improves perception of indoor environmental quality and correlates with improved health. Sleep-wake cycle regulation, circadian rhythms, and seasonal affective disorder show improvements from daylight exposure. Owners, occupants, and the real estate market in general view daylighting as a benefit.

The project team developed a daylight redirecting system to provide daylight in areas of commercial buildings that are 15 to 40 feet from windows. The team designed the system to redirect beam sunlight from the upper area of an east-, south-, or west-facing window to the ceiling plane using a set of automated, variable-width, mirrored louvers. The team also built a tabletop prototype to demonstrate technical feasibility at a macro scale, that is, a 3- to 5-inch slat width. Field measurements in the Advanced Windows Testbed of early prototypes confirmed that the proposed system redirected light deep into the space without discomforting glare.

Simulations indicated that annual lighting energy use was reduced by 0.13–0.73 kilowatt-hours per square foot (kWh/ft.^{2}) or 35–54 percent for east- and south-facing orientations and 9 percent for west-facing orientations compared to a manually operated, matte white venetian blind. The simple payback for all orientations except west was 4–5.5 years, assuming an incremental cost of $10 per lineal foot, for a 2-ft. height.

Dynamic, Integrated Façades

Switchable glazing, motorized shading and daylighting systems, operable windows, and ventilation systems use state-of-the-art, rule-based logic for automated control. Such control provides little to no feedback on how an adjustment of one parameter will affect another parameter, making commissioning, tuning, and maintenance over the life of the installation a trial-and-error process. Rule-based control also has no forecasting capabilities; so if it is foggy in the morning then sunny in the afternoon, the controller

may admit solar gains and daylight to offset heating and lighting requirements in the morning, but increase cooling loads in the afternoon.

Alternatively, model-predictive controls (MPC) use physics-derived mathematical equations and an optimization algorithm to predict how best to manage daylight for the lowest energy cost over a full day, while keeping comfort and indoor environmental quality within bounds. These controls offer a potentially low-cost, transparent, and adaptable alternative to rule-based controls. As utility rates change with the evolving California electricity markets, the model-predictive controller will be able to adapt and support load shift and shed objectives over the life of the installation.

The model-predictive controls were developed and field-tested over a year, using an electrochromic window which modulates from clear to tinted, thus demonstrating feasibility under real-time conditions. The project team evaluated energy cost savings using energy simulations of a south-facing office zone in Oakland and Burbank, California. Compared to rule-based controls, the model-predictive controller was able to reduce daily energy cost by 23–27 percent on sunny days during the summer. The simple payback was four years, given an incremental cost of $1.50–2.00 per square foot of window area.

Daylighting and Shading Optimization Methods

Shading and daylighting systems such as venetian blinds, fabric roller shades, metal mesh overhangs, and sandblasted glass can have an enormous influence on HVAC and lighting energy use, peak demand, and comfort, particularly in sunny, hot regions of California. Today's simulation tools are not able to model the performance of these systems. Since architects and engineers rely on simulation tools to make informed decisions, underlying models need to be accurate and validated.

The project team developed new models based on ray-tracing algorithms, which result in realistic renderings. They validated the models with measured data from full-scale, outdoor test chamber rooms in the LBNL Advanced Windows Testbed and FLEXLAB Testbed. The models agreed with measured data to within 10 percent. The team standardized measurement protocols for characterizing the solar heat gain performance of common shading products. They also developed protocols for evaluating daylighting and comfort performance of shading products.

Technology/Knowledge Transfer/Market Adoption (Advancing the Research to Market)

Technology transfer occurred through public presentations and face-to-face meetings with stakeholders at industry meetings and conferences, open source releases of software and tools, participation on codes and standards development activities, and publications in trade press and open access peer-reviewed publications.

For the highly insulating window, LBNL collaborated with Alcoa to work out essential design elements of the frame for mass manufacturing. The California Partnership for

Advanced Windows convened to identify and overcome technical, regulatory, educational, and financial barriers to promote market transformation toward high-efficiency windows.

The energy recovery-based façade ventilation system and daylight redirecting systems are being promoted in discussions with potential manufacturing partners. For broad market adoption, the daylight redirecting system will need to be further developed as either a between-pane or interior attachment protected by an inboard glazing layer.

The project team held discussions with many of the major dynamic façade manufacturers, with several stating interest in collaborating to develop model-predictive controls. Future work will be focused on improving performance and cost-effectiveness using adaptive tuning and alternate optimization solvers, and then validating performance in the field.

The validated models for determining daylighting and solar heat gains were incorporated into WINDOW, a tool that determines the solar-optical and thermal properties of a user-defined window, Radiance, a ray-tracing tool that renders lighting in buildings, and EnergyPlus, a tool that models building energy use. These were subsequently incorporated into third-party software tools. Technical support was provided with tutorials, on-line forums, and instructional workshops. Standardized procedures for certifying solar control products were developed in collaboration with the Attachments Energy Rating Council for the residential market.

Benefits to California

The project team developed, prototyped, and field-tested a new generation of high-performance building envelope/façade systems. This provided the fenestration and façade industry with potentially cost-effective, grid-responsive solutions to help meet California's zero-net-energy and greenhouse gas reduction goals by 2030. In combination, the technologies developed in this study reduced energy use by reducing thermal losses, cooling loads, and ventilation loads; increased daylighting to reduce electric lighting; and reduced peak load impacts.

Of the three component technologies in this project, both the R-5 window and the local ventilation and energy recovery device are in further development with partner manufacturers. The model-predictive controller will be developed with a partner façade manufacturer if seed R&D funding can be secured, while the open source Modelica models and optimization framework are publicly available to all. There is still substantial work needed to complete design and launch of these innovative technologies. Some of this requires solving additional technical challenges. Advances in self-tuning algorithms and machine learning can also help accelerate development of adaptable, low-cost model-predictive controls. Other tasks are market-oriented, such as evaluating occupant satisfaction with the indoor environment, measuring actual energy savings in occupied buildings, and assessing persistence of savings. Simulation models developed and validated under this study will help accelerate this work and speed market adoption.

This research sets the groundwork for future work in integrated, whole-building, and grid-interactive systems, demonstrating the breadth of potential systems and identifying essential engineering and market-related issues that need to be addressed before full implementation.

When used widely over new and existing building stock, the technologies could be capable of reducing statewide energy use by 6,118 gigawatt-hours, reducing peak electricity demand by 2,250 megawatts, and reducing statewide electricity costs by $867 million/year. This would total to $26 billion over the 30-year life of the technologies. This estimate is based on public information about California commercial building energy use and peak electric cooling demand by building type and floor area, assuming applicability to 75 percent of current floor space, and an average 20 percent reduction in annual energy use and peak demand across new and retrofit applications.

In the long term, the unique tools and prototype technologies developed in this project can result in low-energy buildings that are more flexible and responsive to the variable demands on the utility grid. They will help move California toward achieving an 80 percent reduction in greenhouse gas emissions by 2050.

CHAPTER 1:
Introduction

Innovative window and façade technologies and systems affect heating, ventilation, and air-conditioning (HVAC) and lighting energy use and demand in buildings. Together, these energy uses constitute the largest electricity end uses in California buildings. Given California's goal to double energy savings in existing buildings by 2030, innovative window and façade technologies and systems need to be developed and disseminated as broadly and quickly as possible.

Windows are unique building envelope components. All owners want views, daylight, and connection with the outdoors, so windows are key design features that affect the market value of every building. While most conventional envelope systems, such as insulation, are static, windows can dynamically change energy properties, either intrinsically (for example, with switchable glass) or with the addition of equipment such as blinds, shades, and louvers. Windows affect the operational efficiency of HVAC systems and can be designed to support low-energy heating and cooling strategies. However, despite the potential to achieve significant energy savings, many high-performance window and façade technologies and systems have been slow or unsuccessful in gaining significant market share due to cost and complexity.

This applied research and development (R&D) project focused on developing precommercial technologies and approaches at applied lab-level stages with the goal of feeding the clean energy innovation pipeline with advanced technologies to ensure a reliable, lower-cost, clean, safe, and diverse electricity system for California's investor-owned utility (IOU) ratepayers. Research focused on making breakthrough technological advancements in five key areas:

1. Highly insulating (Hi-R) windows that combine a novel thermal break design for the framing system and nonstructural thin glass triple glazing technology for the insulating glass unit to achieve an R-value of greater than 5 at lower cost.

2. Energy recovery-based façade ventilation systems that use a membrane energy recovery core, wireless sensors, and controls within a window-framing system to address occupant preferences and efficient building HVAC operations.

3. Daylight redirecting systems, based on promising new materials (shape memory alloys and polymers) combined with sensors and controls capable of providing glare-free daylighting to a depth of 40 feet (ft.) in an extended daylight perimeter zone.

4. Daylighting and shading optimization methods for design teams to characterize and optimize the energy- and comfort-related performance of advanced shading and daylighting technologies that cannot be characterized today (such as

complex fins/overhangs, optically complex shading systems, and novel daylight devices).

5. Dynamic, integrated control algorithms that automatically adjust operable window, shading, and daylighting components to meet building-specific energy objectives, including electric utility grid-friendly operation.

Scientists at Lawrence Berkeley National Laboratory (LBNL) conducted research in partnership with manufacturing partners for technology R&D tasks and with industry and research organizations worldwide for activities related to model and tool development that benefit the building industry at large. Separate technical advisory committees were formed for each task so that discussions could focus on task-specific issues.

Research relied on a unique set of modeling capabilities and LBNL facilities that are unparalleled worldwide, including

- The Optics Lab with its scanning goniophotometer for measuring light-scattering materials and systems.

- The Infrared Thermography Laboratory for measuring net heat flow under controlled conditions.

- The Mobile Window Thermal Test Facility (MoWiTT) full-scale outdoor calorimeter for measuring net window heat flow to within 20 watts (W) within a 10-minute (min) time step under dynamic conditions.

- The Advanced Windows Testbed, which measures lighting, comfort, and net window heat flow to within 20–60 W on an hourly time step in three full-scale outdoor test chambers.

- FLEXLAB, which measures light, comfort, and realistic HVAC energy use to within 10 percent on an hourly time step in eight full-scale outdoor test chambers.

The project team conducted design optimization studies using command line versions of WINDOW and Radiance on LBNL's Lawrencium 1148-node (20,436 core) Linux computing cluster. Controls for integrated system interactions were modeled using the LBNL model predictive control (MPC) Python MPCPy platform in combination with Radiance and Modelica/ JModelica open source software.

The project team designed, prototyped, and evaluated technologies using simulations, bench-scale laboratory tests, or full-scale field testing or a combination thereof in LBNL's outdoor testbed facilities. Supporting models and tools were validated in the laboratory and full-scale outdoor testbeds. The scientists addressed technical barriers iteratively through engineering refinements of tabletop or full-scale prototypes, debugging of code or designs when discrepancies were identified between simulated and measured results, and improvements in underlying models or engineering calculations. The team solicited feedback through discussions with the technical

advisory committee, collaborating manufacturers, owners, utilities, and state regulators during face-to-face meetings, conferences, and industry workshops.

The following chapters summarize the research conducted under each of the five tasks, including design objectives, research and development methods, outcomes from testing and simulations, technology transfer activities, and conclusions to date. Future work is discussed, as are benefits to ratepayers.

CHAPTER 2:
Highly Insulating Windows

2.1. Introduction

Commercial window systems are typically constructed with double-pane glazing and thermally broken aluminum framing. Aluminum framing is employed because of the relatively low cost, high strength, easy manufacturability, and long service life. However, even with thermal breaks, the high thermal conductivity of aluminum puts most commercial windows and façades at a serious inherent disadvantage for meeting California building energy efficiency goals. Aluminum frames are often the limiting factor in whole window thermal performance; thermal improvements to the spacer and glazing are nearly irrelevant unless the thermal performance of the frame is first addressed. The low thermal performance of a frame limits the ability of architects and engineers to design energy-efficient buildings without compromising on total window area. In addition, the beneficial view and daylighting benefits that come with windows have resulted in relaxed code compliance requirements for commercial framing, as compared to residential framing. Some framing approaches that increase thermal performance, such as those incorporating pultruded (continuously molded) fiberglass, have been able to meet thermal performance goals but have proven prohibitively expensive for significant market adoption.

In this project, the researchers developed a new thermal break technology that allows aluminum framing to achieve thermal performance comparable to insulating frame materials such as wood and polyvinyl chloride (PVC) while preserving the inherent structural benefits and low cost of the aluminum alloy material. With the thermal performance of the improved frame, the opportunity to realize whole-window performance gains through center-of-glass improvements is presented. The researchers used this opportunity to develop a thin-triple glazing concept. Thin glass is used as the center pane of the triple glazing to reduce window weight and overall glazing width. This report summarizes the development procedures for the aluminum frame thermal break and thin-triple glazing concepts.

2.2 Project Approach

This highly insulating commercial window development project centers on developing an improved aluminum frame thermal break concept. The thermal break design is based on a truss structure. The inherent high strength, low weight, and low thermal conductance make the truss design ideal for a thermal break. The improved thermal performance of the thermal break design of the truss makes it possible for the whole-window thermal impact of the improved glazing performance to be achieved as well. The researchers demonstrated the benefits of the thermal break design of the truss in conjunction with multiple triple-pane insulating glass concepts.

Researchers developed the thermal break design in four major steps. The first step was a market analysis of commercial window framing systems, including a review of state-of-the-art frame profiles. This market analysis provided a baseline for minimum thermal and structural performance that should be achieved with the truss thermal break frame design. After completing the market analysis, the researchers conducted the second step: optimizing the thermal break design to maximize thermal and structural performance.

To ensure that the truss thermal break frame design is practical and easily brought from prototype to market, the third step involved collaborating with industry partners to ensure the final design would meet their cost and performance criteria. The researchers worked closely with Alcoa's Building and Construction Systems group. Alcoa is the world's leading integrated aluminum company. Guidance from Alcoa on essential design elements such as thermal break connection design, thermal break roll crimp, and aluminum extrusion proved crucial in refining preliminary designs.

Finally, the research team produced full-sized prototypes of the truss thermal break frame and thin-glazing unit to validate the simulated thermal and structural performance through laboratory testing. With this step completed, the team demonstrated the viability of the truss thermal break design and the potential effect to the market.

2.3. Results

The results discussion is divided into three sections: (1) the development of the truss thermal break and the related structural and thermal performance, (2) the development of the thin-glass glazing system, and (3) a discussion of the whole-window performance, which includes the highly insulating frame with truss thermal break and a thin-glass glazing system.

2.3.1. Truss Thermal Break

The state of the art in aluminum thermal break technology is mechanically locked designs, where the aluminum frame is extruded with two dies, and glass-reinforced polymer bars (usually two) are crimped between the aluminum to create a single framing cross section. This construction is shown in Figure 2.1(a) with the Kawneer OptiQ^{TM} frame. The standard OptiQ^{TM} frame is one of the most thermally advanced commercial window frames in the U.S. market, and it served as the baseline for thermal and structural performance comparison throughout this project. The truss-based thermal break design developed in this project is shown in Figure 2.1(b). The innovative use of a truss shape provides several key advantages for thermal break design. First, the truss is an efficient structural design, meaning it provides high strength for the amount of material used. Second, this inherent high strength and low material use lead to low thermal conductance. Finally, an additional benefit is that the small triangular chambers created by the truss design disrupt convection heat transfer across the frame width, providing additional thermal performance gains.

Figure 2.1: Thermal Break Profiles of the (a) Kawneer OptiQ™ Frame and (b) Truss Frame
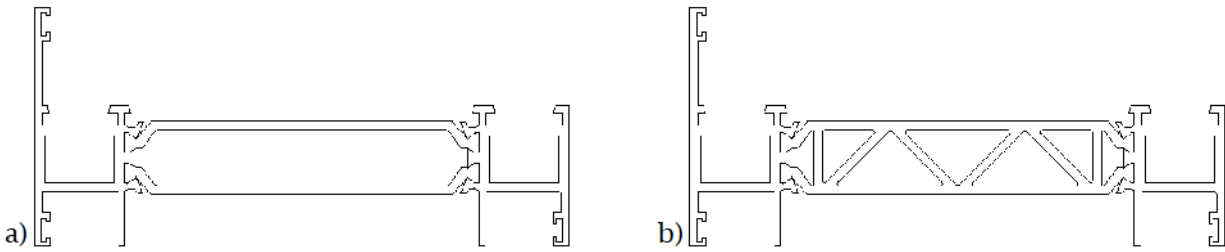
The OptiQ™ frame is used as the baseline for analysis throughout the project. A nonstandard 5-inch frame width was used to integrate with the low-volume energy recovery (LVER) ventilating frame produced in a parallel California Energy Commission project.

Source: Lawrence Berkeley National Laboratory

2.3.1.1. Structural Performance

The optimum shape and extrusion thicknesses for the new thermal break design were determined through a steady-state structural mechanics optimization study performed with COMSOL Multiphysics finite element software (COMSOL 2015). The researchers performed the study with the goal to minimize deflection (bending) under the common loading types identified in AAMA TIR-A8 (AAMA 2008). These guidelines define four loading types that are critical in commercial frame design: tensile (pull), eccentric (twist), shear (lateral shift), and flexural (bend strength). The study focused on several factors of the thermal break, including geometry and material properties. Figure 2 illustrates the three primary geometries (bar, cross, and truss) considered and identifies the primary geometry thickness variables.

The simulation study demonstrated that for any given material property or loading type, the larger the spread, the stiffer the frame. The cross and truss geometries also demonstrated significant improvement, from 30–80 percent improvement over the standard bar design in all loading types when the thickness of the bar is equal for each thermal break type. This improvement in thermal break strength allows a frame designer to choose between having increased frame structural performance or using thinner thermal break dimensions to reduce material cost and increase thermal performance. The thermal break material thicknesses chosen for the prototype in this project are a balance between the two. They offer increased thermal and structural performance over the baseline frame.

Figure 2.2: Basic Thermal Break Construction Types: Bar, Cross, and Truss
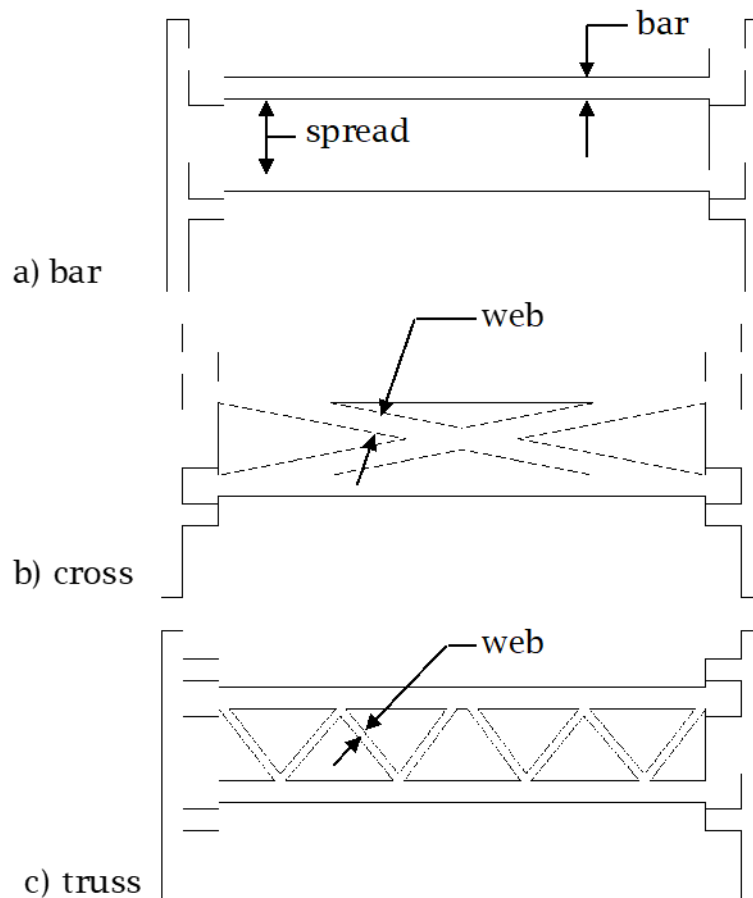
Geometry variables of bar thickness, web thickness, and spread between bars used in the optimization simulation study are identified.

Source: Lawrence Berkeley National Laboratory

The prototype frame built for this project uses the Kawneer OptiQ™ aluminum profiles with a modified truss thermal break and glazing bead to have an accurate baseline of performance. The prototype frame design is based on a 5-inch-wide profile. This profile is wider than typical frames and is done to integrate with the low-volume energy recovery (LVER) ventilating frame produced in a parallel California Energy Commission (Energy Commission) funded task. The baseline Kawneer OptiQ™ frame is also analyzed at a nontypical 5-inch width to provide an accurate comparison between products. Figure 2.3 shows an image of the assembled truss thermal break frame profile.

Figure 2.3: Image of the Assembled Prototype Truss Thermal Break Frame

Source: Lawrence Berkeley National Laboratory

Samples of the prototype frame were sent to a commercial testing lab that regularly performs these tests for industry. The lab compared the deflection measurements to simulation results for several common thermal break polymer types, as shown in Table 2.1 as well as for the standard Kawneer OptiQ™ frame as a basis of comparison. The deflection of the prototype frame profile to these loading types is shown in Figures 2.4 to 2.8. The DuraForm (GF) product was used for the prototype frame, but due to the 3D print method of manufacturing the prototype, the polymer performance is most similar to ultra-high molecular weight polyethylene (UHMW-PE).

Table 2.1: Mechanical Properties of Common Thermal Break Materials

Polymer	Elastic Modulus (MPa)	Shear Modulus (MPa)
Nylon 6/6	2,520	900
DuraForm (GF)	3,106	1,109
Polyurethane (30%GF)	9,830	3,511
UHMW-PE	883	315
Acrylonitrile Butadiene Styrene (ABS) blend	2,100	750

DuraForm (GF) was used in the prototype frame, but the measured performance was closer to UHMW-PE due to the manufacturing method

Source: Lawrence Berkeley National Laboratory

Figure 2.4 to Figure 2.8 show the simulated structural performance of the truss thermal break design compared to the OptiQ™ design with DuraForm polymer under the tensile, eccentric, and shear loading types. These loading types are valuable in determining the overall effectiveness of the thermal break. Tensile loads are common under negative wind pressures, torsional (eccentric) loads are created by gasket pressures when glazing the frame, and shear is the most common loading in frame members designed to resist bending. In all cases the truss thermal break design is shown to be superior to the industry standard bar type thermal break technology (OptiQ™ DuraForm). Eccentric loading in particular highlights the advantages of the truss design over existing technology.

Figure 2.4 Tensile Loading Configuration and Deflection for Common Thermal Break Polymers
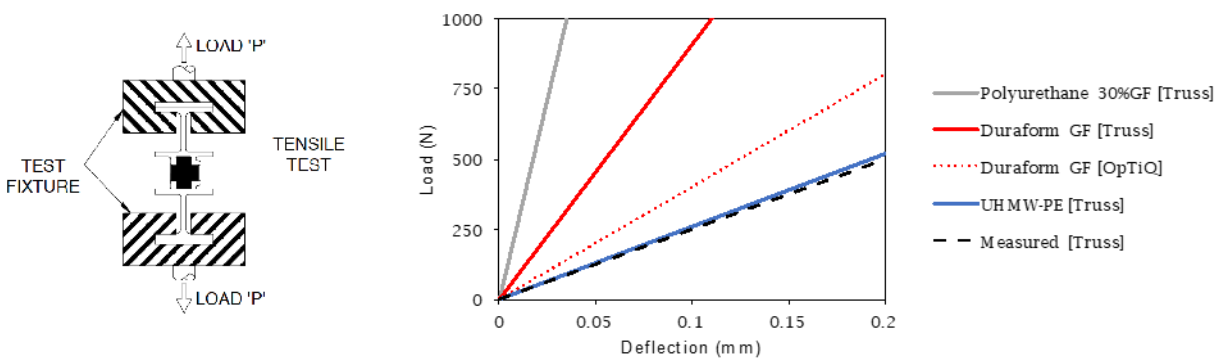
Source: Lawrence Berkeley National Laboratory

Figure 2.5 Eccentric Loading Configuration and Deflection for Common Thermal Break Polymers
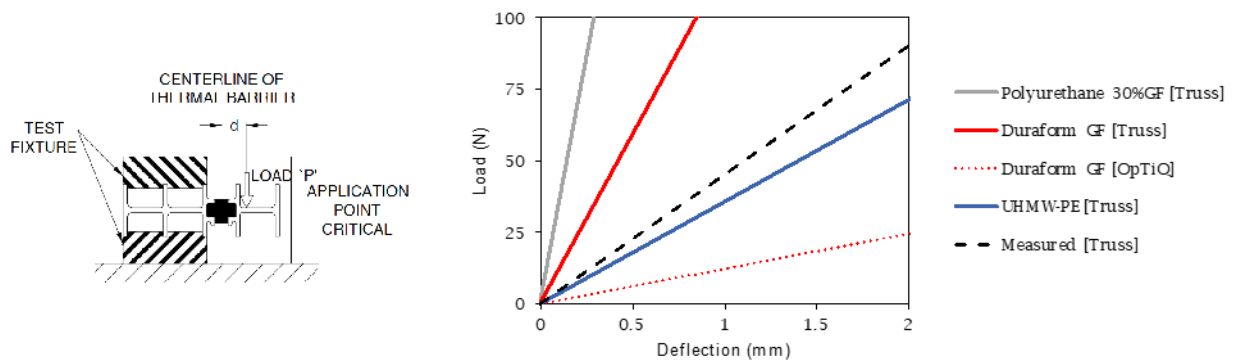
Source: Lawrence Berkeley National Laboratory

Figure 2.6 Shear Loading Configuration and Deflection for Common Thermal Break Polymers
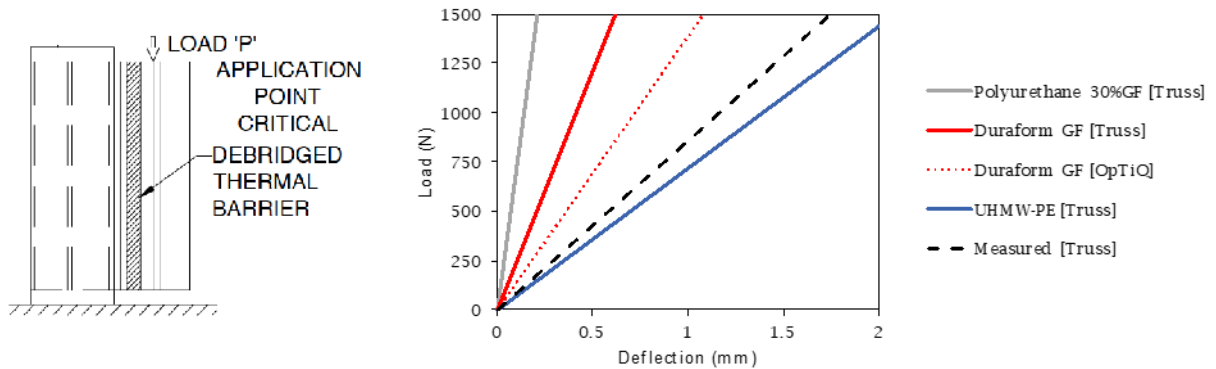
Source: Lawrence Berkeley National Laboratory

The flexural test method is the most commonly recognized metric for frame structural performance. The L/175 deflection criteria (load, P, applied at center of span, L, that results in a deflection of L/175) from this test is typically used by engineers to determine the frame load rating. The results of the flexural tests are shown in Figure 2.7. This measurement is also used to determine the effective moment of inertia (effective second area moment) of aluminum/elastomeric composites, and complex sections, in lieu of calculations. Figure 2.8 shows the calculated moment of inertia for the sample frames. The results show that the truss thermal break design increases the effective moment of inertia by 30 percent over the isobar technology used in the Kawneer OptiQ™ frame.

Figure 2.7 Flexural Loading Configuration and Deflection for Common Thermal Break Polymers

Source: Lawrence Berkeley National Laboratory

18
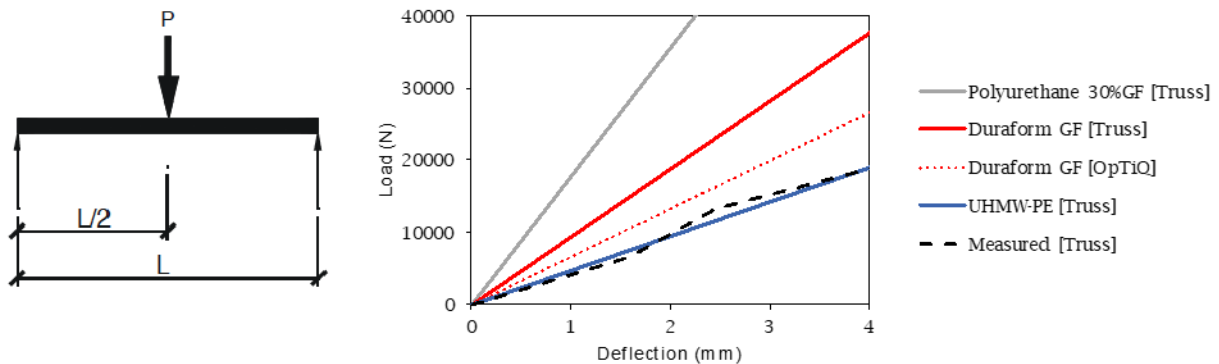
Figure 2.8 Second Moment of Inertia for Prototype Frame with Common Thermal Break Polymers
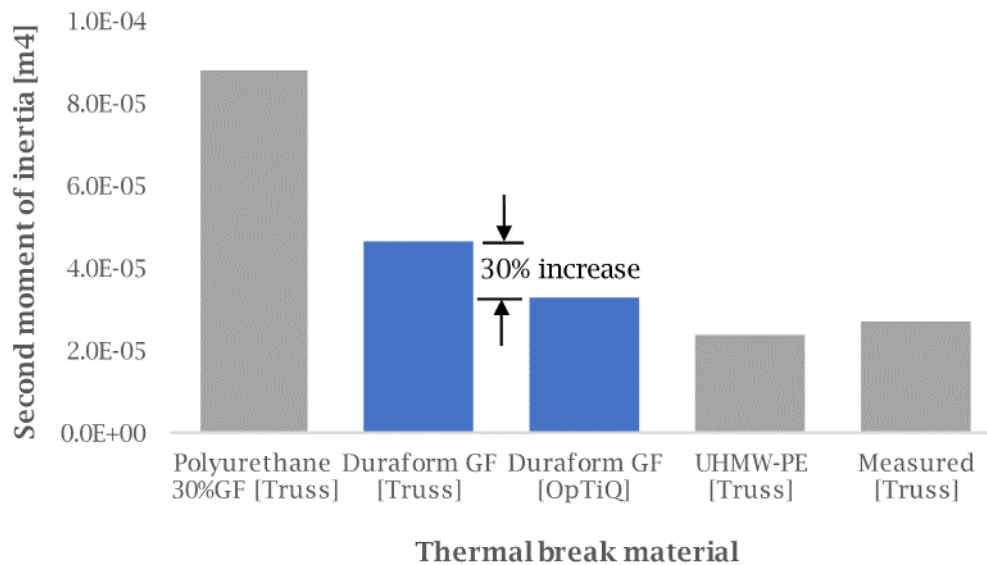
The truss frame design results in a 30 percent increase over the standard OptiQ™ frame when the same polymer is used.

Source: Lawrence Berkeley National Laboratory

This research sought to develop a commercial frame with improved thermal performance. With the minimum structural requirements shown to be met and exceeded with the truss design, the research team analyzed the thermal performance of the truss thermal break design.

2.3.1.2. Thermal Performance

Simulation of thermal transmittance through the truss and Kawneer OptiQ™ frame systems was performed with LBNL's two-dimensional conduction heat-transfer analysis software THERM (LBNL 2016a). THERM is based on the finite-element method. Results of these simulations, as presented in Table 2.2, show that the truss frame design has a 16 percent thermal performance improvement over the OptiQ™ design. Researchers performed the analysis with a typical insulating glass unit composed of double-glazing with low emissivity (low-e) and a warm-edge spacer. The primary source for the improved thermal transmittance with the truss thermal break design is the interruption of convective heat transfer between the two aluminum frame pieces by the intermediate truss webbing. Figure 2.9 shows the representative heat flux through the truss thermal break. The 5-inch-wide frame, composite glazing bead, and thin-glass triple glazing minimize the thermal conduction paths.

Table 2.2: Thermal Transmittance of the Truss Thermal Break Frame Design Compared to the Baseline Frame. Thermal transmittance includes edge of glazing.

Frame	U-factor (W/m²-K)	Improvement over OptiQ (%)
Kawneer OptiQ™ (baseline)	3.76	0
Truss	3.16	16

Source: Lawrence Berkeley National Laboratory

Figure 2.9: Design of Truss Thermal Break Frame and Representative Heat Flux through the Thermal Break.
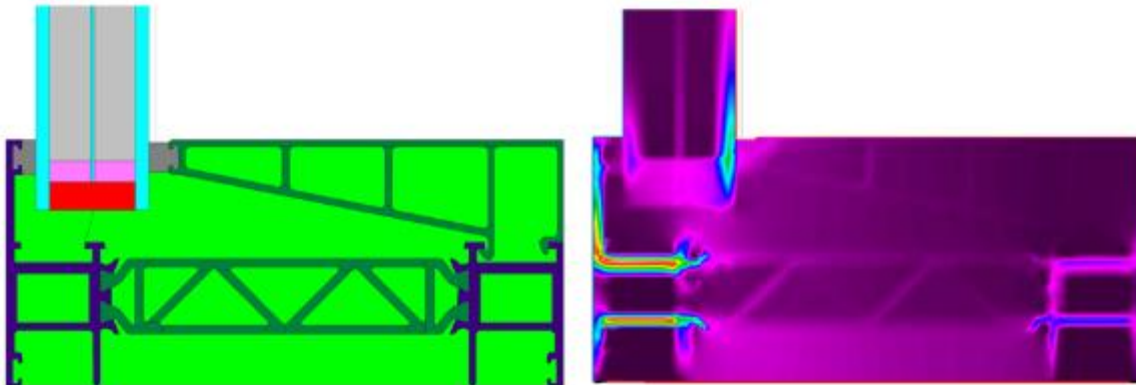
The 5-inch-wide frame, composite glazing bead, and thin-glass triple glazing minimize the thermal conduction paths.

Source: Lawrence Berkeley National Laboratory

2.3.2. Thin-Glass Insulating Glazing Unit

Several strategies for improving the center-of-glass thermal performance of typical windows were examined based on currently available technology. The baseline insulating glazing of double-pane low-solar-gain with argon gas fill (2P-LSG Argon) is typically sized at a 0.74-inch width. This size results from the typical ½-in. between-glass gap width and two layers of single-strength (1/8-in. nominal) glass. The researchers performed a parametric study of U-factor sensitivity to insulating glass unit construction and overall width, as shown in Figure 2.10 (Selkowitz 2018). This study demonstrates that a triple-pane with a 0.7-millimeter (mm.) thick "thin-glass" center layer (3P-TG) and 95 percent krypton gas fill offers the greatest performance potential over a wide range of insulating glass unit widths for all glazing configurations considered. Glass thickness can often rise to 1/4 in. in commercial windows, while the gap between glass layers stays the same. In this case the results in Figure 2.10 remain valid but with a shifted insulating glass unit width of 1/4 in.

Figure 2.10: Center-of-Glass (COG) Thermal Performance Potential Based on Insulating Glass Unit (IGU)
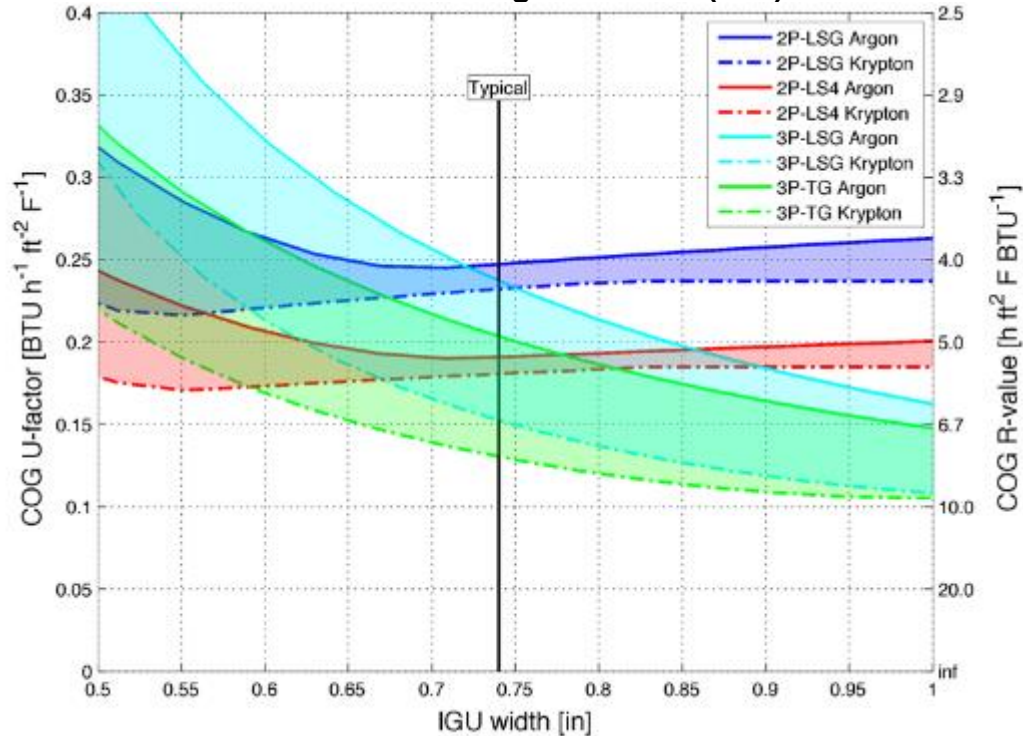
Width with between 95 Percent Argon and 95 Percent Krypton between-Glass Gas Fill and Single-Strength (1/8 in. nominal) glass. 3P-TG uses 0.7 mm glass thickness for center-glass. LSG = low-solar-gain, LS4 = low-solar-gain with surface 4 low-e, TG = thin-glass.

Source: Lawrence Berkeley National Laboratory

A thin-glass insulating glass unit was constructed for the prototype window. The project team constructed the glazing in a low-solar-gain configuration, ideal for the cooling-dominated climates typical in California. Krypton gas fill was used to optimize the thermal performance of the gas gaps. A structural foam warm-edge spacer was used with a polyurethane primary seal to ensure a high-performance edge of glass. The coating and spacer configurations are illustrated in Figure 2.11.

Figure 2.11: Prototype IGU Configuration
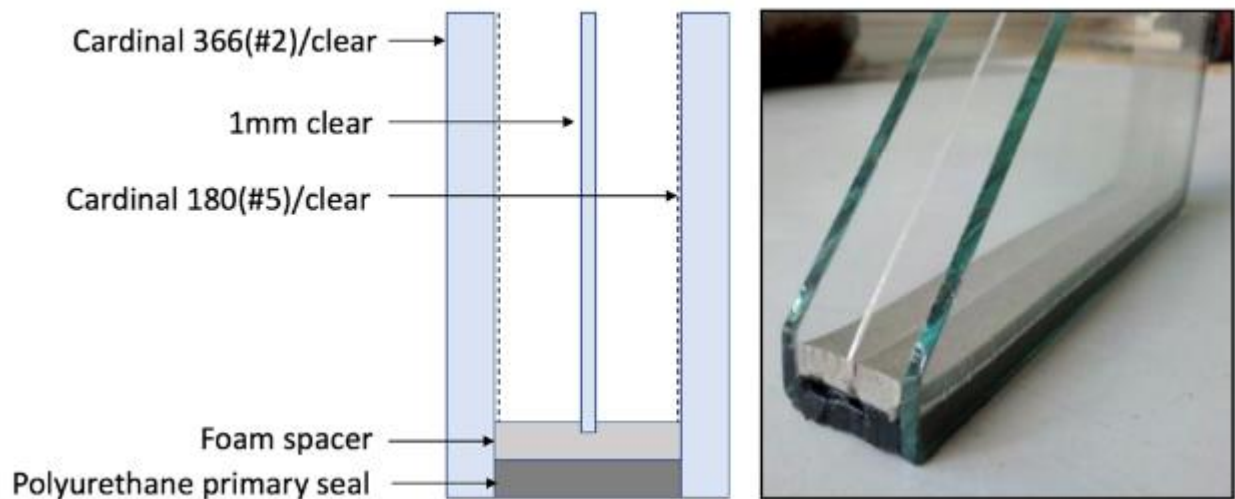
The coating configuration is typical of a low-solar-gain triple-pane IGU.

Source: LBNL

2.3.3. Highly Insulating Window

The assembled truss thermal break frame is shown in Figure 2.12. On the advice of the project team's industry partner, Kawneer, the thermal break was adhered to the aluminum profiles with epoxy (Loctite E-30UT) for the prototype only. This method provides a no-slip condition at the joints, ensuring the structural testing measures the stiffness of the materials and geometry, not the quality of crimping.

Figure 2.12: Image of Truss Thermal Break, Glazing Bead, and Thin-Triple Glazing Assembled Between Kawneer OptiQ™ Aluminum Profiles
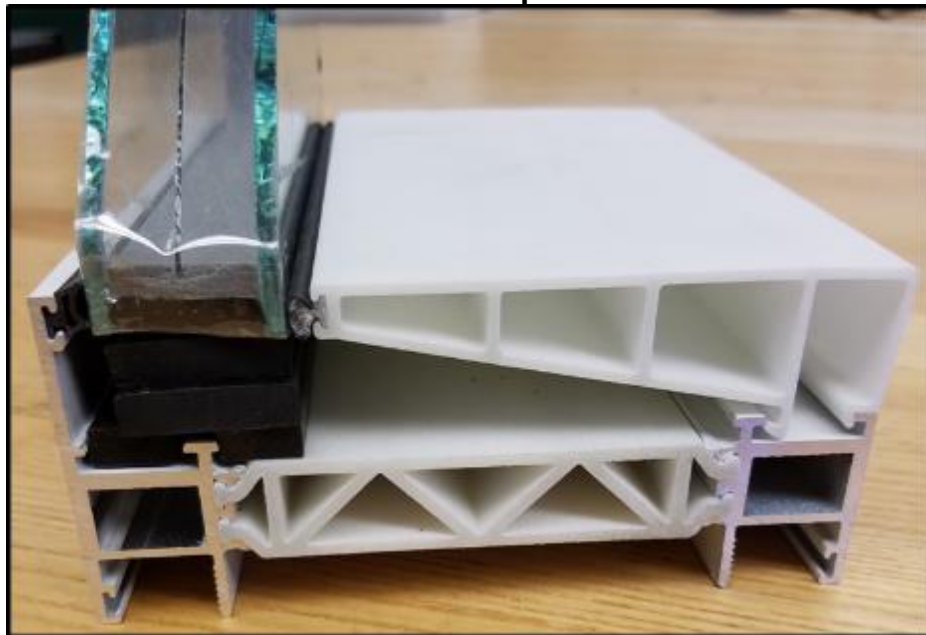
Source: LBNL

A prototype window frame was assembled at 35.75" wide x 41.75" high, as shown in Figure 2.13. The window was constructed per Kawneer guidelines, with mitered corners reinforced by aluminum corner keys. The corner joints were sealed with silicone sealant.

Figure 2.13: Assembled Prototype Frame Showing Mitered and Reinforced Corners
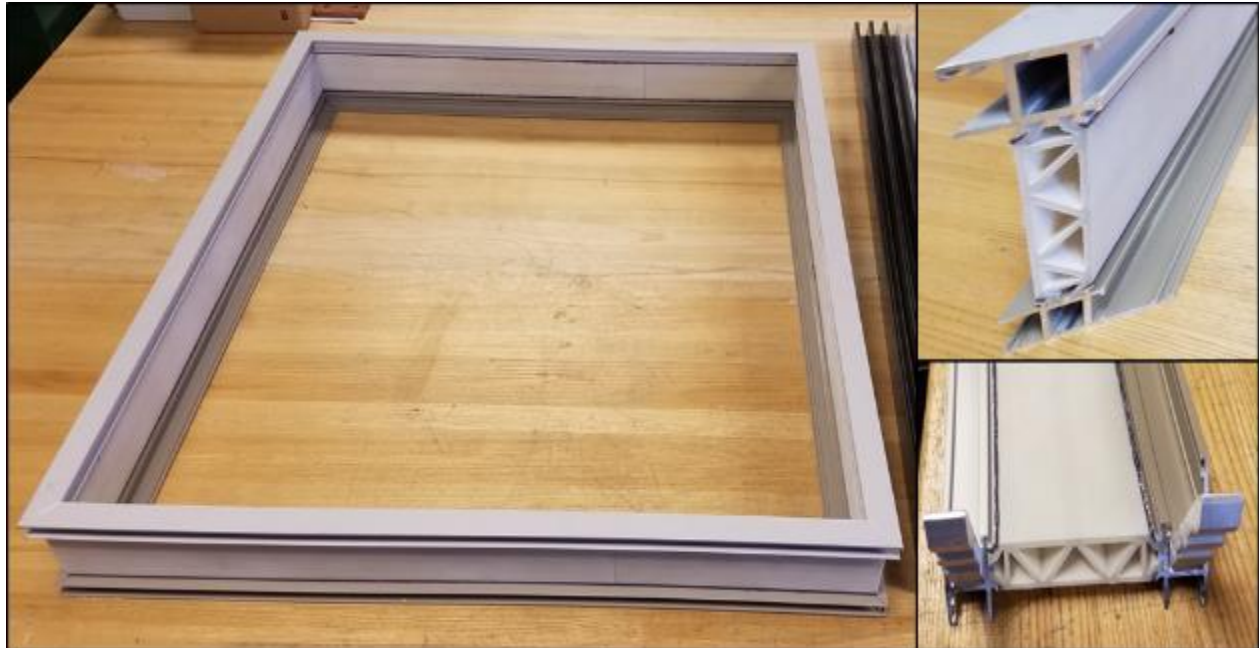
Source: LBNL

The thermal performance of the prototype frame was measured in LBNL's infrared thermography facility and simulated with industry standard LBNL WINDOW software (LBNL 2016b). The measured center-of-glass performance was within 1 percent of the simulated results, as shown in Table 2.3. The whole-window thermal performance is not directly measurable in the infrared thermography lab, but an estimate of the performance was completed through simulation of the frame in THERM and a comparison of the measured and simulated surface temperatures.

Table 2.3: Comparison of Simulated and Measured Center-of-Glass Thermal Performance of Truss Thermal Break Window Prototype

Measurement Method	Center-of-Glass U-factor (Btu/h-ft²-°F)
Simulated	0.094
Measured	0.093

Source: LBNL

Figure 2.14 shows the laboratory setup of the prototype frame in the test chamber and a false color infrared thermography image of the surface temperatures. The temperatures along the vertical centerline are plotted in Figure 2.15 along with the simulated temperatures from THERM. The measured and simulated temperatures along the sill profile matched very well, within 0.5° Celsius (C). The simulated head profile may not accurately account for the convection conditions at the top of the chamber; therefore, the divergence from simulation to measurements at that position is expected. Overall the difference between measured and simulated surface temperatures was within the 2°C range that the authors expected in these tests.

Figure 2.14: Laboratory Setup and Infrared Thermography False Color Image of the Performance Validation Measurements

Source: LBNL

24
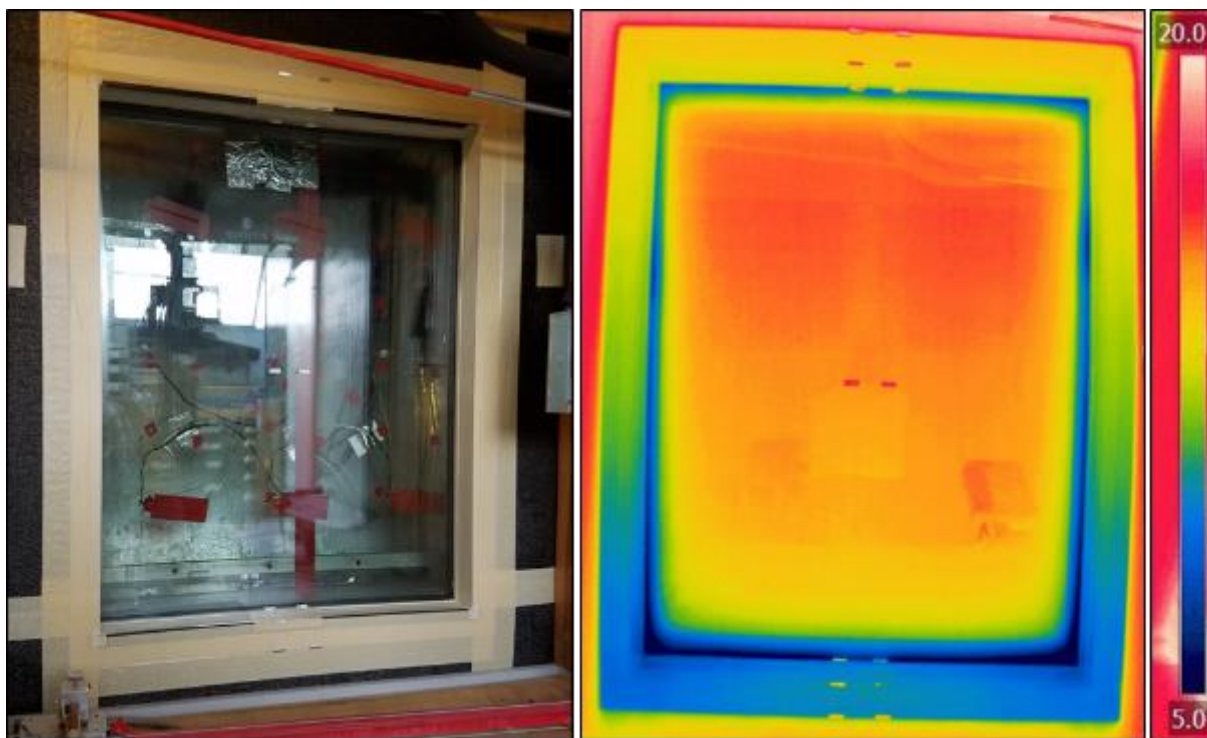
Figure 2.15: Comparison of Measured to Simulated Temperature along the Projected Length of the Test Sample
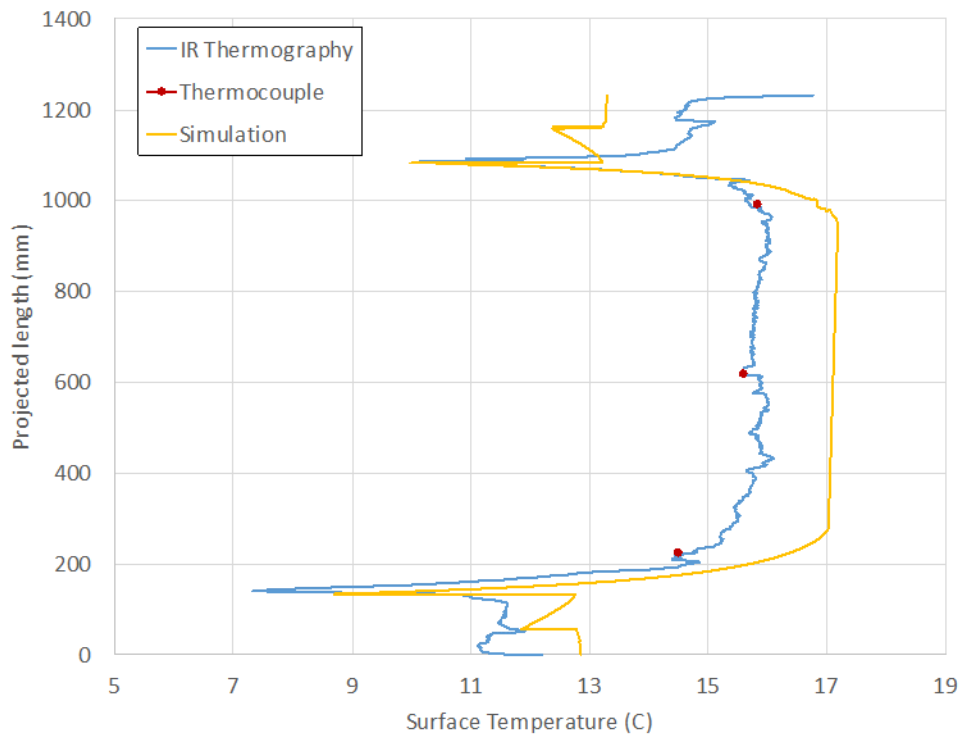
Source: LBNL

Table 2.4 lists the center-of-glass and full window thermal performance of glazing systems modeled in thermally unbroken aluminum, traditional pour-and-debridge thermal break, and the new truss thermal break frame. A basic double-pane low-e argon-filled unit was modeled as typical for commercial installations. High and low solar-heat-gain versions of the thin-triple design were also included. The traditional thermal break frame ranged from 40 to 90 percent improvement over traditional aluminum, and the truss thermal break frame achieved a 20–90 percent further improvement over the traditional thermal break frame (80–170 percent over the aluminum frame).

Table 2.4: Full Window Modeled Thermal Performance of Baseline Double Low-e Glazing and Highly Insulating Thin-Glass Alternatives in High and Low Solar Gain U-Factor (Btu/h-ft^2-°F)

Glazing System	Center of Glass	Full Window Aluminum Unbroken	Full Window Traditional Thermal Break	Full Window Truss Thermal Break
Double low-e (90% argon)	0.24	0.47	0.31	0.26
Thin-triple high-solar-gain (90% krypton)	0.12	0.37	0.24	0.15
Thin-triple low-solar-gain (90% krypton)	0.10	0.36	0.21	0.14

At the National Fenestration Rating Council (NFRC) Fixed Window Size. The traditional thermal break represented here is a pour-and-debridge type.

Source: LBNL

The project team performed annual energy simulations to estimate the effect that the truss frame design with thin-triple glazing could have in a commercial building. The annual energy simulations were performed with CBECC-Com 2016.3.0 SP2 (CABECC 2016a) and the Title 24 medium office prototype (CBECC 2016b). As shown in Figure 2.16, the low-solar-gain truss window shows potential for about 5–7 percent HVAC energy use reduction across all California climate zones.

Figure 2.16: Heating Ventilating and Air-Conditioning Energy Savings Potential of High and Low Solar Gain
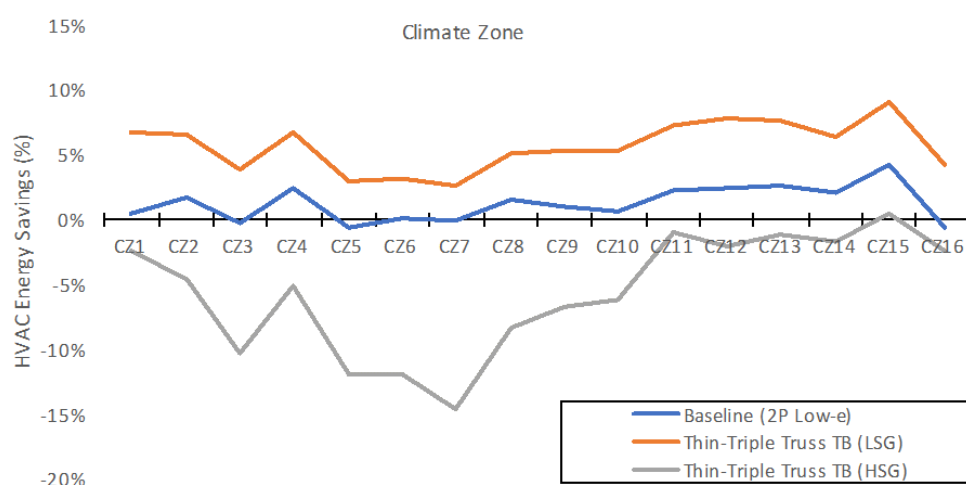
Thin-Triple Truss Thermal Break Windows and Baseline Double-Pane Low-e Window over the Code-Compliant Window. Simulations performed with CBECC-Com Title 24 prototype models: medium office prototype.

Source: LBNL

Some of this reduced energy use can be attributed to the reduced solar heat gain coefficient (SHGC) of triple glazing (SHGC = 0.20) compared to the traditional double-pane window (SHGC = 0.25). For this reason, the high-solar-gain variation of the thin-triple design (SHGC = 0.45) performs poorly and is not recommended for this building type in California climates.

2.4. Technology/Knowledge Transfer/Market Adoption

To ensure the highly insulating window concept is ready for market adoption, the researchers collaborated closely with manufacturing partners, architects, engineers, and utility groups nationwide, with a focus on the California market. The truss thermal break frame design must be practical for manufacturing to be brought easily from prototype to market. The researchers collaborated closely with Alcoa's Building and Construction Systems group throughout the process to ensure the final design meets the group's cost and performance criteria. Alcoa is the world's leading integrated aluminum company.

The project team optimized the truss prototype design for extrusion efficiency by working closely with commercial extruders. The primary design concerns are the wall thicknesses of the chord and web elements, as well as the material base type and glass fiber fill. Thicker profiles provide more strength but are harder to cool and have higher tolerances due to potential gravity sagging.

A patent for the truss thermal break design was filed, and the researchers plan to license the technology to a commercial manufacturer. The development, to date, has focused on commercial punched opening windows, which represent most light commercial and commercial windows sold in California. Most commercial buildings such as small, medium, and large office buildings, schools, and warehouses use this window type. Whether the truss frame technology is ultimately licensed by a manufacturer, the researchers have demonstrated that better frames are possible, and this demonstration should help drive frame manufactures to consider the performance potential when developing new products.

Research and development of the thin-glass triple-pane insulating glass unit is cosponsored by the U.S. Department of Energy (DOE). This work began nearly 30 years ago with a provisional patent (Selkowitz 1991) and continued with thermal performance investigations on nonstructural center layers (Arasteh 2008). Now with large price reductions in thin glass and krypton gas (Selkowitz 2018) the technology is ready for mass-market adoption. The program involves working with supply chain partners (thin glass, low-e, spacers, krypton gas fill), leading window manufacturers, and market pull partners such as building codes, utility rebate/incentive programs, builders targeting net-zero and PassiveHaus (high comfort, low energy) designs, and with tighter northern climate zone ENERGY STAR® criteria. While several insulating glass unit technologies have the potential to meet the same performance achieved with thin-glass construction, the thin triple is the only one that the researchers believe will meet the short-term cost

and industry acceptance requirements. In a longer time frame, new glazing innovations may appear and become market standards, but in the 5- to 10-year "near-term" time frame, the thin-triple approach has a high chance to transform markets.

The thin-triple design depends on volume availability of thin glass with price points that are suitable for mass production of the final insulating glass unit. Historically, this glass has been available for some time but largely for applications such as cell phones, where cost was not a market concern, and in sizes and volumes that were different from windows. However, the rapid market dominance of ever-larger flat screen TVs drove glass manufacturers to develop larger and lower-cost thin glass and make it available in much greater volumes. While there are new challenges with very thin glass (such as handling, cutting, shipping), all of these have been solved by the liquid crystal display (LCD) television industry and can be readily adopted by window companies. There are other challenges unique to windows that must be further explored, such as tempered glass. Prototypes also have focused on typical punched opening window sizes (4 ft. x 5 ft.) so the handling and durability of oversized curtain-wall-sized units is uncertain, but the researchers and industry partners see no fundamental obstacles to the use of thin glass in these windows.

The California Partnership for Advanced Windows (C-PAW) was formed in fall 2018 to identify and overcome technical, regulatory, educational, and financial barriers to ease market transformation toward high-efficiency windows. This partnership is a California-centric collaborative with LBNL, the California Building Industry Association (CBIA), and the Energy Commission leading the effort, with participation from California utilities, window manufacturers, and home builders. The group's current focus is on launching thin-glass window prototypes in residential applications, but the commercial application path is occurring in a parallel effort.

A technical advisory committee was composed of industry, research, and academia, and it included the Energy Commission, thus covering all important stakeholders.

2.5. Benefits to California

The performance requirements for an "ideal" energy-efficient window are difficult to define. In the context of zero-net-energy buildings, the authors find the most suitable definition based in terms of an overall energy balance, for example, a window that is energy-neutral in winter heating mode, where solar gain equals or exceeds thermal losses (Arasteh 2006). Windows meeting this metric enable the building industry to realize the challenging California energy performance goals leading to zero-net-energy commercial buildings by 2030 while maintaining the desirable aspects of windows, such as connection with the outdoors with daylighting and views.

People like large windows for the view and connection to the outdoors, but on the coldest and warmest days, large windows typically present a thermal comfort challenge. Even if average interior air temperature is acceptable, the radiant effects of cold or hot glass and thermal drafts can make space near the window uncomfortable or unusable.

Supplemental perimeter heating and cooling are typically used, even though they are not needed to meet the building thermal load to compensate for these uncomfortable conditions. The highly insulating frame and glazing concept the authors have developed would reduce or eliminate these problems, thus enhancing the marketing story and financial return for these investments.

Based on a 2006 California Energy Commission end-use survey (Itron 2006) and the 5 percent heating and cooling energy savings estimates previously shown for California commercial buildings, the yearly energy savings potential of these high-performance windows over current standards is greater than 1,300 gigawatt-hours (GWh) of electricity and 3.4 trillion-Btus of natural gas. This potential translates to an energy savings of nearly $200 million per year in the commercial sector.

CHAPTER 3:
Energy-Recovery-Based Façade Ventilation Systems

3.1. Introduction

Ventilation in buildings provides fresh air to occupants, and it typically accounts for a significant portion of cooling and heating loads through the energy required to condition outside air to indoor comfort parameters (that is, temperature and humidity). This energy can be reduced through heat or energy recovery systems, where energy recovery accounts for heat and moisture recovery of the exhaust air stream. Energy code typically stipulates a minimum amount of fresh air per occupant, or more recently, based on carbon dioxide (CO_2) sensor readings. In a typical application, outside air is provided at the central HVAC location, where fresh air is mixed with supply air, replacing a portion of the exhaust air that is routed outdoors. In commercial buildings the amount of fresh air exceeds the amount of exhausted air to maintain a slightly pressurized indoor environment, which in turn minimizes infiltration though windows and other parts of building envelope. Rarely, a heat or energy recovery unit is used to reduce energy loss for treating fresh supply air. Due to comfort requirements, outside air may be distributed throughout the building, regardless of HVAC operation, often resulting in additional fan energy to distribute air through buildings. More recently, the use of dedicated outdoor air systems (DOAS) has been proposed, and several systems have been proposed. Generally, DOAS rely on their own distribution, with the idea that dedicated fans and ductwork for moving fresh outside air would be smaller and, therefore, use less energy.

This task addressed the inefficiencies of central distribution systems, including central DOAS, and proposed the use of a local DOAS that is integrated with the windows to provide fresh outside air directly where it is needed, in the adjoining indoor space. This strategy substantially reduces the energy required to move air from a central location through ducts to provide on-demand outside fresh air. The project team designed, developed, and demonstrated an autonomously operated local ventilation and energy recovery (LVER) unit that can replace traditional centralized ventilation designs or replace substantial need for a central system. As part of this design, the team proposed a distributed network of LVERs, integrated into the window/façade framing. Figure 3.1 shows a schematic of the proposed system.

Figure 3.1: Illustration of a Packaged Local Ventilation and Energy Recovery (LVER) Unit

Source: LBNL

3.2. Project Approach

The window-integrated LVER technology provides fresh air through the façade with minimal energy requirements, since air is moved into and out of buildings over short distances through the façade, instead of through a higher centralized pressure drop system. An energy recovery core is incorporated to condition incoming air for temperature and moisture content, saving energy due to decreased temperature and humidity differentials between the supply and room air. Figure 3.2 illustrates the exchange concept.

The window frame-integrated LVER unit consists of an energy recovery core and low-power wireless sensors controlled by a "system-on-a-chip" that minimizes energy use and ensures proper air distribution to perimeter zones. LVER units will be distributed along building façades and mesh-networked with the overall HVAC control systems, including CO_2 sensors in the conditioned perimeter spaces.

The LVER unit development includes several steps: (1) development of the energy recovery core (membrane heat and moisture exchanger; (2) development of the housing that will be integrated with the window; (3) sizing and design of air flow pathways, including dampers and related actuators; (4) development of control logic and board, including sensors; (5) battery and PV modules; (6) packaging and prototype fabrication; and (7) testing and energy savings simulation.

Figure 3.2: Illustration of Packaged Local Ventilation and Energy Recovery (LVER) Unit Operation
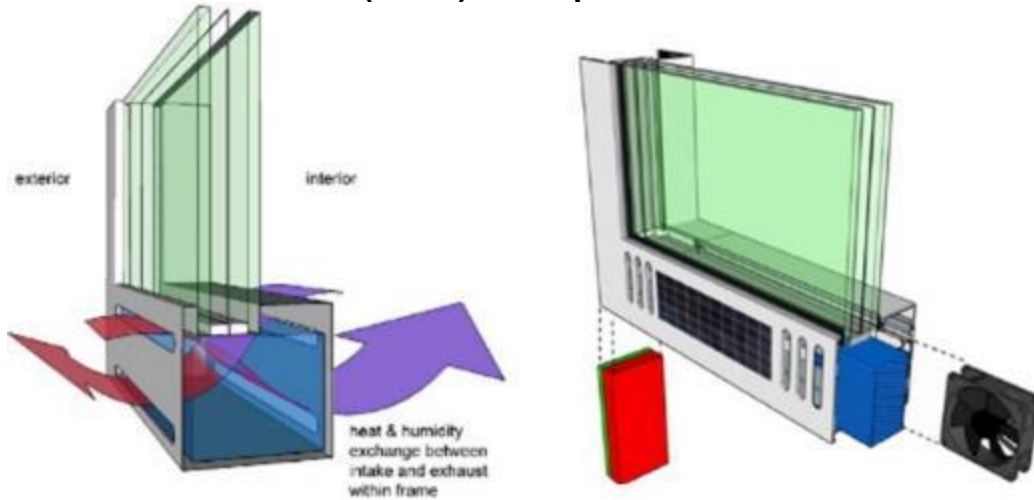
Source: LBNL

3.3. Results

3.3.1. Development of Membrane Heat and Moisture Exchanger

The authors studied and compared several design schemes for the membrane heat exchanger, including spiral, honeycomb, normal concentric cylinder, concentric cylinder with half-turn twist, rectangular solid, and layer-by-layer with aluminum foil supporting types. Figure 3.3 illustrates all design schemes. Green and red were used to distinguish between different air streams.

The energy recovery exchanger works by exchanging heat and moisture between the indoor air stream exhausting outdoors and the outdoor air stream bringing fresh air indoors. Maximizing surface area between these streams theoretically maximizes the energy transfer efficiency. Each of these designs was initially a theoretical exercise, which may ultimately be practical; the project team wanted to keep an open mind and try as many solutions as possible. Some of these designs, such as Figure 3.3e and Figure 3.3f, proved impractical very quickly due to the complex geometry of channels that carry two air streams. After further inspecting the practicality of each design and consultation with a membrane manufacturer, the authors narrowed the choice to the designs Figure 3.3c and Figure 3.3d.

Figure 3.3: Potential Design Schemes for the Membrane Heat Exchanger
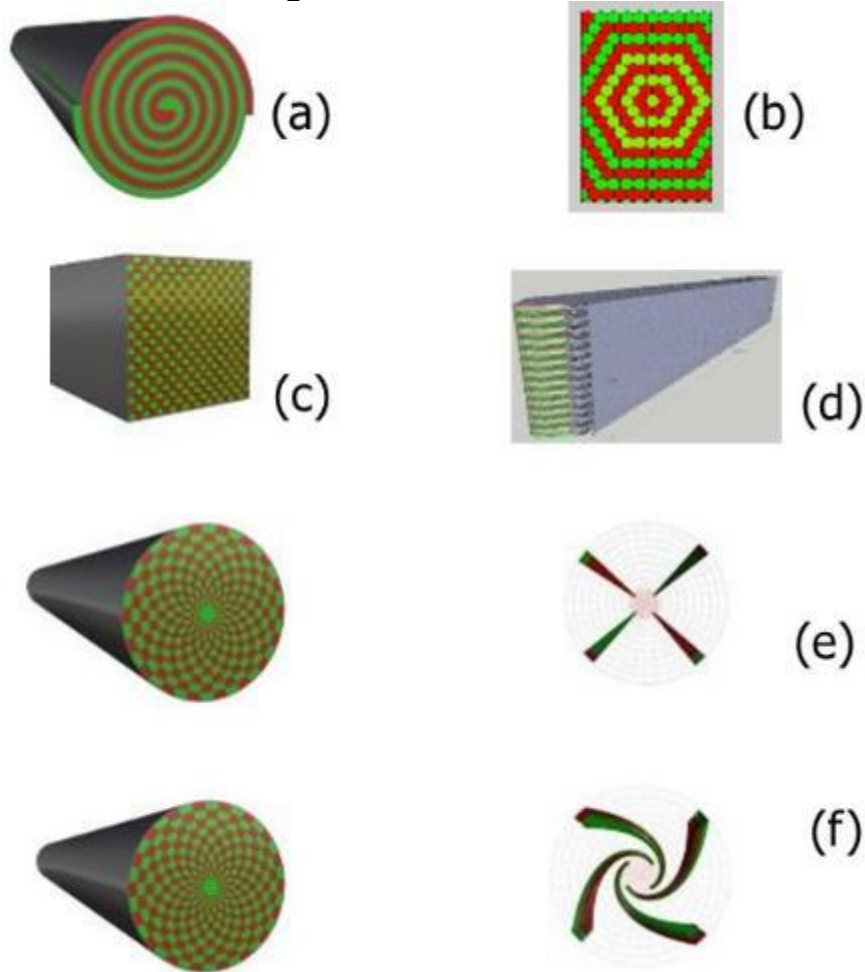
(a) Spiral, (b) Honeycomb, (c) Rectangular Solid, (d) Layer-by-Layer With Aluminum Foil Supporting, (e), Normal Concentric Cylinder, and (f) Concentric Cylinder With Half-Turn Twist

Source: LBNL

3.3.1.1. Rectangular Solid Heat Exchanger

This design is depicted in Figure 3.3c. The challenge when using the rectangular solid heat exchanger (RSHE) is to design an appropriate header to separate fresh air from exhaust air at the terminals of the heat exchanger. Figure 3.4 illustrates the one option for the heat exchanger header. At the terminals of the heat exchanger, fresh air goes in and out through the green tubes that connect the header and the heat exchanger, while exhaust air goes in and out through the gap between the heat exchanger and the header. Thus, the fresh airflow and the exhaust airflow are separated by the green tube at the terminals of the heat exchanger. While this design has higher theoretical efficiency and was a leading candidate early on, further consideration of the practicality

of the design, in consultation with a membrane manufacturer, resulted in the rejection of this design and focus on the layer-by-layer design, described in more detail below.

Figure 3.4: Distribution Header to Separate the Fresh Airflow and the Exhaust Airflow in a Rectangular Solid Heat Exchanger Design
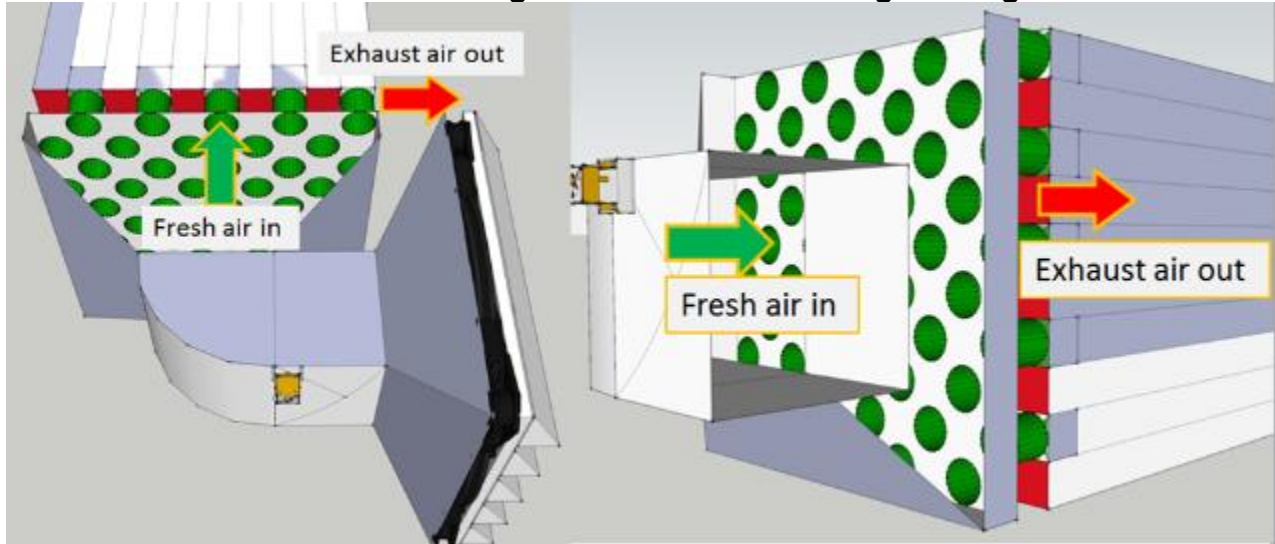
Source: LBNL

3.3.1.2. Layer-by-Layer Heat Exchanger

Figure 3.5 and Figure 3.6 show the details of the layer-by-layer heat exchanger. As the layer height is only 6 mm, the project team inserted a piece of perforated aluminum foil into each layer for support, as shown in Figure 3.5. The team used the perforated aluminum foil because it helps decrease the flow resistance and pressure drop compared to the foil without holes. As shown in Figure 3.6, the exhaust air and fresh air are in crossflow, which contribute to higher heat transfer efficiency. Figure 3.7 shows details of the connections between the heat exchanger and the inlets and outlets of fresh air and exhaust air. Fresh air and exhaust air get into the heat exchanger from the corresponding air inlets and exit the heat exchanger from the respective air outlets. To separate exhaust air from fresh air, the layers are sealed alternately at each inlet/outlet of the heat exchanger. For example, for the fresh air inlet, the layers for exhaust airflow would be sealed to make sure that fresh air can get only into the fresh air layers.

Figure 3.5: Aluminum Foil with Holes

Aluminum foil with
holes for supporting

Layer surface
for separation
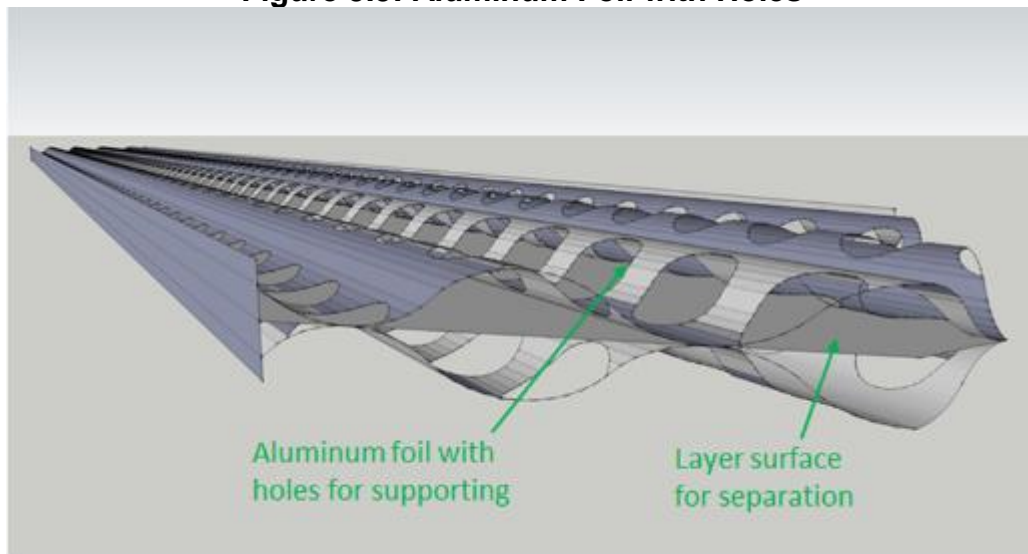
Source: LBNL

Figure 3.6: Layer-by-Layer Heat Exchanger with Aluminum Foil Supporting

Exhaust air out

Fresh air in

1000mm
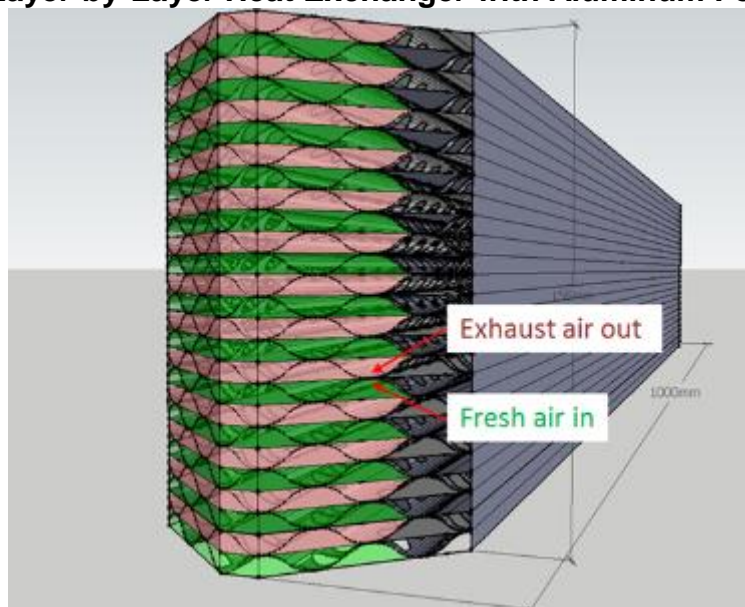
Source: LBNL

Figure 3.7: Connection Details between the Heat Exchanger and the Inlets (a) and Outlets (b)
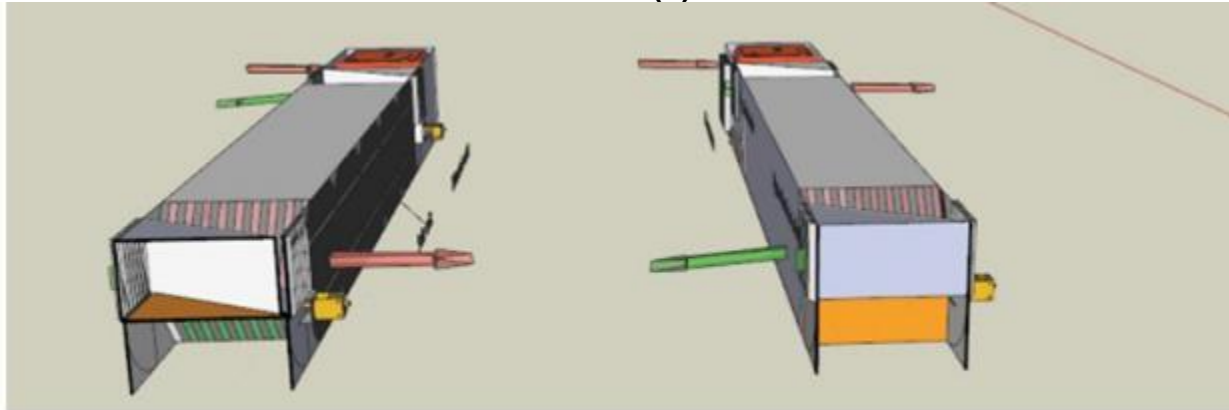
(a)
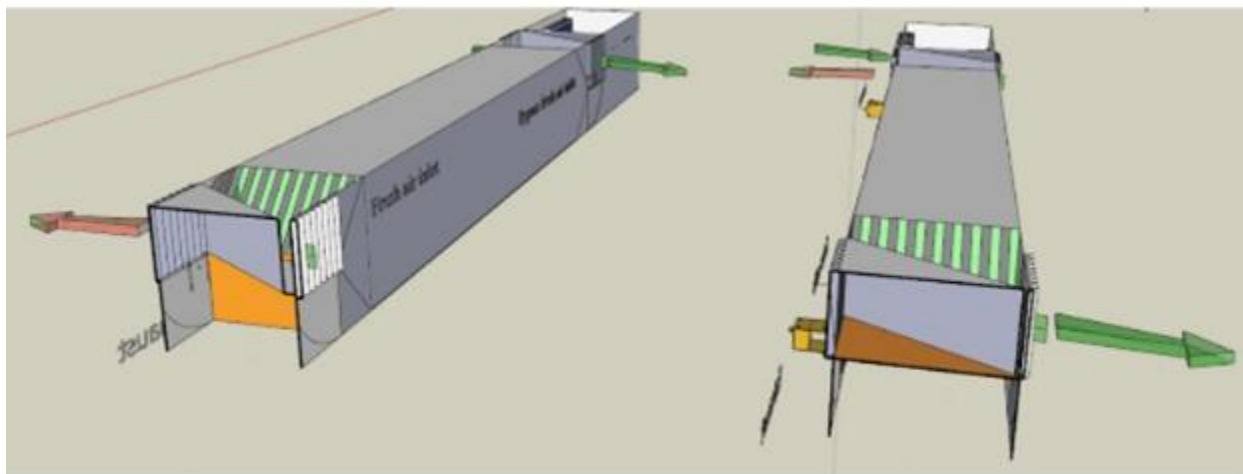
Bypass mode   (b)   Energy recovery mode

Source: LBNL

3.3.2. Design of the Local Ventilation Energy Recovery (LVER) Unit

The project team designed the LVER unit to be integrated with the window frame developed as part of this project (see Chapter 2 for details), so the unit dimensions were specified according to the dimensions of the prototype window. These dimensions are flexible, although at minimum the cross section of the housing needs to be at least 100 mm x 100 mm to fit the energy core with meaningful performance. The LVER consists mainly of the membrane heat exchanger, the airflow distribution header, the fans, the air inlet and outlet louvers, the bypass ducts, the photovoltaic (PV) array, and the associated maximum power point tracking controller and battery. Bypass ducts are used for fresh air and exhaust air, bypassing the heat exchanger in transition seasons. A small PV system was proposed to power the LVER system and have it operate autonomously. The generated DC power from the PV system is supplied to the electricity-consuming devices of the unit, such as the fans, controllers, and sensors. The

surplus electricity, if any, would be stored in the battery that will provide electricity to the devices during nights and days with low solar exposure. Figure 3.8 shows the LVER design using the layer-by-layer heat exchanger.

Figure 3.8: Layout of the LVER Unit Using a Rectangular Solid Heat Exchanger
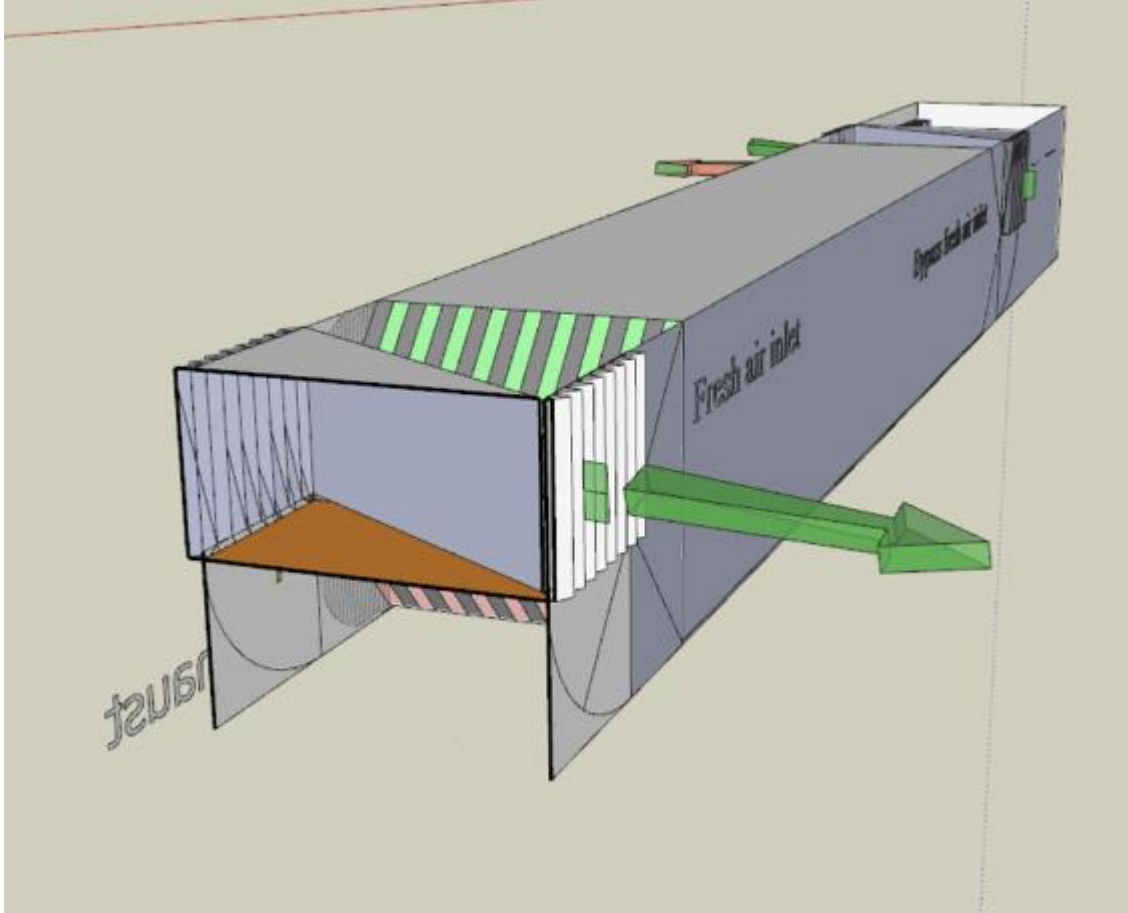
Source: LBNL

3.3.2.1. Operating Modes

The LVER unit has two operating modes: energy recovery and bypass (that is, economizer) mode. When the ambient outdoor air temperature and humidity do not meet the indoor thermal comfort requirement, the LVER unit operates in the energy recovery mode. When the ambient outdoor air temperature and humidity can meet the indoor thermal comfort requirement, the LVER unit operates in bypass mode. Figure 3.9 shows a schematic diagram of the energy recovery mode of the LVER unit using a rectangular solid heat exchanger. The fresh outdoor airflow (marked with green arrows) exchanges heat and moisture with the exhaust airflow (marked with red arrows) in the exchanger to achieve the goal of energy recovery. After passing through the energy core, fresh air flows inward (into the room), and the exhaust air discharges to the outdoor environment.

37

Figure 3.9: Schematic Diagram of the Heat Recovery Mode of the LVER Unit Using Layer-by-Layer Heat Exchanger
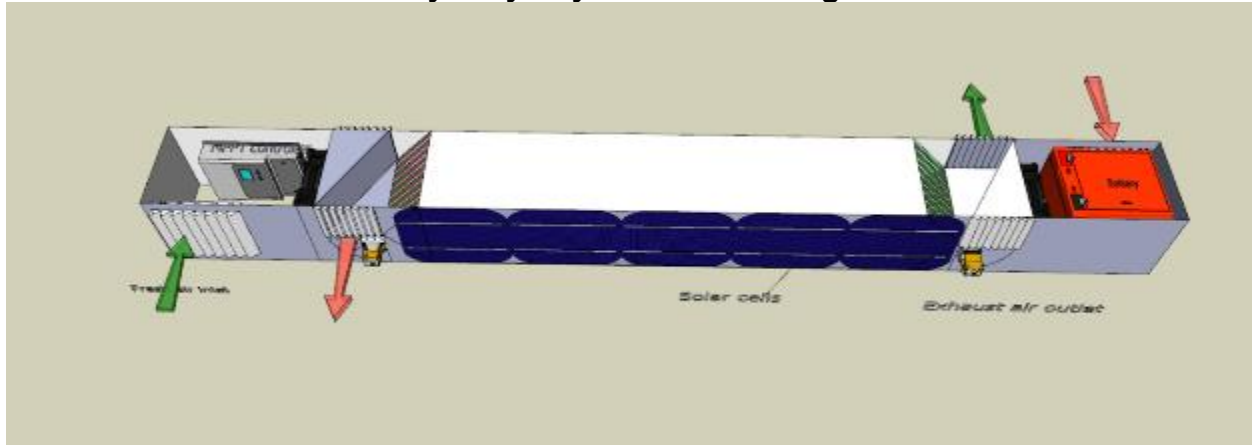
Source: LBNL

Figure 3.10 shows the schematic diagram of the bypass mode of the LVER unit The dampers of the bypass ducts are open in bypass mode, so the outdoor fresh air is supplied directly from the outdoor environment to the indoor room space while the exhaust air is directly discharged from the indoor room space to the outdoor environment. No heat or moisture transfer occurs in the heat and moisture exchanger.

Figure 3.10: Schematic Diagram of the Heat Recovery Mode of the LVER Unit Using a Layer-by-Layer Heat Exchanger
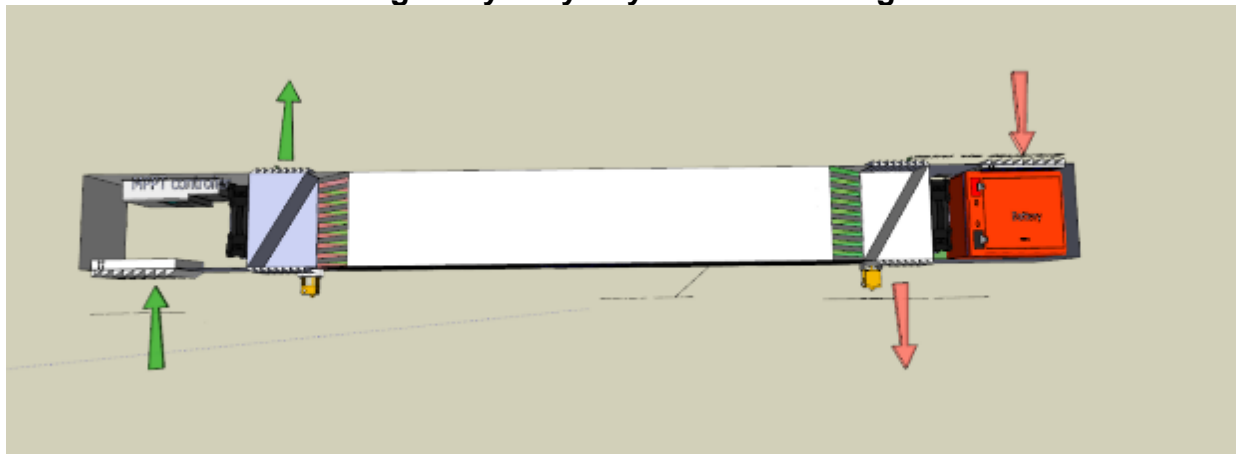
Source: LBNL

3.3.2.2. Zone Ventilation Requirements

The zone ventilation requirement for the preliminary design was derived by modeling a small office prototype building for the ASHRAE 90.1-2010 code package (ASHRAE 2010a) in EnergyPlus. The provided minimum outdoor airflow rate has been checked against the requirement of ASHRAE 62.1 (ASHRAE 2010b). The prototype office building is shown in Figure 3.11. The building is composed of a single-floor conditioned space and an unconditioned attic. The total conditioned floor area is 511.16 square meters

(m^2), which is subdivided to one central core zone and four perimeter zones. Basic zone conditions are summarized in Table 3.1. A total of 20 windows are installed on the four perimeter zones, leading to a total installation capacity of 20 LVER units.

Figure 3.11 3D Model of the Small Office Prototype Building
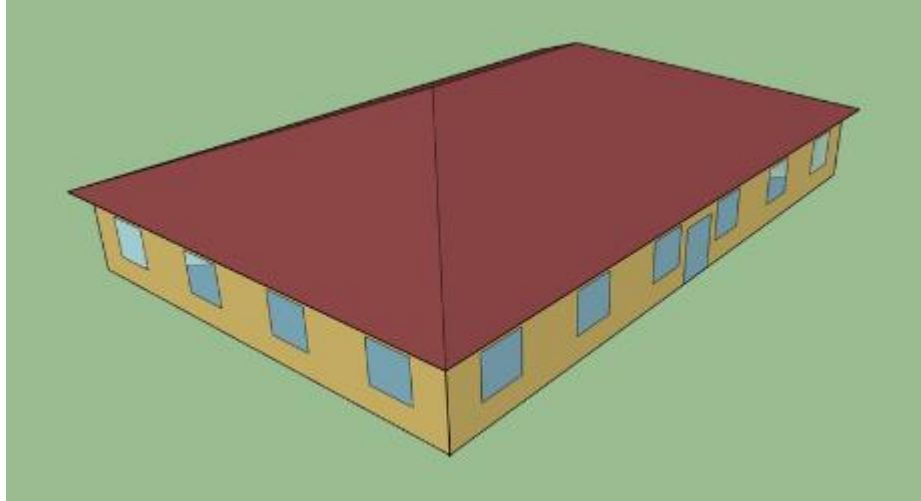
Source: LBNL

Table 3.1: Summary of Building Geometry

	Area (m^2)	Volume (m^3)	Gross Wall Area (m^2)	Window Glass Area (m^2)
CORE_ZN	149.66	456.46	0	0
PERIMETER_ZN_1	113.45	346.02	84.45	20.64
PERIMETER_ZN_2	67.3	205.26	56.3	11.16
PERIMETER_ZN_3	113.45	346.02	84.45	16.73
PERIMETER_ZN_4	67.3	205.26	56.3	11.16
Total	511.16	1559.02	281.50	59.69

Source: LBNL

Based on the air flow/floor area method in ASHRAE 62.1 chosen for the outdoor air module in EnergyPlus, the minimum outdoor airflow rate is calculated per zone, as shown Table 3.2. These results are further compared with the mandatory minimum ventilation rates in breathing zones, which is a superposition of the people outdoor air rate (i.e., 0.0025 square meters per second per person [m^{2}s·person]) and the area outdoor rate (i.e., 0.0003 m^3/s·m^2) as specified by ASHRAE 62.1. Combing the total outdoor airflow rate of 0.221 m^3/s and total LVER units of 20, the fresh airflow rate per each unit was calculated to be 0.011 m^3/s.

Table 3.2: Validation of Minimum Outdoor Airflow Rate

	Outdoor Air Flow per Zone Floor Area (m³/s-m²)	Minimum Outdoor Air Flow Rate (m³/s)	Minimum Outdoor Air per ASHRAE 62.1 (m³/s)
CORE_ZN	0.00043	0.065	0.058
PERIMETER_ZN_1	0.00043	0.049	0.044
PERIMETER_ZN_2	0.00043	0.029	0.026
PERIMETER_ZN_3	0.00043	0.049	0.044
PERIMETER_ZN_4	0.00043	0.029	0.026
Total		0.221	0.197

Source: LBNL

3.3.2.3. Fan Selection

This section presents theoretical calculations for a generalized heat exchanger. Final performance criteria were obtained by the measurements on the actual energy recovery core later on.

The fan was selected based on airflow requirements and pressure drop. Considering that pressure drop is a function of hydraulic diameter, the project team made the selection by considering the hydraulic diameter that would allow the fan to fit into the proposed housing. The team estimated the pressure drop of each LVER unit using the membrane and moist air properties shown in Table 3.3: Summary of Properties of Moist Air and Membraneand Equations 3-1 to 3-3. According to the preliminary design of the LVER unit, the heat exchanger channels can be approximated by a double-pipe heat exchanger, as shown Figure 3.12. In the double-pipe heat exchanger, the outer and inner diameters (d_i and d_o) of the inside pipe, as well as those (D_o and D_i) of the outside pipe, were considered equal, given the thickness of membrane.

Table 3.3: Summary of Properties of Moist Air and Membrane

Membrane Properties	Symbol	Units	Value
Thickness of the membrane	δ	m	1.00E-04
Thermal conductivity of the membrane	λ_m	W/m·K	2.00E-01
Air temperature in the membrane	T	K	293
Water vapor permeability in the membrane	P/l	gpu	6000
Water vapor permeability in the membrane		$cm^3(STP)/cm^2scmHg$	0.006
Water vapor permeability in the membrane		m/s	0.0048941
Thermal properties of air			
Air density	ρ	kg/m^3	1.205
Dynamic viscosity	μ	kg/m·s	1.82E-05
Thermal conductivity	λ_a	W/m·K	0.0257
Mass diffusivity (water vapor)	D_v	m^2/s	0.000024
Specific heat capacity (air)	C_p	J/kg·K	1005
Specific heat capacity (water vapor)	C_v	J/kg·K	1840

Source: LBNL

$$Re = \frac{u\rho d_h}{\mu} \qquad (3\text{-}1)$$

$$f = \frac{64}{Re} \qquad (3\text{-}2)$$

$$\Delta P = f\frac{L}{D_e}\frac{\rho}{2}u^2 \qquad (3\text{-}3)$$

Where d_h is the hydraulic diameter (equal to d_i); Re is the Reynolds number; D_e is equivalent diameter; f is the friction factor in laminar flow (i.e., Re < 2300); ΔP is the friction head loss along the pipe; L is the length of the pipe; and u is the airflow velocity.

Figure 3.12: Approximation of the Designed Exchanger with the Double-Pipe Heat Exchanger

a. Transform of the designed heat exchanger (D = 2d = 20 mm)

Counterflow

b. Axial view of the double-pipe heat exchanger
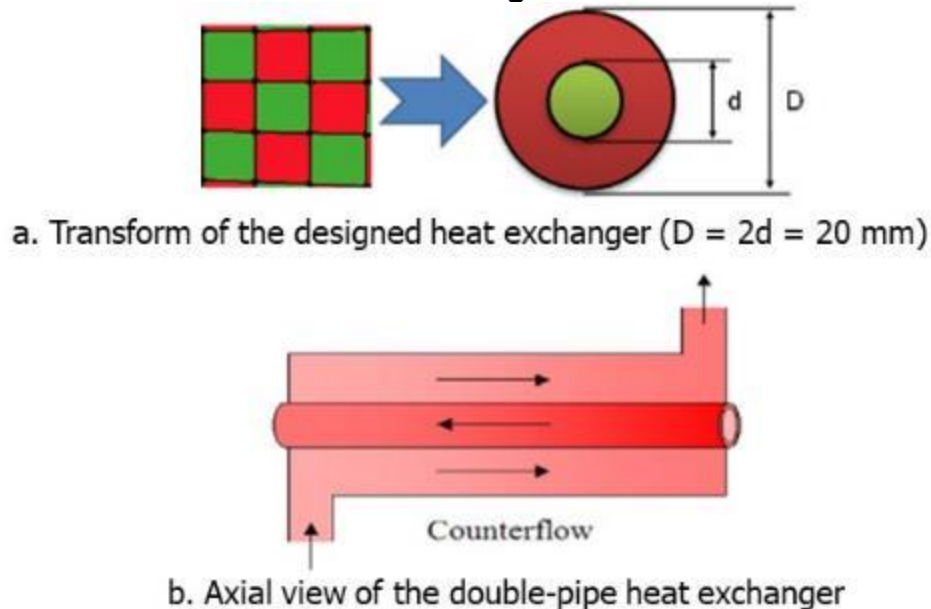
Source: LBNL

For the 10 mm hydraulic diameter, determined after several iterations of required airflow, the pressure drop through the heat exchanger was calculated to be 7.97 Pascal's (Pa, a unit measure of pressure). The project team estimated the pressure loss of the air filter with reference to the efficiency requirement in ASHRAE 52.2 (ASHRAE 2014) and experimental data in existing literatures (Zaatari, Novoselac, and Siegel 2014). Because filters with minimum efficiency reporting value (MERV; i.e., values between 1-16, where higher values are more effective at trapping airborne particles) 8 are suitable for application in commercial buildings, the filter loss for a typical MERV 8 filter, such as those in the 3M Filtrete 600 Series of products, is no more than 17.42 Pa when the surface airflow speed is lower than 1.25 meters per second (m/s). Assuming an inlet grid dimension of 0.12 m x 0.12 m, the fresh air speed on the filter surface is 0.76 m/s, so the induced pressure drop should be lower than 17.42 Pa. Therefore, the pressure drop through the heat exchanger and filter adds up to 25.39 Pa. Considering the extra pressure drop in headers and other fittings, the value above was multiplied by a safety factor of 20 percent, so the final total head loss was preliminarily estimated as 30.47 Pa. A CF Series – CF112 compact axial fan from Fantech Pty Ltd., which was selected because it can fit into the compact LVER design, can be then selected to provide airflow for the LVER unit. The dimension of the selected fan is illustrated in Figure 3.13. The rated input fan power is determined to be 4 W according to the technical data of the product catalogue shown in Table 3.4. The fan performance curve between the pressure drop and flow rate is shown in Figure 3.14. If the hydraulic diameter is reduced to 5 mm, the pressure drop of the heat exchanger increases to 31.90 Pa. Given the same assumption of air filters and miscellaneous losses, the total

pressure loss of the unit was estimated to be 59.18, where the previously selected fan is no longer suitable. The newly selected fan exceeds the designed housing dimension, and the details are presented in Table 3.5, Figure 3.15, and Figure 3.16.

Figure 3.13: Dimension and 3D View of the CF112
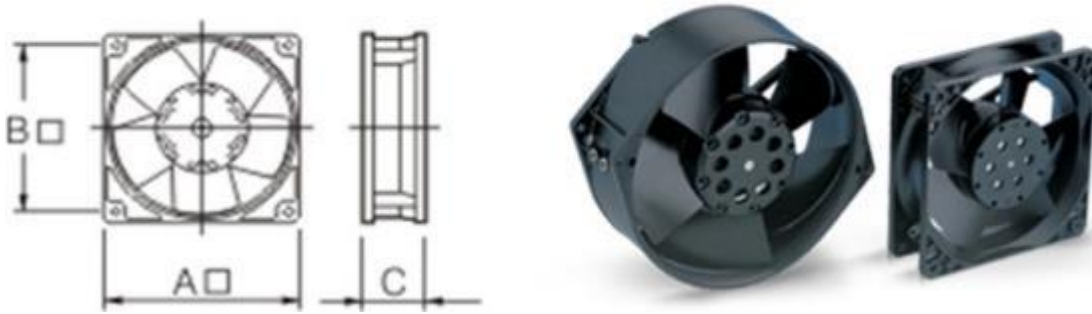
(A = 119 mm, B = 105 mm, C = 38 mm)

Source: LBNL

Table 3.4: Technical Data of CF112

Speed (rps)	Avg. dBA @ 3 m	kWatts (Input)	Amps	Max.°C	Approx. Weight (kg)
55	36	0.004	0.04	72	0.55

Source: LBNL

Figure 3.14: Performance Curve of CF112 (Red Line)

Source: LBNL

43
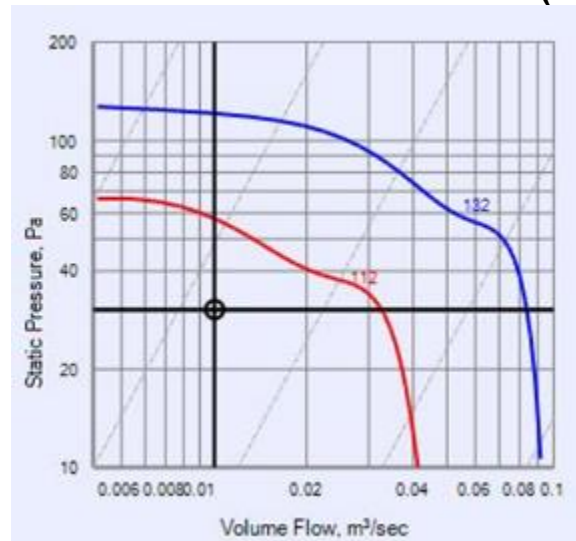
Table 3.5: Technical Data of HCM-225N

Speed (rps)	Avg. dBA @ 3 m	kWatts (Input)	Amps	Max.°C	Approx. Weight (kg)
28	40	0.04	0.3	40	2

Source: LBNL

Figure 3.15: Dimension and 3D View of HCM-225N
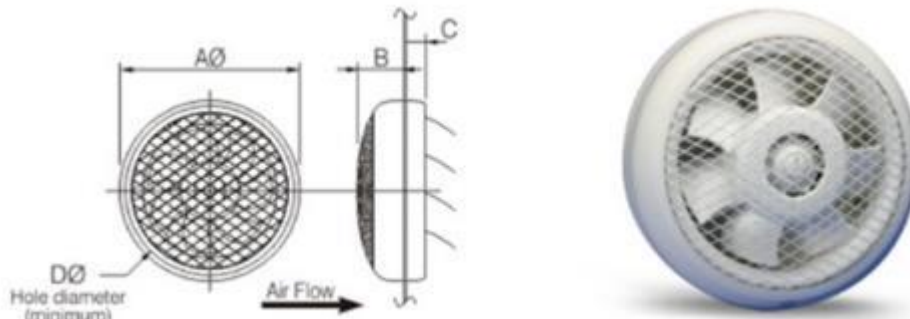
(A = 298 mm, B = 90 mm, C = 35 mm, and D = 262 mm)

Source: LBNL

Figure 3.16: Performance Curve of HCM-225N (Red Line)
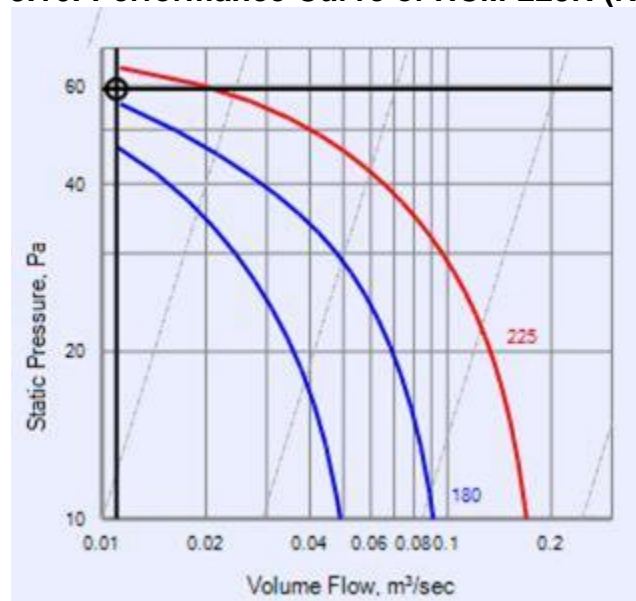
Source: LBNL

3.3.2.4. Effectiveness of the Heat Exchanger

The sensible effectiveness of a heat exchanger (ε) is defined by the number of transfer units (NTU) in the counterflow condition per Equations 3-4 and 3-5, when the heat capacity of hot fluid and cold fluid is considered equal in this case and C_{min} is the product of the specific heat and air mass flow rate.

$$\varepsilon = \frac{NTU}{1+NTU}$$

(3-4)

$$NTU = \frac{UA}{C_{\min}}$$

(3-5)

The overall heat transfer coefficient (U), convective heat transfer coefficient (h), Nusselt number (NU), and the Prandtl number (PR) are defined by Equations 3-6 to 3-9. Equation 8 is an imperial formula to caculate the Nusselt number in laminar flow, where $(\mu/\mu_w)^{0.14}$ is a correction factor of the dynamic airflow viscosity (Zhang and Jiang 1999).

$$U = \frac{1}{\dfrac{1}{h_i}\dfrac{d_o}{d_i} + \dfrac{d_o}{2\lambda_m}\ln\dfrac{d_o}{d_i} + \dfrac{1}{h_0}}$$

(3-6)

$$h = \frac{Nu\,\lambda_m}{d_h}$$

(3-7)

$$Nu = 3.658 + \frac{0.085\left(\mathrm{Re}\,\mathrm{Pr}\left(d_h/L\right)\right)}{1+0.047\left(\mathrm{Re}\,\mathrm{Pr}\left(d_h/L\right)\right)^{0.67}}\left(\frac{\mu}{\mu_w}\right)^{0.14}$$

(3-8)

$$\mathrm{Pr} = \frac{C_p\mu}{\lambda_m}$$

(3-9)

The latent heat transfer effectiveness in a mass transfer process can be compared to the sensible heat transfer effectiveness in a heat transfer process. Therefore, the Sherwood number (Sh) is considered equal to Nu, as defined by Equation 3-10. The letter k is the convective mass transfer coefficient. The overall mass transfer coefficient, K, is then defined by Equation 3-11, where P is the water permeability through the membrane.

$$Nu = Sh = \frac{kd_h}{D_V}$$

(3-10)

$$K = \frac{1}{\frac{1}{k_o} + \frac{1}{P} + \frac{1}{k_i}}$$

(3-11)

The sensible and latent heat transfer effectiveness in the counter flow condition is then summarized in Table 3.6, where the hydraulic diameter is decreased from 10 mm (current design) to 2 mm. It is clear that the effectiveness of the heat exchanger can be improved with smaller diameters. However, the pipe pressure loss is greatly increased with the decreasing exchanger dimensions, leading to a requirement of larger ventilation fans, which would exceed the external housing of the current LVER unit.

Table 3.6: Heat Exchanger Effectiveness and Pressure Loss in Different Pipe Dimensions

Scenarios	Hydraulic Diameter (m)	Pressure Drop (Pa)	Sensible Heat Transfer Effectiveness (%)	Latent Heat Transfer Effectiveness (%)
1	0.010	7.97	51.26	37.15
2	0.005	31.90	79.31	60.54
3	0.002	199.37	95.81	82.86

Source: LBNL

3.3.3. Fabrication and Functional Testing

Figure 3.17 shows the schematic design of the LVER unit. The project team made design modifications to produce a prototype with as many off-the-shelf components as possible. Total length of the unit was limited to 35.75″ so it would fit into the test chamber. The depth of the unit was chosen to correspond to the prototype High-R window, which was 5″.

Figure 3.17: Schematic Layout of the LEVR Design
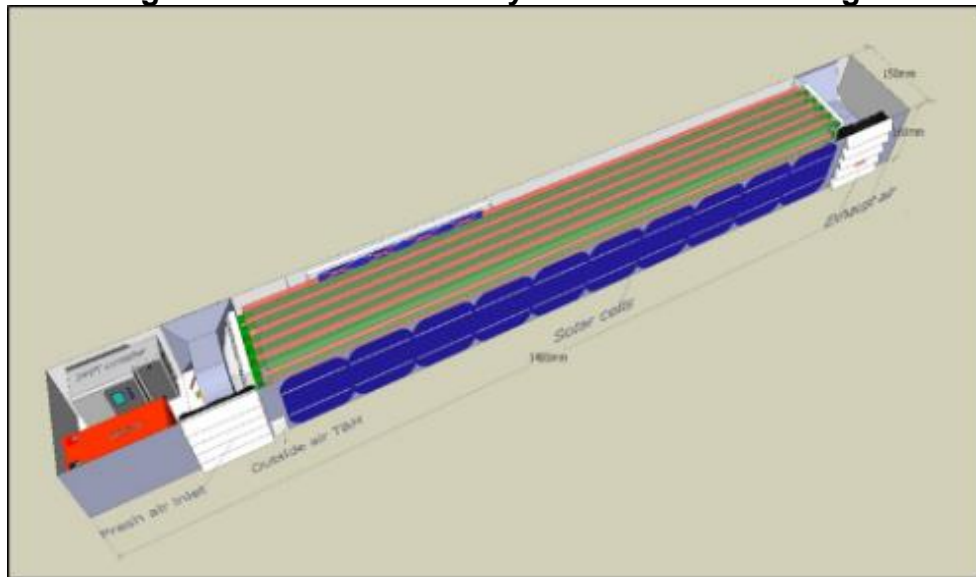
Source: LBNL

A set of smaller fans than those initially intended were used because of limited space in the prototype. Figure 3.18 shows these fans and associated configuration. The fan sets are mounted to use the available volume efficiently and operate at low power. As built, the airflow through the energy recovery core was measured to be 0.00283 m/s (6 cubic feet per minute [cfm]) by timing the fill of a plastic bag with a known volume. The design could have accommodated a fan capable of up to 0.015 m/s (30 cfm) with some modifications.

Figure 3.18: As-Built Fan and Bypass Louver Assembly
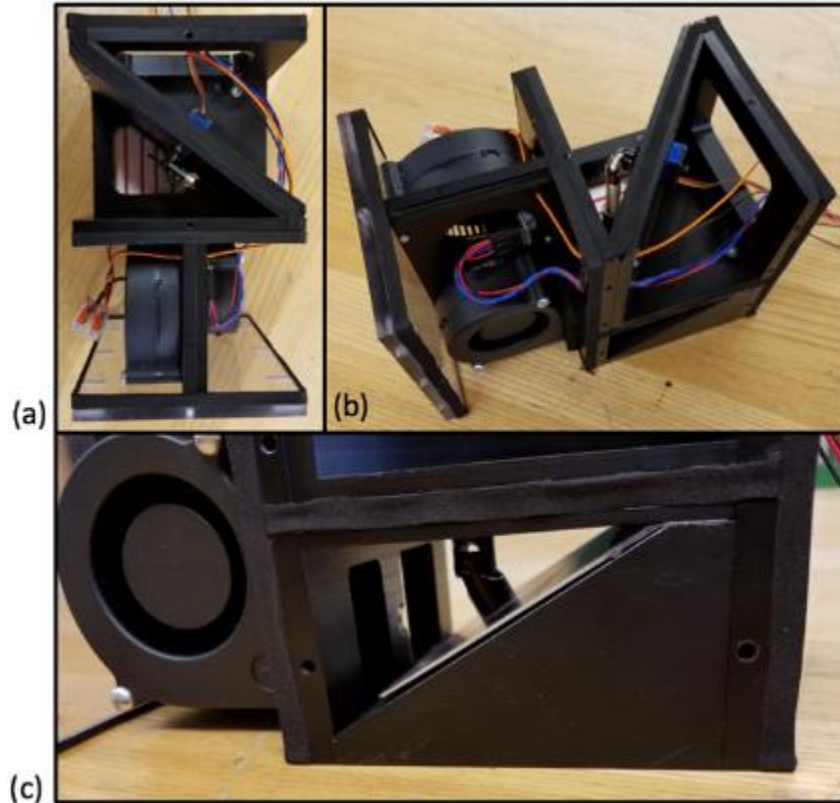
(a) Top View Showing Dual-Fan Configuration; (B) Side View Showing the Hole Through Which Air Flows When in Energy Recovery Mode; (c) View of the Lower Chamber with the Louver in Bypass Position. The two small holes on the left are inlets from the fans.

Source: LBNL

The energy core bypass louvers are operated by a rod connected to a servo motor mounted in the air stream. This linkage is shown in Figure 3.18 and Figure 3.19. Position (a) shows the louver in the energy recovery position, (b) shows the louver in the bypass position, and (c) shows the fan and louver assemblies mounted in the housing with control system and wiring, but without the energy recovery core.

Figure 3.19: As-Built Fan and Bypass Louver Assembly
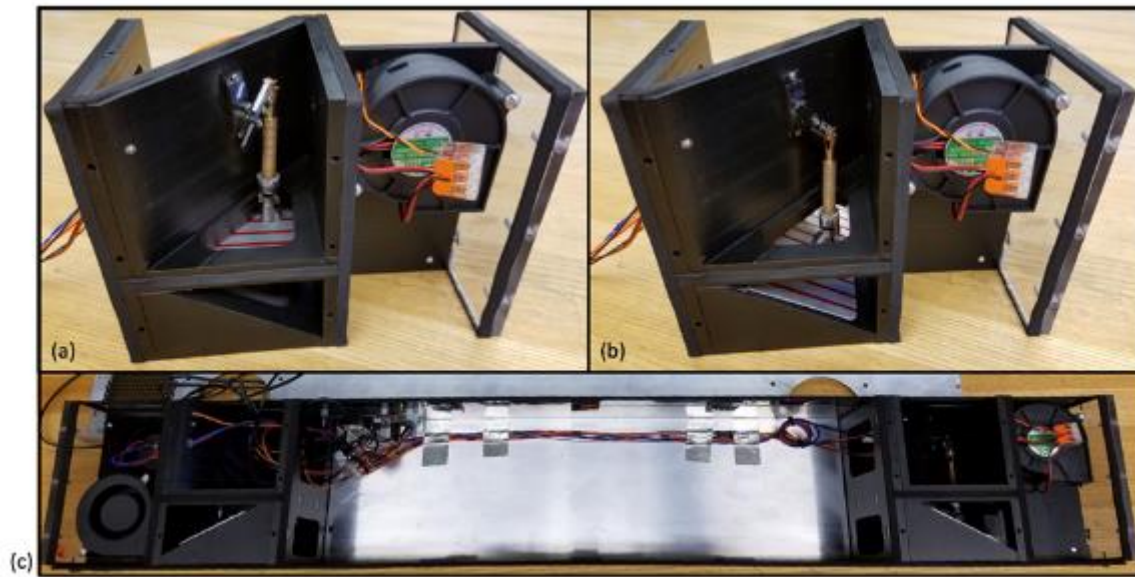
(a) Side view showing closed louver (Energy Recovery Mode); (b) Side view showing open louver (Bypass Mode); and (c) Louver assemblies mounted in the housing with Control System and wiring.

Source: LBNL

The prototype energy recovery core was hand-built by the team's partner organization, Architectural Applications, to fit within the prototype dimensional restrictions. The unit was air sealed with gaskets at all joints to prevent unwanted bypass. The effectiveness of the energy recovery core was measured at the manufacturer's facility. The measured effectiveness of the core at the test conditions was:

$\varepsilon_{sensible} = 0.76$

$\varepsilon_{latent} = 0.57$

Figure 3.17 shows the energy core, as installed into the housing. The fully assembled LVER and corner section of the highly insulating window are shown in Figure 3.18 and Figure 3.19.

Figure 3.20: Assembled LVER Unit
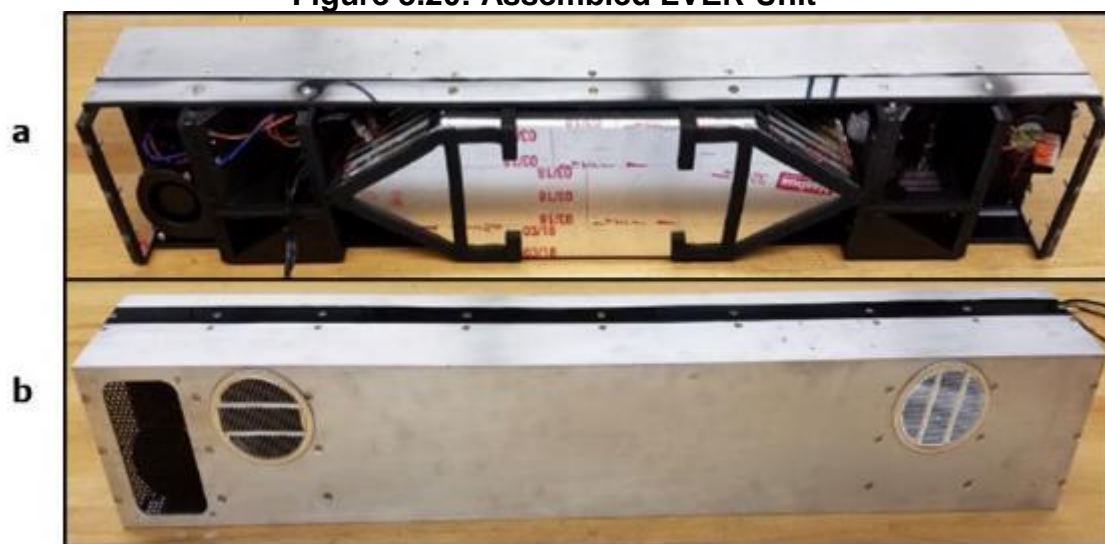
a) Fan and Bypass Louvers Surround the Energy Recovery Core; (b) Fully Assembled Units Showing Air Intake on Far Left, and Round Outlets. The unit is thermally broken with a 1-inch-wide polymer strip.

Source: LBNL

Figure 3.21: LVER Prototype

Source: LBNL

Figure 3.22: LVER Prototype, Along With a Section of the Hi-R Window
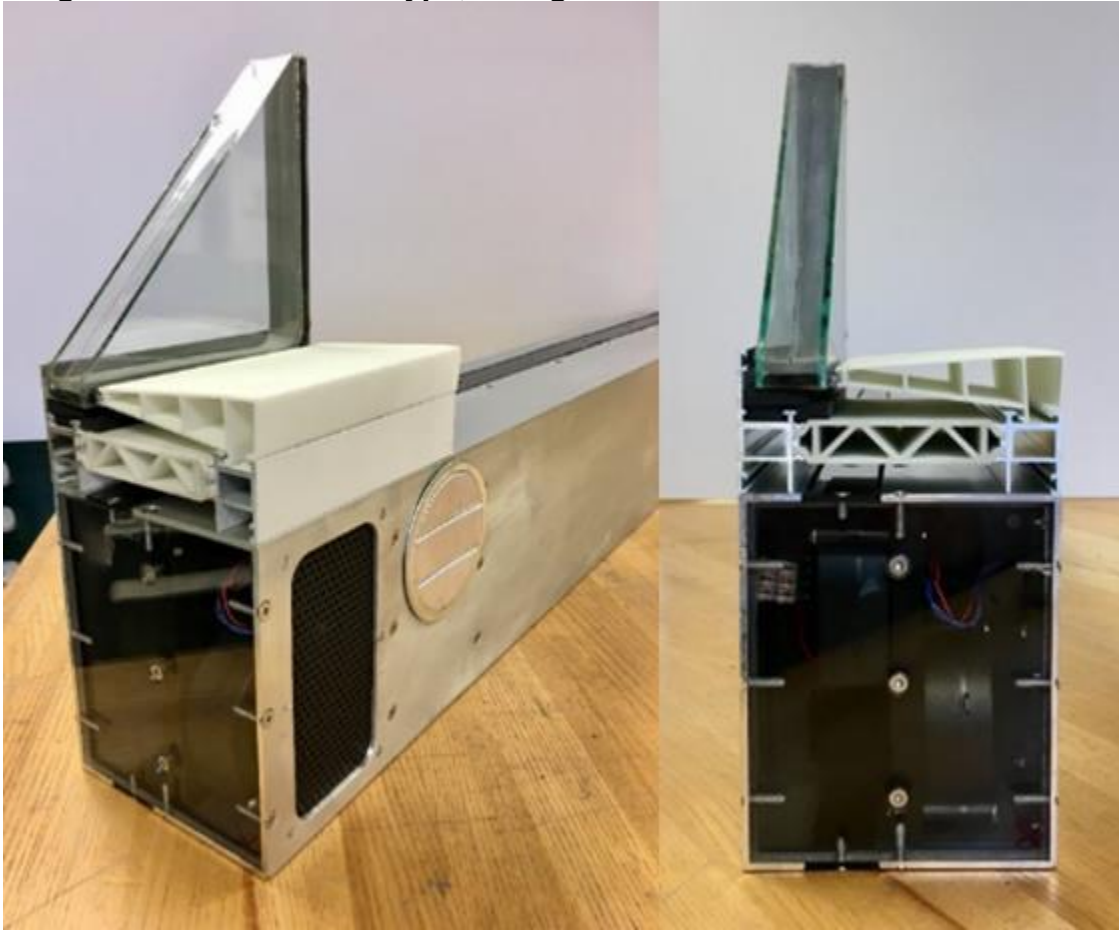
Source: LBNL

A list of significant components purchased for the prototype construction is in Table 3.7. The project team selected the components to be of minimal size and power use to allow the use of solar cells on the exterior of the housing.

Table 3.7: Bill of Materials for Off-the-Shelf Parts Used in Design

Qty	Part Number	Manufacturer	Description
4	AV-F7530MB	MB Ambeyond	75-mm x 30-mm centrifugal blower fan 12 VDC ~2 W
2	MG92B	Tower Pro	servo motor
1	LoPy4	Pycom	Control microprocessor
2	SHT31-D	Adafruit	Temp/RH sensor (I2C interface)
1	TB6612	Adafruit	Motor driver board (for fans)
2	2122K107	McMaster Carr	MERV 7 inlet air filter
36	Maxeon	Sun Power	1/6-cut high-efficiency (21%) solar cell (future implementation)
1		Architectural Applications	Custom energy recovery core
1	88875K396	McMaster Carr	1/8" wall 6" square extrusion cut into 2 halves for a 6" tall and 5" deep unit with thermal break

Source: LBNL

3.3.4. Performance Testing

Testing of the LVER prototype in the LBNL IR thermography lab environmental chamber (LBNL 1998) allowed controlled temperature conditions (and scheduled temperature changes) on the interior and exterior sides of the device. The project team performed this testing to confirm product performance. The remainder of this section describes the sample preparation, test protocol, and measurement results.

The team installed the LVER sill assembly in a foam mask wall cut to fit, with taped seams for air tightness. Additional sensors internal to the LVER assembly were added to allow the team to measure the temperature and relative humidity of the input and output sides of the energy recovery core to allow verification of the core exchange efficiency.

3.3.4.1. Test Protocol

A series of controlled states was established on both sides of the specimen (as shown in **Error! Reference source not found.**). The chambers did not have humidity controls, but the humidity could be modified by introducing dry air from a house-compressed air line or running a humidifier in one of the chambers.

Table 3.8: Series of Controlled States (Steps 1-5)

	1. Exterior	1. Interior	2. Exterior	2. Interior	3. Exterior	3. Interior	4. Exterior	4. Interior	5. Exterior	5. Interior	$T_{heating}$	$T_{cooling}$
Test 1	12°C RH low	**22°C** RH low	12°C RH low	**20°C** RH low	12°C RH low	**22°C** RH low					17.5°C	20°C
Test 2	12°C RH **high**	22°C RH low	12°C RH **low**	22°C RH low	12°C RH **high**	22°C RH low	12°C RH **low**	22°C RH low	12°C RH **high**	22°C RH low	17.5°C	20°C
Test 3	22°C RH low	24°C RH low	22°C RH low	20°C RH low	20°C RH low	18°C RH low	20°C RH low	22°C RH low			20°C	22°C

Source: LBNL

3.3.4.2. Test Setup

The first test setup, shown in Figure 3.23, demonstrates cooling bypass operation based on interior temperature criteria. During this portion of the test, the exterior humidity was always below 55 percent, and the exterior temperature was always below the interior temperature. The operation was initial direct vent because the interior temperature was 22°C and could benefit from "free" cooling using exterior air. When the interior temperature fell below 21°C, it switched back to energy recovery mode to prevent it from overcooling the interior space. After rising back above 21°C, it switched back to direct vent mode.

Figure 3.23: Cooling Bypass Operation Based on Interior Temperature Criteria
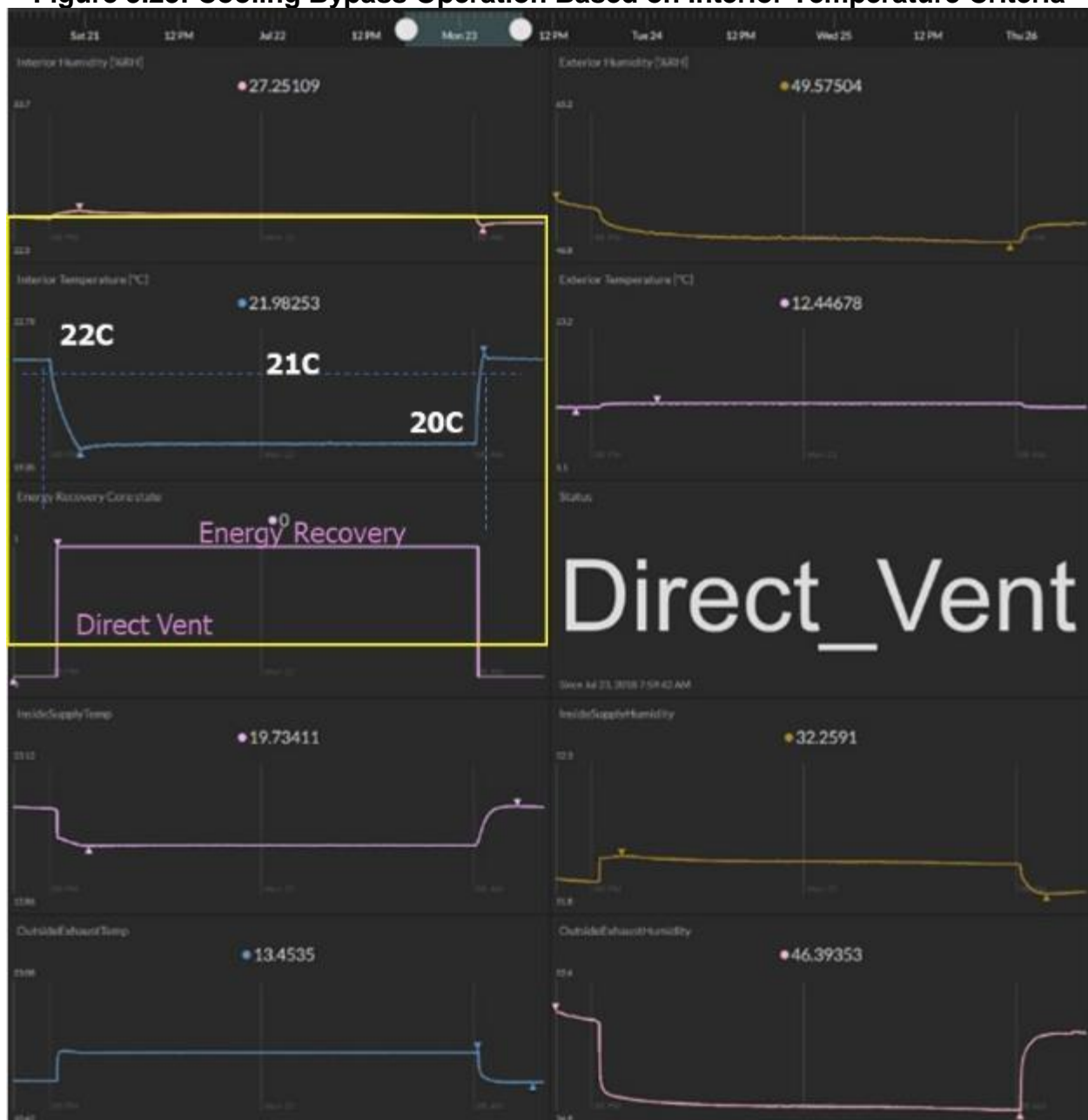
Source: LBNL

The second test setup, shown in Figure 3.24, demonstrates cooling bypass operation based on exterior temperature criteria. During the switching period of this test, the interior temperature was always above 21°C, and the exterior temperature was always cooler than the interior, which favors direct vent operation. However, it initially ran in energy recovery mode because the exterior humidity was above 54 percent (selected to avoid bringing in excess moisture to the room air). It switched to direct vent operation when the exterior humidity fell below 54 percent and then switched back and forth again following the changes in exterior humidity.

Figure 3.24: Cooling Bypass Operation Based on Exterior Temperature Criteria

Source: LBNL

3.3.5. Control Logic

The implemented control strategy started with the assumption that ventilation is needed and runs the fans all the time. (In future implementations, fans could be turned off based on schedule, occupancy, or air quality indicators). Based on temperature and humidity measurements of the room air and outside air, the control unit determines whether the dampers flow directly through the energy recovery core or bypass the core for direct air exchange. Figure 3.25 shows the defined criteria.

The first control sequence tested for whether direct ventilation cooling (economizer) was helpful, and the second tested for whether direct ventilation heating was helpful. The humidity consideration was fairly simple, by setting a maximum relative humidify (RH) threshold for direct venting. Future refinements of the concept may include more sophisticated algorithms using moisture ratios and enthalpy, when testing in real conditions. Two more temperature and humidity sensors could also be added to the output stream (after energy recovery core) to characterize the exchange performance of the core.

Figure 3.25: Control Logic for LVER Operation
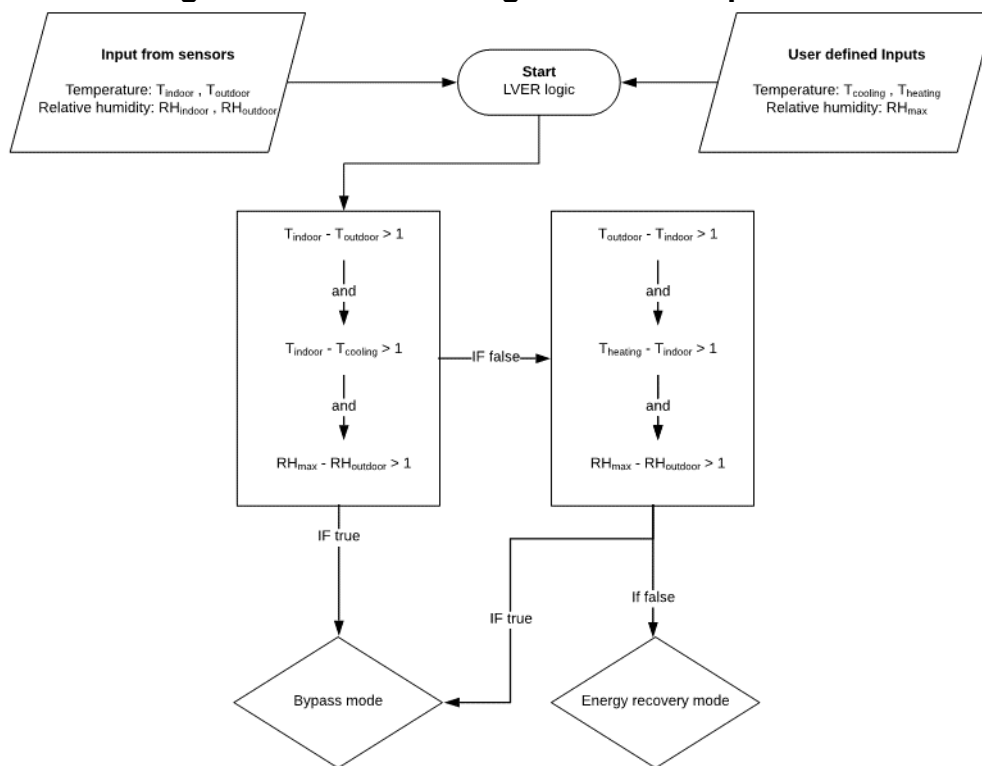
Source: LBNL

3.3.5.1. Test Results

The LVER unit was tested in the LBNL MoWiTT facility to measure the energy required to make up for heating in direct vent and energy recovery modes, when the exterior temperature is colder than the room temperature. The rest of the measurement aperture was filled with 4 inches of foam, so most of the heat load was associated with the fresh air ventilation, as well as some conduction through the LVER unit. The MoWiTT net heat measurement was compared to a heat calculation based on airflow and temperature difference of the supply air stream to the room. An earlier experiment estimated the airflow rate at 6 cfm, but this was likely not highly accurate. The calculated heat associated with 6 cfm did not match the MoWiTT results, but it agrees quite well when scaled to 14 cfm. Even though the absolute value did not match (likely because of inaccuracies in measuring the flow rate), the ratio of energy recovery and direct vent cases shows close agreement. A time series of MoWiTT measurements and the resulting energy flow in LVER is shown in Figure 3.26. Table 3.9 shows energy recovery results.

Figure 3.26: Time Series of Measurements in MoWiTT
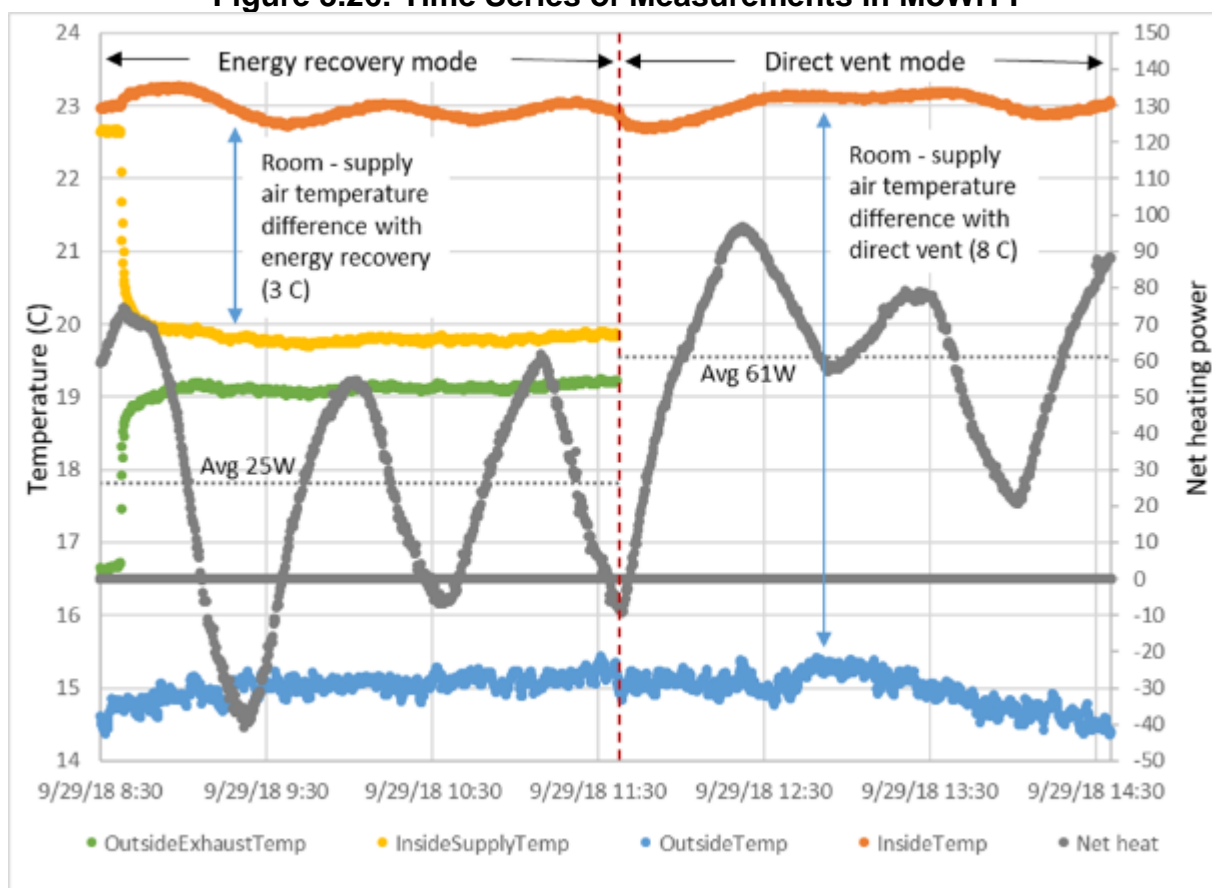
Source: LBNL

Table 3.9: Energy Recovery Results

Mode	Outside Temp, °C	Inside Temp, °C	Outside Exhaust Temp, °C	Inside Supply Temp, °C	Net Heat, W	Net Heat Based on 14 cfm, W
Energy Recovery	15.02	22.97	19.01	19.94	24.92	24.00
Direct Vent	14.97	23.00			61.03	62.60

Source: LBNL

3.3.5.2. IR Thermography Results

All IR thermography images were taken from the warm side (22°C–24°C), with the cold side at 10°C. Three characteristic states were considered:

1. For the baseline image, shown in Figure 3.27, ports were sealed with tape (no airflow). Thermally broken structural elements (plastic intermediate between the two aluminum skins) provided good thermal performance and uniform warm surface temperatures. Seventeen watts per square meter (W/m^2) was measured by a heat flux sensor between the center location markers.

2. For the heat recovery mode, shown in Figure 3.28, cold air entering the core at right was not sufficiently insulated from the interior skin, so it showed colder-than-expected temperatures. This situation can be improved by including insulation in that area. Air warmed by the core heat exchange enters the room through the circular vent on the left (warmer than the right-side temperatures and much warmer than the direct vent bypass case below). The heat flux sensor measured 32 W/m^2.

3. For the heat exchange core bypass case (direct vent), shown in Figure 3.29, the project team raised the warm-side environment to 24°C to engage direct vent bypass. Much colder air enters the room through the right circular vent. Thirty-eight W/m^2 was measured by a heat flux sensor.

Figure 3.27: Static Baseline
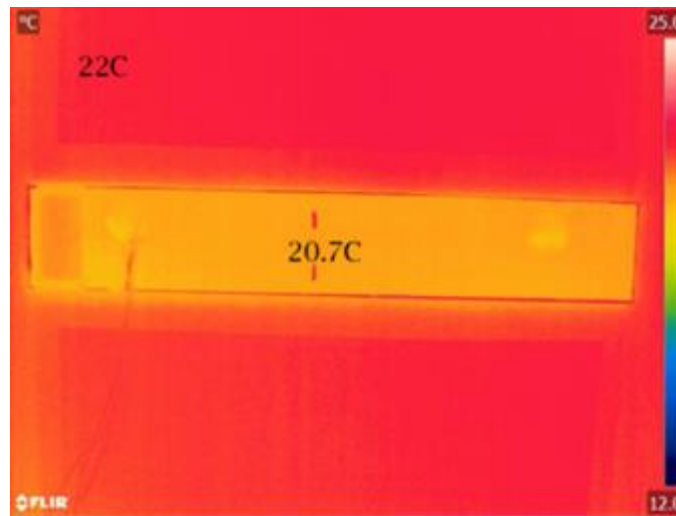
Source: LBNL

Figure 3.28: Core Heat Recovery Mode
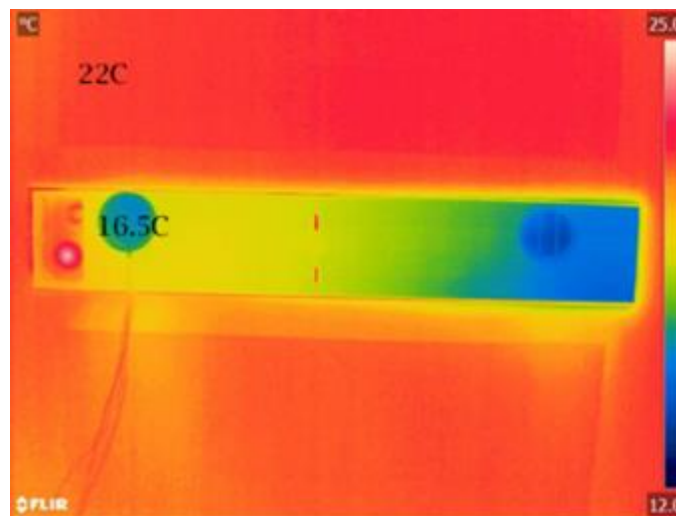
Source: LBNL

Figure 3.29: Core Heat Recovery Mode
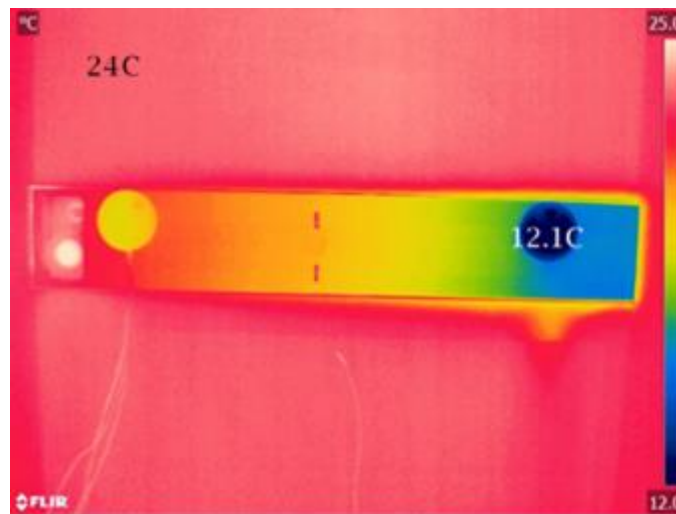
Source: LBNL

3.3.6. Simulation Results

3.3.6.1. Simulation of PV Production

This project used PVWatts, a Web-based PV production calculator, to simulate solar production (NREL 2018). The PV production was calculated for several cities and California and elsewhere, showing the average watt-hours per day of solar production for a 15 W solar panel powering the LVER unit (based on the number of cells that were able to be installed on the prototype). South, west, east, and north orientations are presented for the best and worst summer and winter months, assuming a vertical façade. The LVER prototype consumes between 8 and 12 W of electrical power, primarily for fans. The microprocessor control measured less than 1 watt. Because the fans do not have to run for ventilation at all times, the needed energy per day may vary between 10 watt-hours (Wh) for 1 hour of ventilation to 240 Wh for 24-hour continuous ventilation. Only the north-facing orientation in the winter was limited to a single hour of ventilation operation per day under these assumptions. In most cases there was sufficient power to run the ventilation 2–5 hours per day. Of course, larger units and larger solar arrays would enable even longer run times.

61

Solar Wh per Day	South	West	East	North
Sacramento Summer	26.8	50.8	51.2	23.8
Sacramento Winter	43.9	17.5	16.3	6.5
Los Angeles Summer	21.7	51.3	44.2	23.5
Los Angeles Winter	56.2	22.4	23.9	8.2
San Francisco Summer	26.5	46.0	45.8	24.7
San Francisco Winter	51.4	18.0	17.7	7.0
Washington, D.C. Summer	25.5	38.9	41.0	22.3
Washington, D.C. Winter	50.8	18.2	17.2	6.8
Miami Summer	17.4	40.5	39.7	22.9
Miami Winter	55.1	25.3	26.2	10.3
Minneapolis Summer	30.1	43.3	43.9	22.9
Minneapolis Winter	50.6	13.5	14.8	5.5

Source: LBNL

3.3.7. Building Energy Use Simulation

To investigate the benefits of this technology, the authors used the EnergyPlus building energy simulation program to simulate a single-zone building model in three climates in California: San Francisco (3C), Los Angeles (3B), and Siskiyou (5B). The authors made the simulation runs for an office building type and two HVAC models: (1) base case: a fan coil unit with a dedicated outdoor system, and (2) LVER case: a fan coil unit plus the LVER, which serves as a zone energy recovery ventilator (ERV), with EMS control logic employed to control the LVER. Table 3.11 shows a summary of the assumptions used in the simulation, and the location of the three cities is listed in Table 3.12. Based on the experimental testing data, the sensible and latent efficiencies of the LVER unit are listed in Table 3.13. The authors also show the hourly temperature profiles for a typical summer day and winter day.

3.3.7.1. Modeling Assumptions

The EnergyPlus model, illustrated in Figure 3.30: EnergyPlus Single Zone Model, is a 400 ft^2 single zone with a slab-on-grade floor and one double low-e (40% WWR) south-facing window. The project team used the schedules, internal loads, wall constructions

per climate, and outdoor air requirements from the DOE EnergyPlus commercial prototypical building models, 90.1-2010 version. The schematic drawing of the LVER is in **Error! Reference source not found.**, **Error! Reference source not found.**, and **Error! Reference source not found.** and include the schematic drawing of the two HVAC models.

The project team considered two cases:

- Case 1: Baseline Case: a fan coil unit with a dedicated outdoor system (DOAS) and no economizer

- Case 2: a fan coil unit plus the LVER, which serves as a zone ERV. EMS control logic was employed to control the LVER.

To model the zone-level LVER, the project team used a special EnergyPlus object—a ZoneHVAC:EnergyRecoveryVentilator. This object consists of a heat exchanger, a supply fan, an exhaust fan, and an ERV controller. The team used EnergyPlus Energy Management to write the energy management system (EMS) code to improve the controller function and provide more cooling or heating, when possible.

Table 3.11: Summary of Simulation Assumptions

Parameters	Assumption
Floor Area	400 ft^2 (20 ft × 20 ft)
Foundation	Slab-on-grade
Insulation	Envelope insulation levels are based on location
Infiltration	0.672 ach
Window	South-facing, double-clear low-e, 40% WWR
Internal Loads: People (㎡/person)	18.58
Internal Loads: Light（W/㎡）	8.83
Internal Loads: Equipment （W/㎡）	8.07
HVAC System: Case1	Base case: fan coil unit with a dedicated outdoor system
HVAC System: Case2	LVER case: a fan coil unit plus the LVER, which serves as a zone ERV
HVAC Efficiency: Ventilation rate (m^3/s/Area)	0.00043
HVAC Efficiency: LVER fan supply air (m^3/sec)	0.016
Thermostat Setting: Cooling	75°F (24℃)
Thermostat Setting: Heating	70°F (21℃)
Locations	San Francisco, Los Angeles, and Siskiyou
Weather Data	All TMY3

Source: LBNL

Table 3.12: Information For Three Selected Cities

City	Climate Zone ID	Climate	Annual Average Temperature (℃)
San Francisco	3C	Warm, marine	13.79
Los Angeles	3B	Warm, dry	16.84
Siskiyou	5B	Cool, dry	11.36

Source: LBNL

Table 3.13: Local Ventilation and Energy Recovery Unit Effectiveness

	Efficiency
Sensible	0.76
Latent	0.57

Source: LBNL

Figure 3.30: EnergyPlus Single Zone Model

Source: LBNL

65
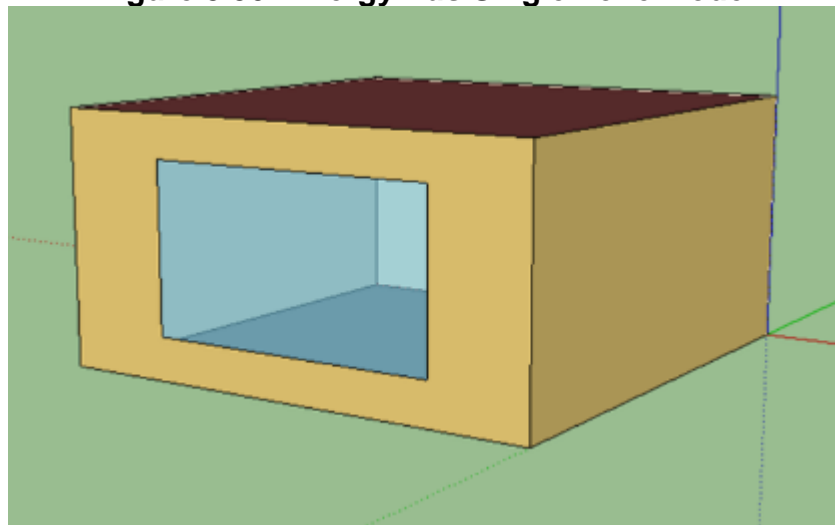
Figure 3.31: Schematic of the LVER Unit
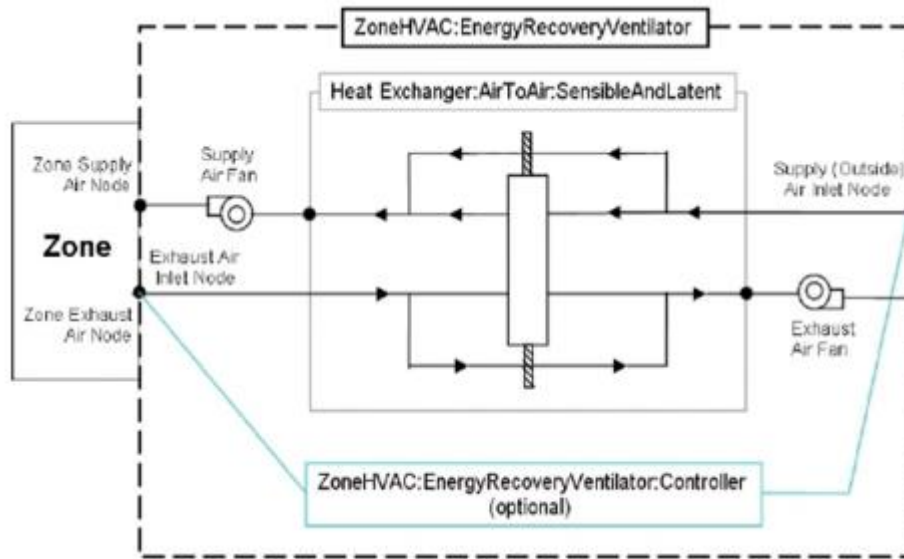
Source: LBNL

Figure 3.32: Schematic Fan Coil Base Case System
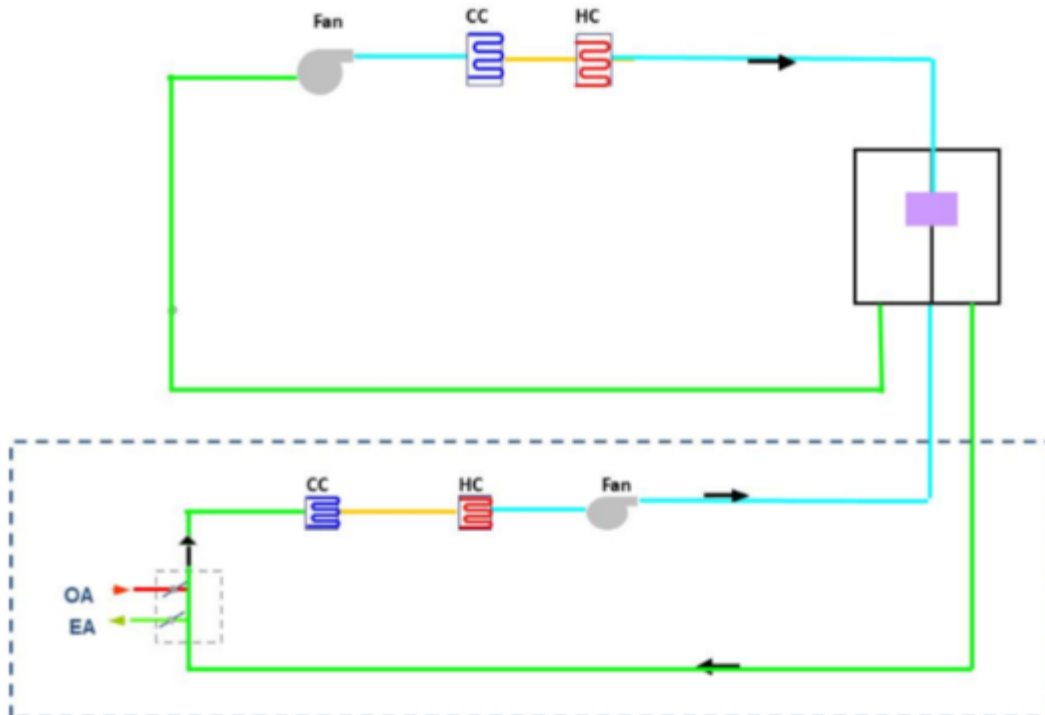
A Fan Coil with Dedicated Outdoor Air System, OA-Outdoor Air, EA-Exhaust Air, CC-Cooling Coil, HC-Heating Coil

Source: LBNL

Figure 3.33: Schematic for Fan Coil System with a Local Ventilation and Energy Recovery Unit I
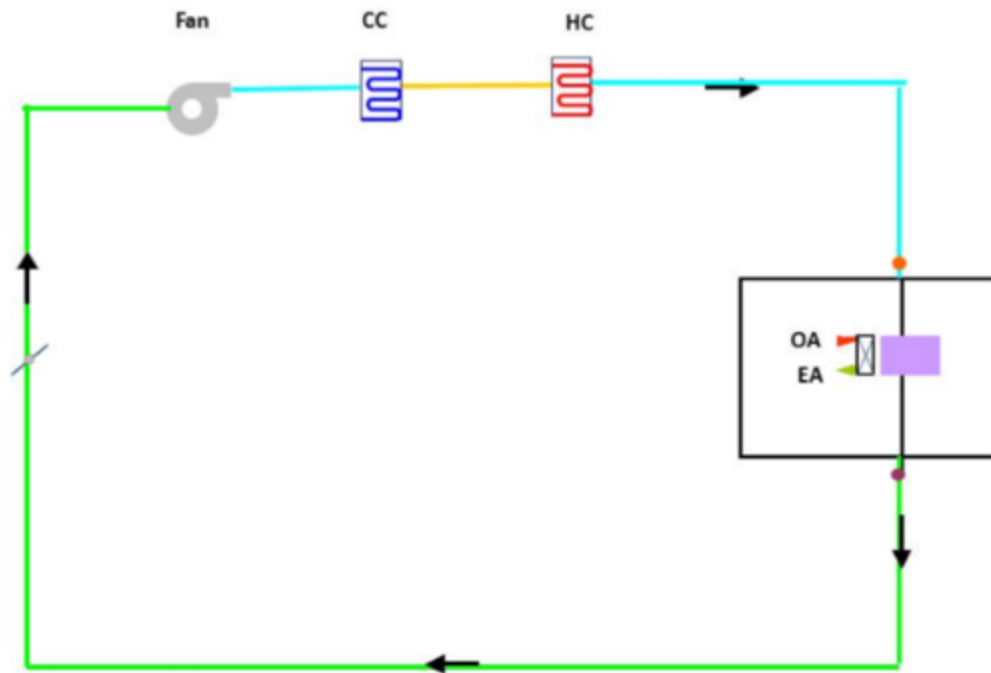
Integrated at Zone Level, OA-Outdoor Air, EA-Exhaust Air, CC-Cooling Coil, HC-Heating Coil

Source: LBNL

3.3.7.2. Results

The project team conducted energy simulation for four locations: two cooling locations (marine and dry hot), one heating location in California, and one comparative location in a U.S. cooling climate (Atlanta). The results are presented in Table 3.14 as a breakdown among heating, cooling, fan energy, and total energy. Table 3.15 shows percentagewise energy savings between the baseline and LVER-equipped building. Overall, the energy simulation showed heating and cooling savings anywhere from 17 to 39 percent.

Table 3.14: Energy Simulation Results (gigajoules)

City	Climate Zone	BAE Heating	BAE Cooling	BAE Fan	BAE Total	BAE+ZoneLERV+EMS Heating	BAE+ZoneLERV+EMS Cooling	BAE+ZoneLERV+EMS Fan	BAE+ZoneLERV+EMS Total
Atlanta	3A (warm, humid)	2.96	7	0.57	10.53	1.83	4.09	0.55	6.47
San Francisco	3C (warm, marine)	11.36	10.54	0.89	22.79	10.54	4.76	0.87	16.17
Los Angeles	3B (warm, dry)	5.79	15.2	0.98	21.97	5.29	7.44	0.96	13.69
Siskiyou	5B (cool, dry)	21.01	10.26	1.19	32.46	18.86	6.99	1.17	27.02

BAE = Baseline Annual Energy)

Source: LBNL

Table 3.15: Energy Savings

City	Climate Zone	Heating (%)	Cooling (%)	Fan (%)	Total (%)
San Francisco	3C (warm, marine)	7	55	2	29
Los Angeles	3B (warm, dry)	7	51	2	38
Siskiyou	5B (cool, dry)	7	32	2	17

Source: LBNL

3.4. Technology/Knowledge Transfer/Market Adoption

A local ventilation energy recovery (LVER) unit is an innovative technology that was developed in this project as a proof of concept, so it is in an early stage of technology market acceptance. To promote the concept, the authors have been working with window manufacturers and energy recovery technology manufacturers. Architectural Applications, a company that develops and markets wall-integrated local ventilation energy recovery units, has been part of the project and has participated in the design and development of the prototype. Arconic, which is the parent company of the largest commercial window and façade manufacturer in the United States, has also been engaged in an observer and advising role.

The authors plan to continue to engage with industry and discuss further commercialization efforts for the technology.

A technical advisory committee was composed of industry, research, media, academia, and the Energy Commission; thus, all important stakeholders were covered.

3.5. Benefits to California

California has variety of climates, from a mild marine/coastal climate to more extreme cooling and heating climates in the interior. Testing and simulation, detailed in this chapter, have shown that the LVER technology studied has significant energy savings potential. Windows that provide local ventilation with energy recovery will help the building industry achieve the challenging California energy performance goals leading to zero-net-energy commercial buildings by 2030 while maintaining the desirable aspects of windows, such as connection with the outdoors with daylighting and views.

One original role for a window was to provide connection to the outdoors (i.e., to avoid a cave like feeling). Ventilation provides a physical manifestation of this connection by providing fresh outdoor air through the façade. The proposed design and prototype embody an autonomous package that requires no wiring or complicated installation. Local dedicated outdoor air systems (DOAS) technologies are the best DOAS implementation because they avoid the large central fans needed to move air through building ducts, expending large amounts of energy in the process. Instead, local DOAS

provide fresh outdoor air where it is needed, replacing large central fans with small and efficient fans the size of a typical computer fan.

Based on the *California Commercial End-Use Survey* (Itron 2006) and the 30 percent heating and cooling energy savings estimates previously shown for California commercial buildings, the yearly energy savings potential of these high-performance windows over current standards could be about 8,000 GWh in electricity and about 200 million Therms of natural gas. These amounts translate to a savings of nearly $1 billion per year in the commercial sector.

CHAPTER 4:
Daylight Redirecting Systems

4.1. Introduction

The objective of this task was to develop cost-effective, versatile, daylight-redirecting systems for new and retrofit commercial building applications in California, with the goal of saving 25–50 percent in annual lighting energy use in a 15- to 40-ft deep perimeter zone. Qualitative objectives included improved daylight quality with no negative effects on visual comfort. Historically, achieving this ideal in practice has proven more elusive than the simplicity of the idea may suggest. Static systems, such as prismatic films (Thanachareonkit et al. 2014; McNeil et al. 2017) or reflective slats (Konis and Lee 2015), can work well at certain times of the day or year, but these solutions generally cannot maintain high performance over the full range of solar conditions. Dynamic systems, such as automated venetian blinds, overcome this issue but have limited light redirection efficiency when simultaneously controlled to avoid glare. The characteristics of a successful light redirection system for this project were therefore defined as follows:

1. Deep room penetration: The system must be able to provide deep sunlight penetration (up to 40 ft.) without glare to the occupants, when installed in the upper clerestory of a vertical façade, above eye level (nominally 7 ft. to ceiling level).

2. Optimal/smart operations: The system is assumed operable and automated such that available incident direct beam radiation is used as much as possible, while glare is minimized under all conditions without the use of secondary indoor shades.

3. Low maintenance: The system should operate within an insulated glazing unit (IGU) with a nominal 20-year life or within a glazing unit with a removable panel.

4. Low-powered: The design must have power requirements that are low enough to be supplied with low-voltage wiring or self-powered using a small, vertically mounted photovoltaic strip mounted on the daylight-redirecting system.

5. Adjustable, commissionable: The device must enable changes to the associated control algorithm after installation to, for example, meet new needs or allow control by a building management system.

An issue limiting light redirection performance and related cost-effectiveness of reflective slat systems is that to prevent the downward transmission of direct sunlight, slats must be closed more than would be ideal for redirecting light to a certain depth within the space. Conversely, if slats are positioned at an angle that provides redirection to the desired depth, at most times some of the incident sunlight will not hit any slat

and will be transmitted straight down through the window, causing glare to the occupants.

In 1977, an idea was proposed by LBNL researchers (Rosenfeld and Selkowitz 1977) that circumvented this problem. By making the spacing between the slats depend on the solar profile angle (Figure 4.1), it could be ensured not only that *all* direct sunlight would be redirected upward, but that it would be redirected to the required depth. This concept can also be implemented by varying the width of the slats while keeping the spacing between the slats constant (Figure 4.2). The two concepts are geometrically equivalent in terms of light redirection toward the ceiling and blocking of sunlight transmitted downward.

Figure 4.1: Variable Slat Spacing Blind Concept – Configuration A*
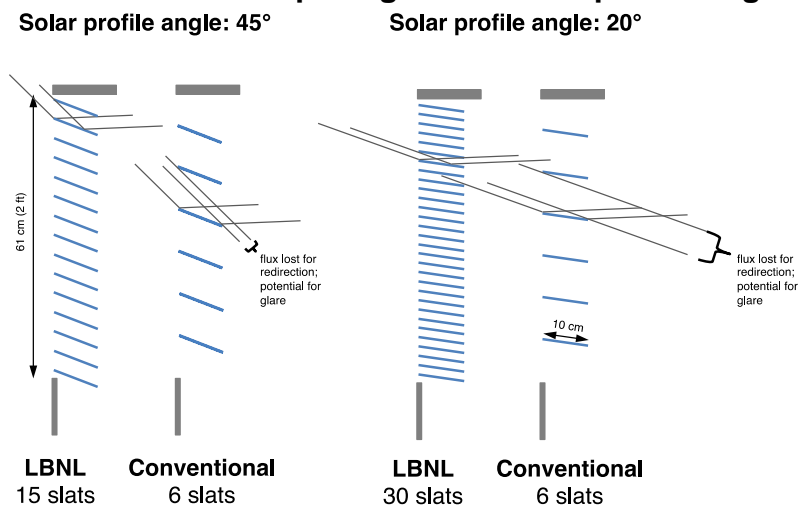
* While equivalent to the variable-width concept shown in Figure 4.2, this concept was not analyzed in this study.

Source: LBNL

Figure 4.2: Variable Slat Width Blind Concept -- Configuration A

Solar profile angle: 45°   Solar profile angle: 20°

61 cm (2 ft)

flux lost for redirection; potential for glare

flux lost for redirection; potential for glare

10 cm

LBNL
30 slats

Conventional
6 slats

LBNL
30 slats

Conventional
6 slats
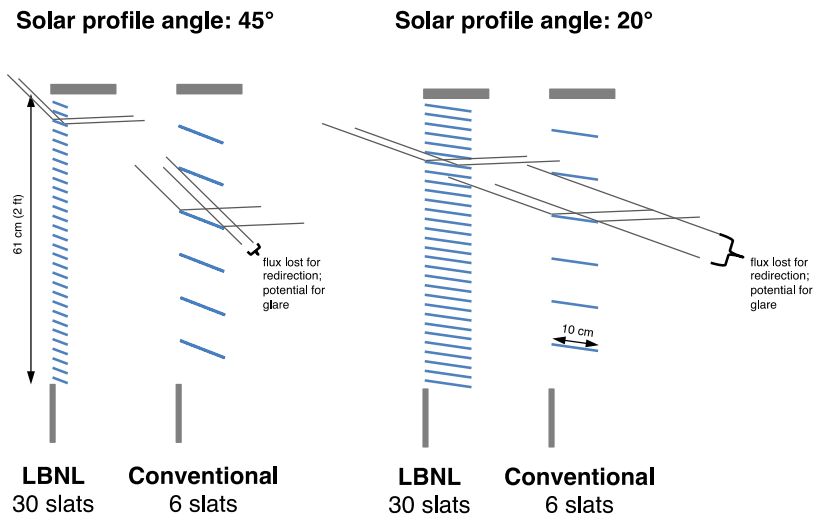
Source: LBNL

In a preliminary analysis, the concept appeared to satisfy the initial design objectives. Not only could the system adjust to a variety of solar conditions (and sky conditions, such as by retracting the blind when the sky is overcast), it could also perform highly efficient light redirection to a specified depth while controlling glare from direct sunlight. The system was based on a proven technology: automated venetian blinds. Recent advances in communications hardware and motors suggested that implementing automation and controls would be feasible at a reasonable cost.

4.2. Project Approach

The performance of this concept was evaluated using Radiance ray-tracing simulations (Ward Larson and Shakespeare 1998) to estimate annual lighting energy savings and cost-effectiveness, as well as discomfort glare. Simulations were performed for every hour of the year for five façade orientations (East, SE, West, SW, South) using climate data for four locations (Bakersfield, Oakland, Sacramento, San Diego), which represented inland and coastal climates in Northern and Southern California. The performance of the proposed concept with automated, flat, mirrored slats and variable-spacing slat configuration (Figure 4.1, Configuration A) was compared to two benchmarks:

1. Automated, flat, mirrored slats with fixed spacing between the slats (similar to a conventional venetian blind) and controlled to block downward transmission of sunlight (Configuration B)

2. A conventional matte white venetian blind operated manually (Configuration C)

As an extension to the simulation study, the project team conducted field tests to check the redirection geometry (i.e., does the proposed system redirect light in the expected manner), evaluate the daylight quality of the proposed light redirection system, and assess comparatively the effects of slat curvature and surface finish on light redirection

73

and glare. These tests were performed periodically over the initial period of prototype development at LBNL's Advanced Windows Testbed (Figure 4.3 and Figure 4.4).

Figure 4.3: Field Test Setup in the Advanced Windows Testbed
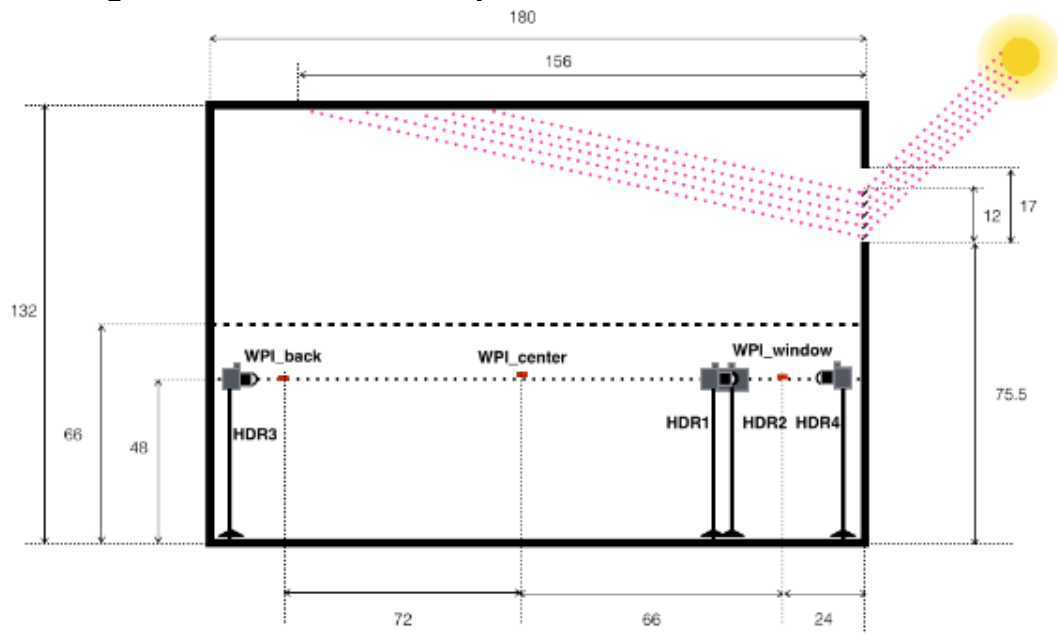
Section view looking east with south-facing window to the right of the image. Dimensions are given in inches. WPI = work plane illuminance; HDR = high dynamic range.

Source: LBNL

Figure 4.4: Setup of Daylight-Redirecting Slats in the Upper Clerestory of the Window
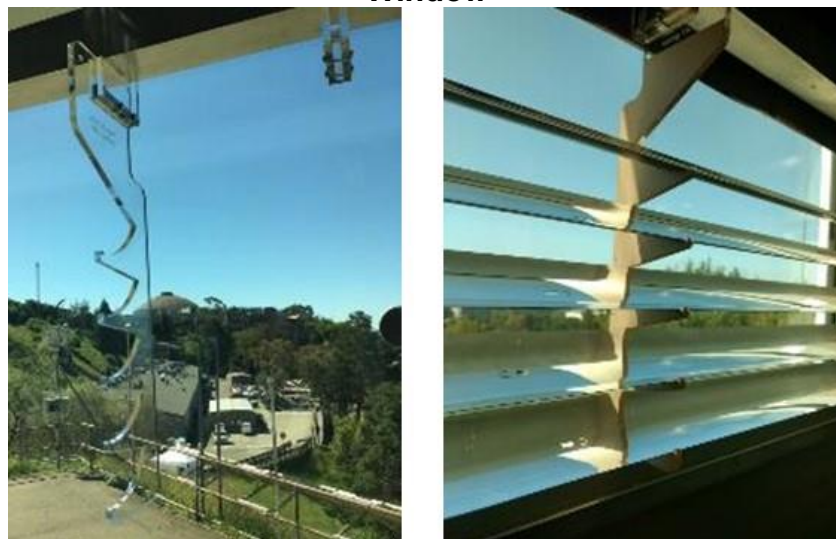
Custom slat holders were devised to hold the slats at the appropriate angle and spacing for a particular date and time of day. Left: Slat holder without slats. Right: Slat holder with slats mounted.

Source: LBNL

To further evaluate the feasibility for commercialization of an operable unit, the project team fabricated a tabletop prototype of the design to explore motorization and automated control of the slats. The prototype went through several design iterations to develop a practical, feasible solution. The prototype was shown to industry stakeholders to obtain feedback on the viability of commercialization.

4.3. Results

4.3.1. Annual Performance

Results from the annual Radiance simulations showed that the proposed concept delivered a significant amount of daylight into zones that were 15–40 ft. away from windows without causing glare to the occupants. The system provided additional savings in the 15 ft. nearest the window, but the project team assumed that the lower view window with shading would provide adequate daylight to this primary zone. Assuming an installed lighting power density (LPD) of 0.75 W/ft^2 and a design work plane illuminance of 300 lux, annual lighting energy use in the secondary 15–40 ft.-deep zone was reduced significantly with the prototype design (with flat, mirrored slats and no lower view window in all cases):

- The savings compared to the same flat, mirrored blind but with conventional slat spacing and automatically controlled to block direct sunlight (Configuration B) were 0.20–0.46 kWh/ft.^{2}, or 14–42 percent, depending on climate and orientation.

- Savings compared to a conventional, manually operated venetian blind (Configuration C) were 0.13–0.73 kWh/ft.^{2}, or 9–54 percent, depending on climate and orientation.

Figure 4.5 shows the results for Oakland. The prototype (Configuration A) also maintained acceptable visual comfort throughout the year.

Figure 4.5: Annual Lighting Energy Consumption in Oakland
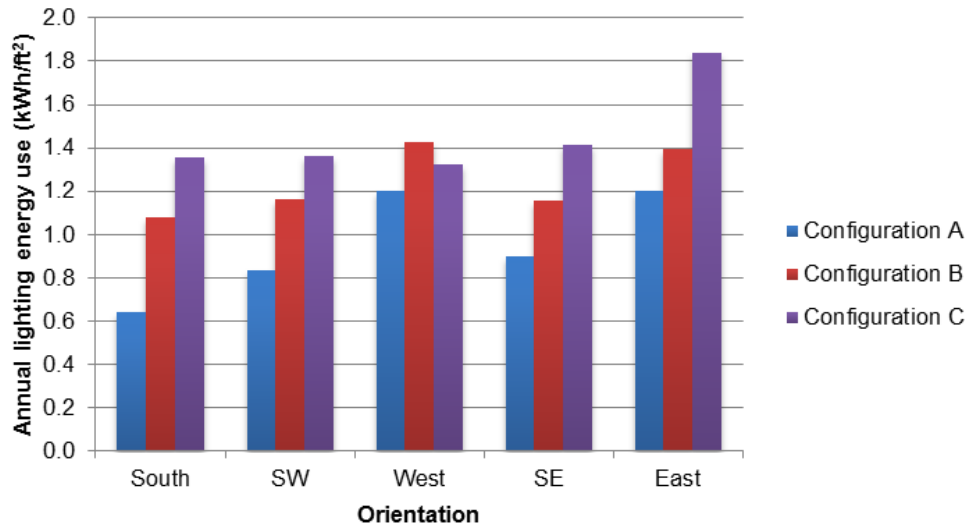
Annual lighting energy consumption in Oakland for an installed LPD of 0.75 W/ft^2 and design work plane illuminance of 300 lux. Configuration A: prototype design, B: automated reflective blind, C: manually
operated venetian blind.

Source: LBNL

Figure 4.6: Simple Payback (Years) for Oakland, California
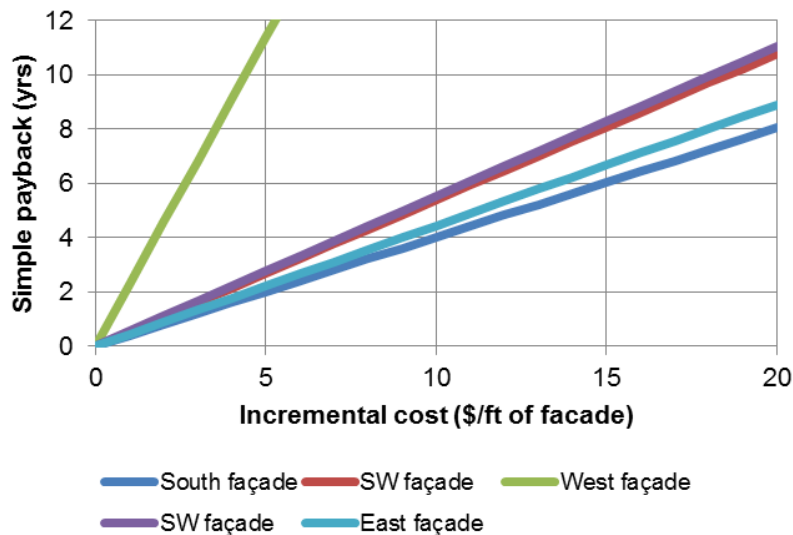
Source: LBNL

Relative to conventional windows (Configuration C), the simple payback was 4–6 years if the incremental cost of the prototype system was $10/lineal ft. of the façade or 8–11 years if the incremental cost was $20/lineal ft. of the façade. These paybacks are given for the south- and east-facing window orientations (Figure 4.6). Payback times were

higher for the west orientation. These calculations assumed 50 weeks of operation per year, five days per week, 10 hours per day (8 a.m. to 6 p.m. standard time), and an electricity cost of $0.14 per kWh.

Using results from these annual simulations, as well as data from national and California building characteristics databases (Energy Commission 2006; EIA 2016), an estimate of statewide energy use impacts was calculated, assuming use in east-, west-, and south-facing open-plan areas throughout California office buildings. Total annual lighting energy savings relative to a manually operated venetian blind were 187 million kWh, which was equivalent to $26.1 million in cost savings at an energy price of $0.14/kWh. A detailed report of the simulations is given in Fernandes et al. 2018a.

4.3.2. Outdoor Field Tests

4.3.2.1. Verification of Redirected Daylight

The project team performed field tests to confirm that the slat configuration of the proposed system redirected sunlight in a manner consistent with the initial calculations and simulations. The tests were performed with flat slats—the same slat geometry used in the annual simulations. To overcome the limitations of the testbed chamber geometry, the team placed the slats at a height between 6.5 and 7.5 ft. above the floor and 3.5 ft. below the ceiling. In an actual installation, the top of the slat system would be placed as close to the ceiling as possible to redirect daylight across the entire ceiling plane. Slats were angled so that the maximum redirection depth was 13 ft.—2 ft. short of the depth of the testbed cell. These tests confirmed that the expected redirection occurred as predicted by the simulations. A detailed report is given in Thanachareonkit et al. 2018.

4.3.2.2. Aesthetic Evaluation of Daylight Quality

Slat shape and finish can affect the aesthetic quality of redirected sunlight and, thus, user acceptance of the technology. Mirrored slats are known to be more efficient at redirecting light. The quality of the redirected sunlight can make a space look more lively and cause uncomfortable contrasts. Curved and flat mirrored slats were tested. A curved slat with a prismatic surface was also tested. The day lit appearance of the outdoor testbed chamber was evaluated under sunny sky conditions. Images of the test chamber are given in Figure 4.7.

- Curved slats produced light reflection patterns on the interior walls and ceiling that were more spread out than the flat slats. Bright spots were visible on the curved slats but did not occur with the flat slats.

- The mirrored slats (curved or flat) produced sunlit and shadow patterns that were readily identifiable, lending a more harshly day lit quality to the space.

- The prismatic slats produced light reflection patterns that were softer, diffuse, and less noticeable.

Figure 4.7: Appearance of Reflected Sunlight in the Advanced Windows Testbed

Flat, mirrored slats vs. curved, mirrored slats

Curved, mirrored slats vs. curved, prismatic slats

Left image: Appearance of reflected sunlight on walls and ceiling with flat, mirrored slats (left side) and curved, mirrored slats (right side). Right image: Appearance of reflected sunlight on walls with curved, mirrored slats (left side) and curved, prismatic slats (right side).

Source: LBNL

4.3.2.3. Light Redirection

The project team evaluated the efficiency and distribution of sunlight redirection for different types of slats. The evaluation focused on light redirected toward the back of the room (10 ft. from the window), which was the area targeted by the flat slat design for these field tests. Indoor measurements were normalized to the incident outdoor vertical irradiance to control for the different times of the day and year that the experiments took place. This "daylight delivery efficacy," or DDE, was defined as the ratio (in units of lumen/watt) of horizontal illuminance at the work plane at the back of the room (lux) and vertical irradiance at the façade (watt/m^2). A higher DDE value indicated a better ability to deliver daylight to the interior space.

- For the flat slats, DDE at the back of the room was more consistent and, for most of the time, greater than for both types of curved slats (Figure 4.8–Figure 4.10).

- The curved mirrored slats appeared to distribute light so that it concentrated in the center of the room; whereas, with the curved prismatic slats, most light was nearest to the window.

Figure 4.8: Daylight Distribution and Efficiency with Flat Mirrored Slats
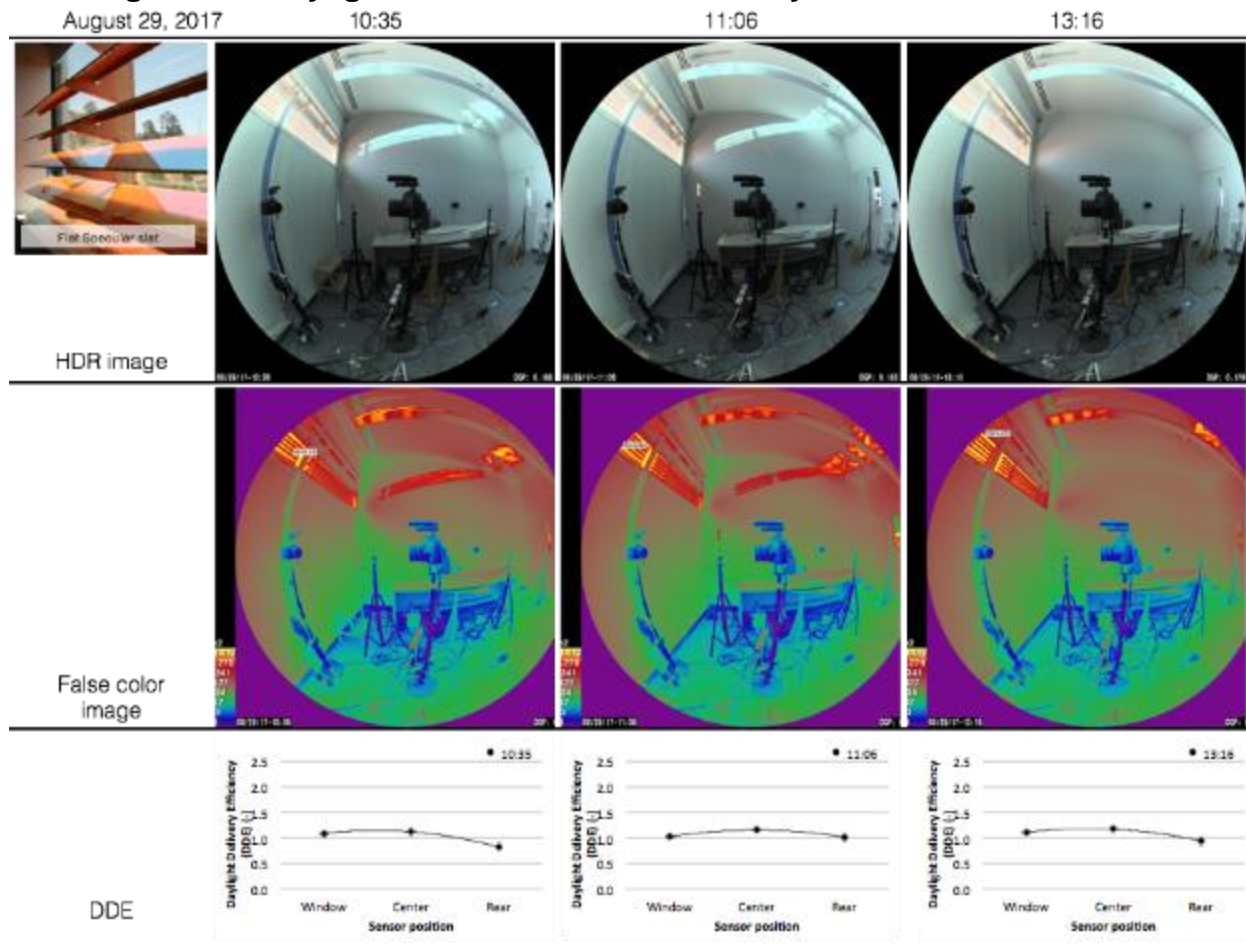
Fish-eye photographs, false color luminance image, and daylight delivery efficacy (DDE) obtained with the flat mirrored slats at three times on August 29, 2017.

Source: LBNL

Figure 4.9: Daylight Distribution and Efficiency with Curved Mirrored Slats
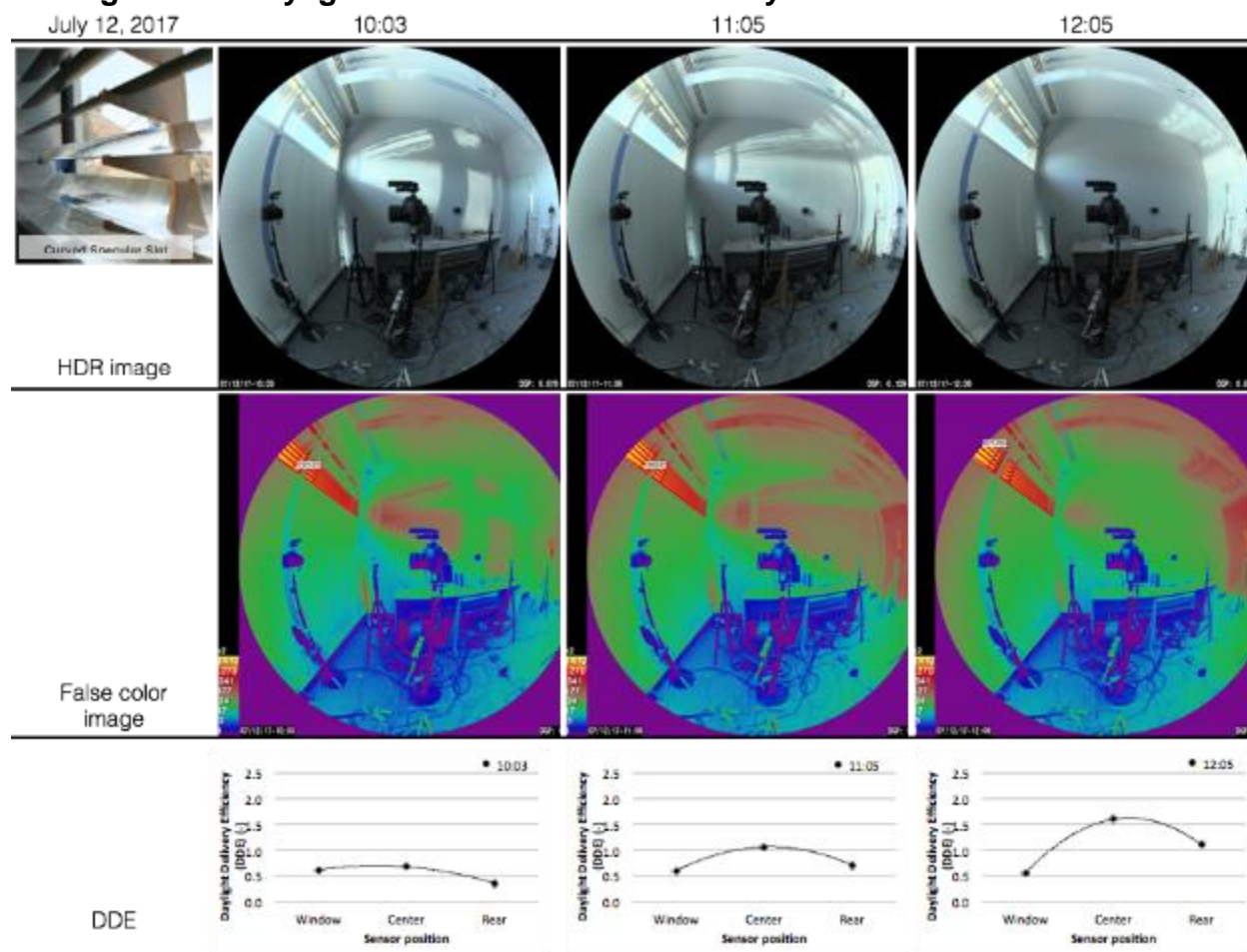
Fish-eye photographs, false color luminance images, and daylight delivery efficacy (DDE) obtained with the curved mirrored slats at three times on July 12, 2017.

Source: LBNL

Figure 4.10: Daylight Distribution and Efficiency with Curved Prismatic Slats
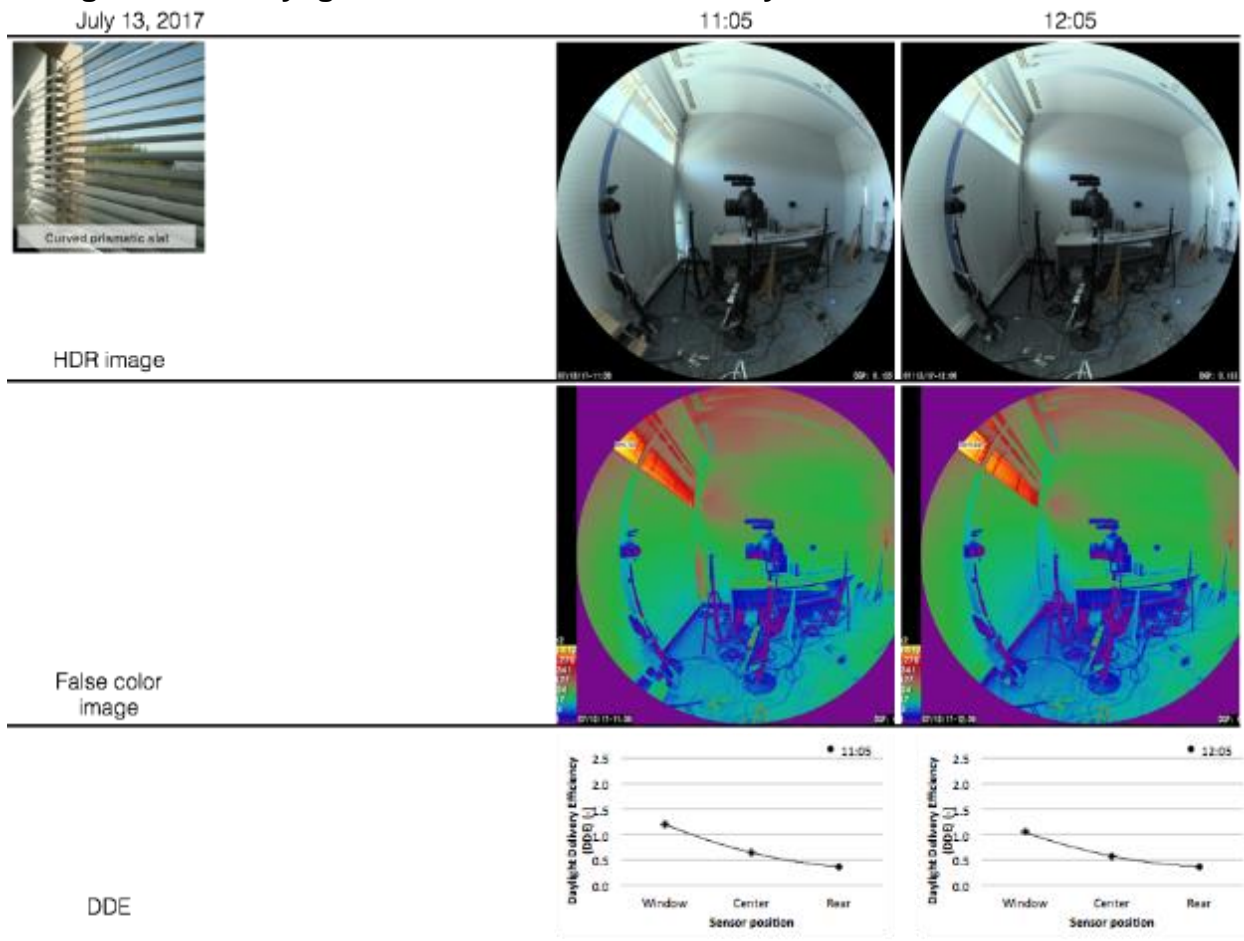
Fish-eye photographs, false color luminance images, and daylight delivery efficacy (DDE) obtained with the curved prismatic slats at three times on July 13, 2017.

Source: LBNL

4.3.2.4. Glare

The project team conducted a similar field evaluation regarding glare. When assessed using the Daylight Glare Probability (DGP) metric (Wienold and Christoffersen 2006), the three types of slats resulted in acceptable levels of glare for all the tests conducted, with the exception of one instance of DGP slightly above the glare threshold of 0.35 (the measured value was 0.36) when using the curved mirrored slats (Figure 4.11).

Figure 4.11: Comparison of Discomfort Glare for Four Slat Designs
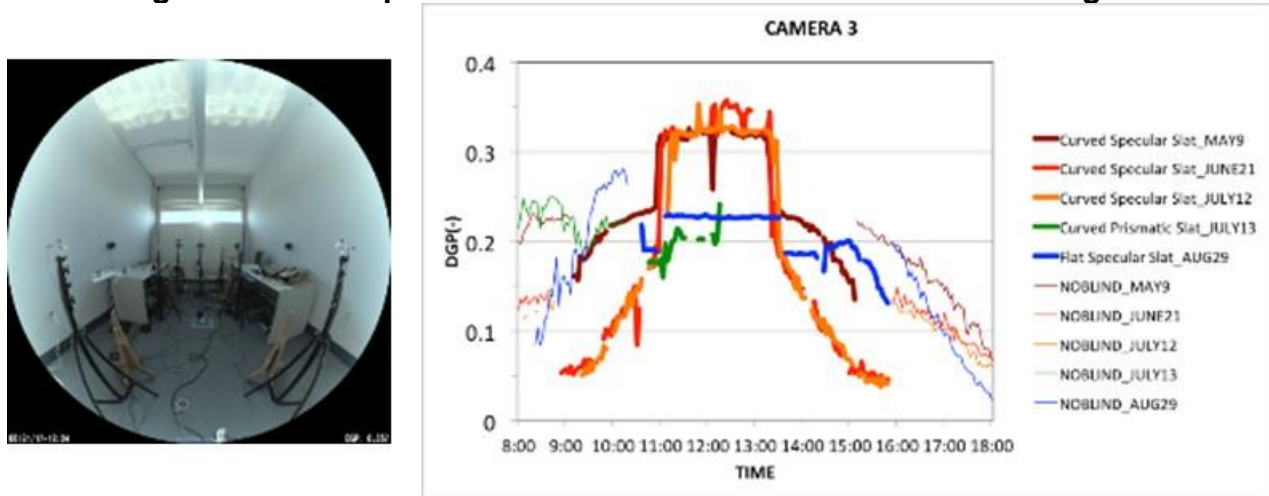
Comparison of DGP of three slat systems for four occupant locations.

Source: LBNL

4.3.3. Prototype Development

4.3.3.1. Design

A proof-of-concept prototype of the proposed system was developed to assess technical feasibility for manufacturing and commercialization (Fernandes et al. 2018b). While at the outset the variable slat spacing concept shown in Figure 4.1 appeared promising, it proved challenging to implement in practice. Therefore, the project team abandoned this concept, and the variable slat width concept (Figure 4.2) was pursued instead. An implementation was developed based on stacking three equal-width slats and expanding them with two coordinated rotational actuators such that two of the three slats slide out, in opposite directions, from the center, stationary slat (Figure 4.12).

The team constructed the prototype (Figure 4.13) using modified parts from a conventional venetian blind, with the addition of custom parts. The frame, slats, and rods were fabricated out of aluminum and steel, using machine-cut methods. In mass production, some parts are likely to be made of injection-molded plastic.

Figure 4.12: Stacked Slats and a Vertical Rod Actuation Pivot
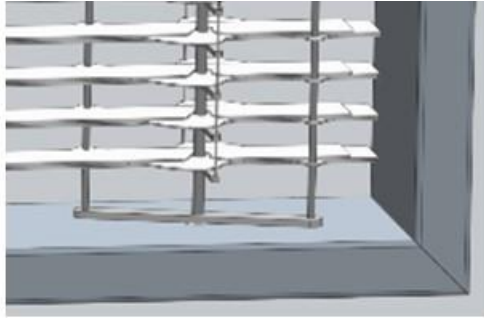
Stacked slats and a vertical rod actuation pivot: computer rendering (top) and actual prototype (bottom).

Source: LBNL

Figure 4.13: Prototype of Variable-Width Blind Assembly

Prototype of variable-width blind assembly: computer rendering (top) and actual 432 x 711 millimeter (17 x 18 inch) prototype (bottom).

Source: LBNL

4.3.3.2. Controls

To achieve daylight redirection and prevent glare throughout the year, the two slat degrees of freedom (angle and width) must be adjusted throughout the day. This adjustment was implemented, as is typical for conventional automated venetian blinds, using a system of small motors controlled by a microprocessor. The control software running on the microprocessor used latitude, cardinal orientation, day of year, time of day, and desired light-redirection depth to calculate the correct position for tilt and slat width. When the concept is implemented in a commercial product, latitude and cardinal

orientation can be determined from sensors or from user inputs during installation and commissioning. Redirection depth can be preprogrammed and adjusted by users at installation and over the life of the installation.

4.4 Technology Transfer

Feedback was provided by the technical advisory committee members throughout the project. Feedback on the initial concept was positive because of the potential for significant energy savings and satisfaction of occupant needs, such as visual comfort, daylight quality, and connection to the outdoors. Aesthetic appearance of the technology and the indoor day lit space is paramount to achieving broad market acceptance and occupant satisfaction. Members advised that the system be designed to consider ceiling finish and that a range of products be developed with different slat and ceiling finishes.

Upon review of the analysis results and prototype development, committee members commented that the current prototype depth was too wide; it would project too far into the room from the window surface. This issue can be addressed with the current prototype design by increasing the number of slats and making them narrower. To broaden acceptance of the system, members advised that a semi-reflective finish that would produce softer reflected patches should be considered. This can be achieved readily with the current prototype design by replacing the specular slats with slats that have a more diffusive finish. Reflective coatings can be procured with a wide range of specular and diffusive properties, which is useful because too diffusive a surface has been shown to reduce overall performance.

This system opens some new opportunities for the use of daylight in deeper open plan spaces and in other large building spaces. Modern office design often uses partitions for optical and acoustic privacy, and these typically intercept and reduce the available daylight received directly through the window from the sky vault. Because this design bounces light from the vertical façade off the horizontal ceiling plane, it can deliver illuminance directly to a horizontal task location in a cubicle at any distance from the façade. It can also redirect the light above partitions to the upper portion of the back wall. Daylight redirected to the upper 2 feet of the interior rear wall instead of just the ceiling was thought to have a high potential for positive emotional impact in some room designs, based on outcomes from prior field studies. The current control algorithm can be readily configured to redirect light onto the interior rear wall. Industry reviewers thought the system had the potential to provide positive psychological benefits due to a better connection with the dynamic aspects of daylight introduced from the outdoors. The study did not address whether requirements for a positive physiological circadian effect were met, but the system is capable of delivering appropriate high light levels in the rear of the room that would be impossible to achieve with a conventional window design. These performance attributes might add to the business value of the technology.

The physical prototype was shown to industry stakeholders to obtain feedback on viability of commercialization. One manufacturer of automated shades expressed a degree of interest in looking into manufacturing options for the prototype. The initial intention of this work was to investigate low-cost, microscale methods for precision actuation that would not rely on conventional motors. However, this manufacturer commented that recent advances and price reductions in small motors for robotic applications could make the use of conventional motors feasible for this type of system. This investigation occurred at the conceptual level, with reduction to practice to occur once the initial value proposition and feasibility of a macroscale prototype design were investigated. Addressing practical issues such as protection from dust, durability of the mechanical operations, and maintenance requirements over the life of the installation will involve additional engineering. Invention disclosures have been filed to document potential intellectual property developed during this project.

4.5. Conclusions

The project team developed a variable-width slat system with automated controls to redirect daylight up to 40 feet from the window.

- Simulations of the flat mirrored slat prototype in four California climates estimated up to 54 percent annual lighting energy use savings for south-, southeast-, and southwest-facing orientations compared to manually operated, conventional venetian blinds. The simple payback was 4–6 years if the incremental cost of the system was $10 per lineal foot of the façade or 8–11 years if the cost was $20/ft. Visual comfort was maintained throughout the year. HVAC energy-use impacts were not simulated. Energy cost trade-offs between daylight admission versus solar control are expected to be small because the total window area involved in the clerestory is small. These impacts could be minimized using optimization methods described in Chapter 6.

- Field tests showed that the proposed system redirected sunlight deep into the space without measurable glare using the DGP metric.[1] The day lit appearance of the space varied considerably depending on the slat profile and finish. The slat finish should be selected according to specific applications and ceiling types, since redirected sunlight can cause ceiling-mounted objects to cast shadows or shiny objects to reflect bright light. Mirrored slats produced local areas of bright sunlight on the ceiling and upper areas of the walls. Use of curved prismatic slats softened this redirected daylight but reduced the depth of redirection and, therefore, energy savings.

- The project team built a tabletop physical prototype that demonstrated technical feasibility of the variable-width slat concept. A control system was implemented

---

[1] The appropriate thresholds for discomfort glare using the DGP metric are an open topic of research (which is outside the current scope of this project). A DGP threshold of 0.35 was used in this study.

with a touch-screen user interface to actuate the motorized system. While the concept is potentially feasible for mass manufacturing, the depth of the current prototype is probably too large; this can be addressed by reducing the depth of the slats while increasing the number of slats. Concepts for microactuation were explored with a goal of producing a prototype design that could be fit within a 1-inch-deep insulating glass unit.

- The prototype technology would be most applicable to buildings situated in sunny climates with curtain wall façades that have minimal obstructions from overhangs, fins, deep reveals, or nearby buildings. The technology would be most effective in large-area open-plan spaces with minimal vertical obstructions within the 7–9 ft. zone above the floor.

- Building-type applications such as gymnasiums, supermarkets, airports, atria, laboratories, fabrication spaces, and warehouses where aesthetics may not be an overriding concern would enable use of the most efficient system (flat mirrored slats). For office environments with lower ceilings such as open-plan offices, a semi reflective slat may provide better lighting quality in the space.

- Blockage of view through the upper clerestory portion of the window may be a concern, particularly in open-plan office areas with high partitions where the view would be available only to those sitting next to the window. The prototype technology raises the slats when sunlight, solar control, and glare are not of concern, but for times when the sun is within view of the window, the slats would block views to the outdoors. Under those conditions, most windows with conventional shades or blinds will have them pulled, obstructing the view as well.

- The daylighting system affords greater connection to the outdoors through the provision of variable, natural daylight to a greater area of the floor plate. With mirrored slats, there is no shift in spectrum of the admitted daylight. The system also could be designed and controlled to deliver sufficient daylight to satisfy physiological needs to support circadian rhythm in many applications.

4.6. Benefits to Ratepayers

Reduction of lighting energy use through daylighting supports California's overarching goal of reducing greenhouse gas emissions by improving building energy efficiency. This foundational research sets the groundwork for subsequent technology R&D that could potentially leverage micro actuation methods (e.g., shape memory alloys, linear motors, polypyrrole actuators, and magnetic actuators) to produce a cost-effective, market-acceptable solution. It also supports trends to develop and implement more grid-friendly dynamic solutions in buildings that deliver high quality working conditions. This work quantified energy cost savings, payback, and the physical and functional aspects of a novel daylight redirecting prototype. This information can be used by companies seeking to expand their product offerings and by researchers in subsequent work to develop promising new designs.

CHAPTER 5:
Daylighting and Shading Optimization Methods

5.1. Introduction

Shading and daylighting fenestration systems can have an enormous influence on HVAC and lighting energy use, peak demand, and comfort in both residential and nonresidential buildings in California—particularly in sunny, hot climates such as the Greater Los Angeles Area, Central California, and areas in San Diego (Figure 5.1). Over the past 30 years, researchers have sought ways to model the light-scattering or "optically complex" properties of these fenestration systems for building performance evaluations.

Systems can be classified as *coplanar* or *noncoplanar*. *Coplanar* systems are those where the shade surface is parallel to the window glazing, such as roller shades, venetian blinds, prismatic glazings, or sand-blasted glass. *Noncoplanar* systems are those where the shade surface extends out from the exterior face of the window glazing, such as awnings, overhangs, fins, and even skylight systems such as tubular daylight devices. Architects and engineers, facility owners, regulators, and manufacturers need accurate, time-efficient energy simulation tools to evaluate new and conventional products.

Figure 5.1: Example of Optically Complex, Noncoplanar, Exterior Shading

Annual energy performance of these perforated metal vertical fins and sand blasted glass overhangs can be modeled quickly and routinely using the models developed and validated in this study.

Source: LBNL

In a prior California Energy Commission project, new algorithms were developed to model the solar, daylight, and thermal performance of complex fenestration systems (Lee et al. 2009). Work in this subsequent project focused on validating the algorithms, developing methods for characterizing the light-scattering behavior of complex fenestration systems, and developing the supporting tutorials and tools to promote the use of the algorithms by end users.

5.2. Project Approach

Radiance is free, open-source, ray-tracing simulation software that is used extensively by engineering firms for innovative lighting, solar control, and daylighting design to improve building energy efficiency. Lawrence Berkeley National Laboratory, in collaboration with Anyhere Software and the open source community, has been developing Radiance in coordination with companion tools Optics, WINDOW, and EnergyPlus. Many software tools, including EnergyPlus, rely on radiosity-based methods (i.e., light or radiation from a source is reflected diffusely before arriving at a point in the room) to determine the effects of solar radiation on building energy consumption. These methods assume that fenestration systems exhibit Lambertian (perfectly diffuse) scattering properties, which can result in significant errors in simulated performance for fenestration systems that have diffuse and specular properties, such as fabrics that scatter light diffusely and allow direct sunlight to pass straight through for some sun angles.

To increase modeling accuracy of optically complex fenestration systems, the project team developed new ray-tracing algorithms in a prior phase of Energy Commission-funded research. Instead of using simplifying assumptions, fenestration systems are characterized using "bidirectional scattering distribution functions," or BSDFs, which define the intensity of transmitted, reflected, or absorbed radiation for paired incident and exiting angles (Figure 5.2). In other words, for a single ray of light hitting a fenestration system, the distribution of transmitted light in any direction through the system is recorded in a BSDF matrix data file. BSDFs are based on empirical measurements, vastly improving the modeling accuracy of fenestration materials and systems such as fabrics, venetian blinds, fritted glass, prismatic films, and perforated metals.

To calculate point-in-time performance, matrix algebraic methods were developed that rely on a set of flux-transfer, ray-tracing calculations to produce scene-specific matrices. These matrices, combined with the BSDF matrix for the fenestration system, are used in a time-step calculation to produce annual simulations within a fraction of a time needed by brute-force, ray-tracing methods (that is, a few minutes rather than days or months). The BSDF matrix is interchangeable, enabling efficient modeling of *operable* fenestration systems; for example, to model 20 slat angles of a venetian blind, one simply needs to substitute a BSDF file (for Angle 1) for another BSDF file (for Angle 2).

Figure 5.2: Bidirectional Scattering Distribution Functions (BSDFs)
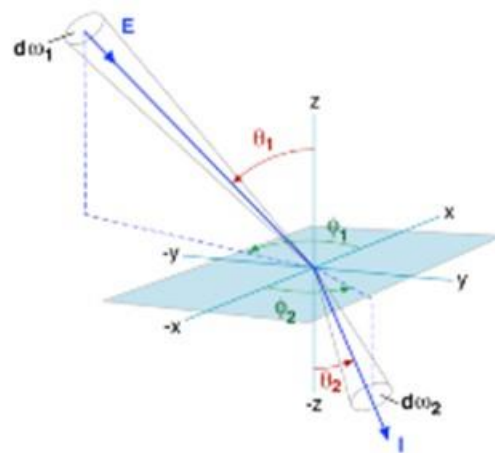
Transmitted radiation intensity (I) shown for a paired incident (θ_1, ϕ_1) and exiting angle (θ_2, ϕ_2).
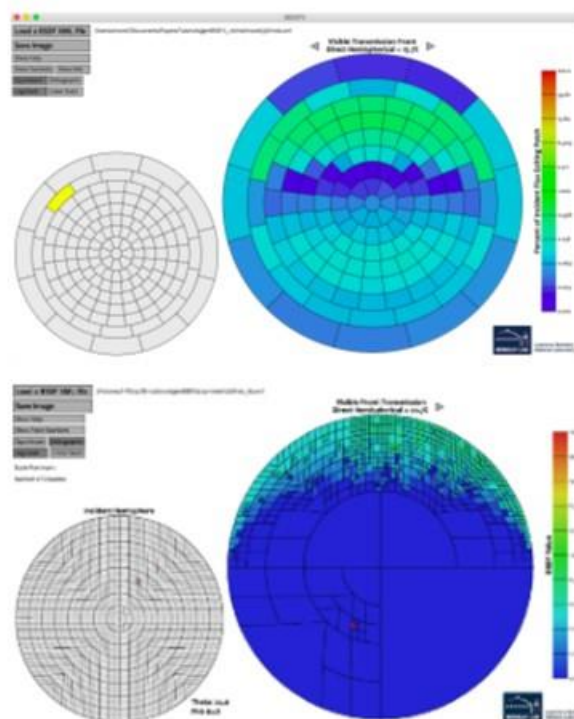
Example BSDF data for a horizontal venetian blind. Left: Direction of incident light is shown with a yellow patch or "X." Right: Distribution of scattered light in exiting direction. BSDF data are given with low angular resolution (upper image, 145 x 145 matrix with 10°–15° angular resolution for each patch) and with a high angular resolution (lower image, tensor tree, 3° angular resolution for smallest patch).

Source: LBNL

There are several variations on the matrix method, where (a) calculation of flux transfer from the sun is made separately from the sky to improve accuracy (Figures 5.3 and 5.4), and (b) calculation of flux transfer from a noncoplanar shading system to the window is represented with a separate matrix to enable modeling of operable systems (for example, adjustable awnings) or parametric analysis (for example, to select the awning fabric) or both. This project focused on first validating the various methods, then providing tools and guidance that users can use to make more informed decisions when employing matrix algebraic methods in building energy simulations.

Figure 5.3: Matrix Methods for Coplanar Systems
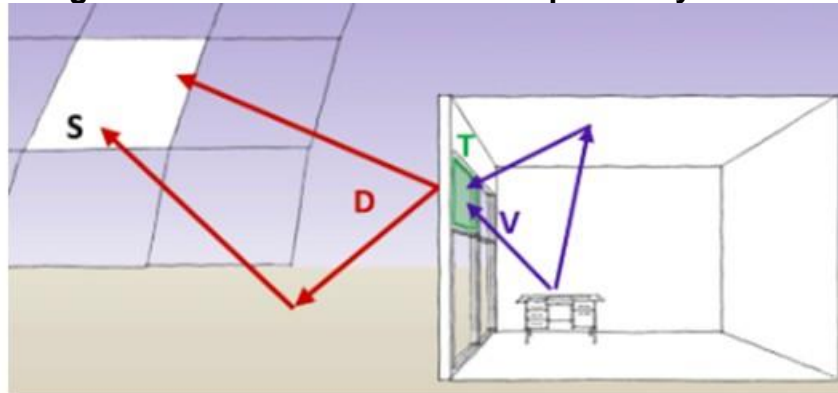
Three-phase method: Flux transfer from an indoor point location mapped to the window surface is represented by the view matrix (V); flux transfer from incident light to outgoing light from the fenestration surface is represented by the transmission matrix (T); flux transfer from the outdoor window surface to the subdivided skydome hemisphere is represented by the daylight matrix (D); the intensity of each sky patch is represented by the sky matrix (S). Total flux incident at the indoor point is a summation of flux from each subdivision of the skydome hemisphere using a matrix calculation (=VTDS, [Ward et al. 2010]).
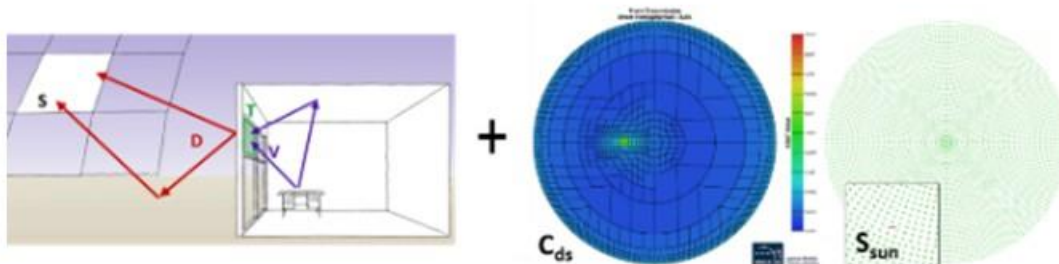
Five-phase method: To increase accuracy, the contribution of flux transfer from the sky (left image) is calculated separately from the contribution from the sun (right image); then the two contributions are summed. For the direct sun (ds) contribution, the BSDF has high angular resolution; i.e., the "C_{ds}" BSDF matrix patch size is very small in areas of peak transmission (shown in yellow), enabling accurate determination of flux from the sun (i.e., S_{sun}, red point).

L_{3phase} $- Lds_{-3phase}$ $+ Lds$ L_{5phase}
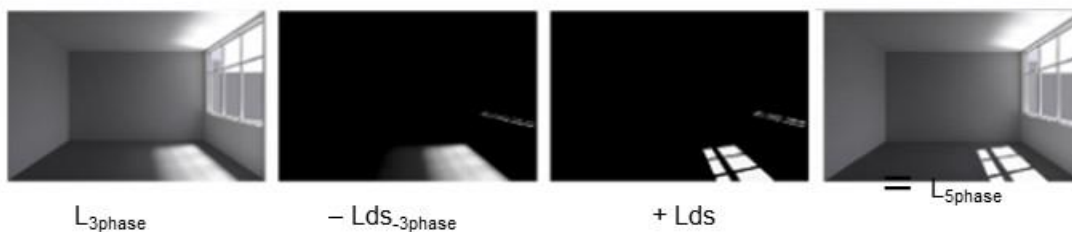
Five-phase method: Renderings of the luminance (L) contributions in an indoor space with clear glazing. Results from the three-phase method are shown in the left most image. Results from the five-phase method are shown in the rightmost image. The intensity is significantly greater in areas of direct sunlight with the five-phase method.

Source: LBNL

Figure 5.4: Matrix Methods for Noncoplanar Systems

$$i = V\ T\ F\ D\ s$$

| View matrix | × | Transmission matrix | × | Facade matrix | × | Daylight matrix | × | sky matrix |
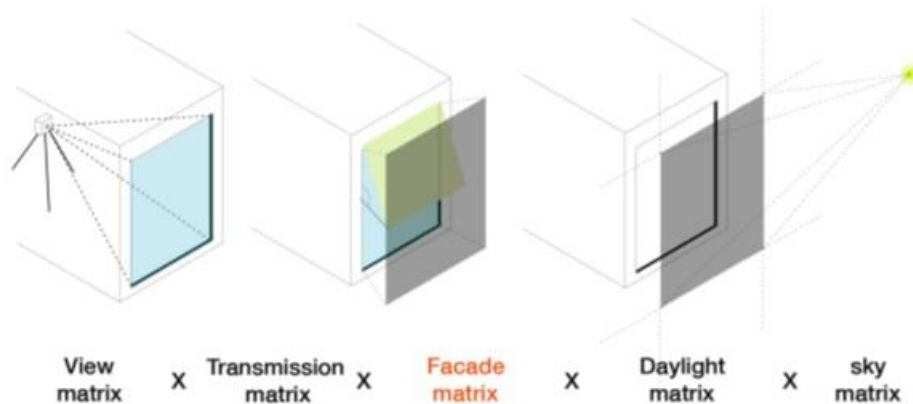
Four- and six-phase methods: For fenestration systems that are not parallel to the surface of the window (e.g., awning shown in the middle image), flux transfer between a virtual (gray) plane at the outermost edges of the awning and the face of the window glazing is represented by the façade matrix (F). The three-phase method becomes the four-phase method with the addition of the F matrix; the four-phase method becomes the six-phase method when the sky and sun components are separately calculated.
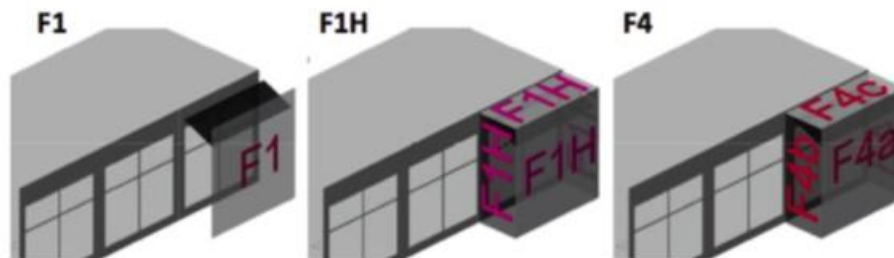
The F matrix has a few variants (lower image): F1, F1H, and FN, where flux is mapped from a single (F1, F1H) or number (FN) of virtual planes that bound the non-coplanar shading system on all sides.

Source: LBNL

5.3. Results

5.3.1. Validation of Matrix Methods

The research team validated and debugged the matrix methods using comparisons to full ray-tracing simulations and to measured illuminance and luminance data from full-scale, outdoor field tests. The initial three-phase matrix method was field validated in a prior California Energy Commission study (McNeil and Lee 2012). The four-, five-, and six-phase methods were field validated as described in the following sections.

5.3.1.1. Field Validation of the Five-Phase Method

The project team validated the five-phase method through comparisons with measured data in the full-scale LBNL FLEXLAB testbed with four daylighting or shading systems installed in the windows (Figure 5.5 and Figure 5 6, [Lee et al. 2018]). Workplane and vertical illuminance, luminance, and discomfort glare data were generated using three-

and five-phase simulations. The team monitored illuminance and luminance during the equinox period, where one week of 5-minute data for each of the systems were used for the comparisons. Results showing the frequency of deviation (expressed as the percentage of the monitored period) of simulated results from measured data are shown in Figure 5.7. The ideal would be simulated results that achieve less than 5 percent deviation from measured results for 100 percent of the monitored period. Points above the diagonal line indicate the higher percentage of time when the five-phase method produced results with a deviation of less than 10 percent from measured results compared to the three-phase method.

Figure 5.5: LBNL FLEXLAB

Indoor view of the FLEXLAB test chamber showing instrumentation and furnishings used for the validation study.

Source: LBNL

Figure 5 6: Fenestration Systems Used for Five-Phase Method Validation

DL-L1   DL-L2   DL-P   S-Dyn

Three daylight-redirecting films were tested (three left-hand images). Each was designed with microscopic features to redirect sunlight for a specific range of angles. The film was applied to the upper third of the window with the lower two-thirds covered by a venetian blind set to a fixed cut-off angle. An exterior solar screen (S-L) was also tested, consisting of matte black slats (i.e., 1.25 mm wide, 0.22 mm thick, fixed cut-off angle of 40°) that covered the entire window.

Source: LBNL

Figure 5.7: Frequency of Deviation between Simulated and Measured Results
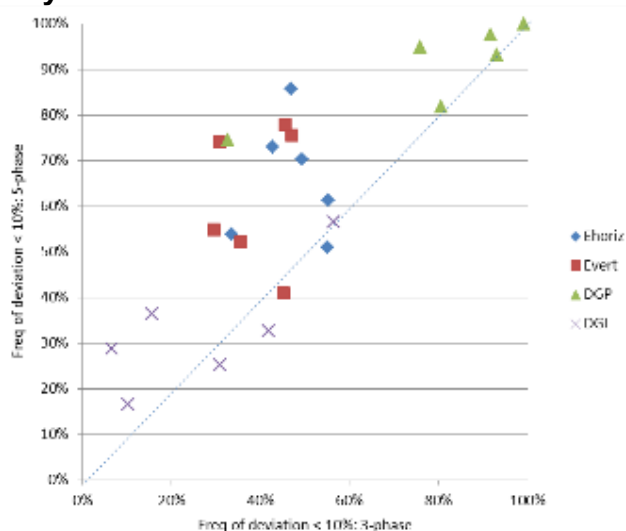
Frequency of deviation (percentage of the equinox monitored period) when the difference between the simulated and measured data was less than 10 percent, where the simulated data were determined using the three-phase (x-axis) or the five-phase (y-axis) method. Each point represents one week of monitored data for each of the six systems.

Source: LBNL

95

For horizontal and vertical illuminance, the five-phase method deviated from measured data less frequently than the three-phase method by about 20–40 percent of the monitored period. The daylight glare index (DGI) proved the most difficult to match. This metric relies on accurate modeling of the spatial distribution and intensity of glare sources within the field of view, so small shifts in view angle can result in significant errors between predicted and measured results (Figure 5.8 andFigure 5.9). The daylight glare probability (DGP) index is strongly correlated to vertical illuminance at the eye and depends less on spatial accuracy of glare sources. Here, the three- and five-phase methods produced similar DGP results, in part because direct sun was blocked by the fenestration system in four of the six cases.

Figure 5.8: Illuminance Distribution in the FLEXLAB Space
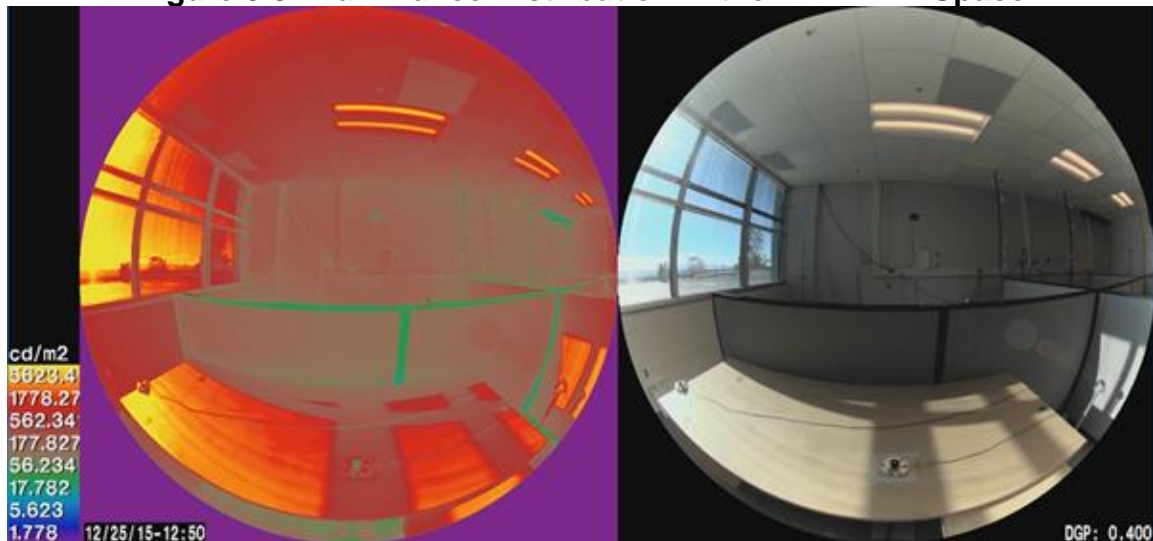
High dynamic range (HDR) image (left) and photograph (right) of the full-scale testbed with the S-L exterior screen system showing the shadow pattern on the workplane illuminance sensor in the foreground, while the sensor to the left is in direct sunlight, December 25, 12:50 p.m.

Source: LBNL

Figure 5.9: Illuminance Distribution from Simulations
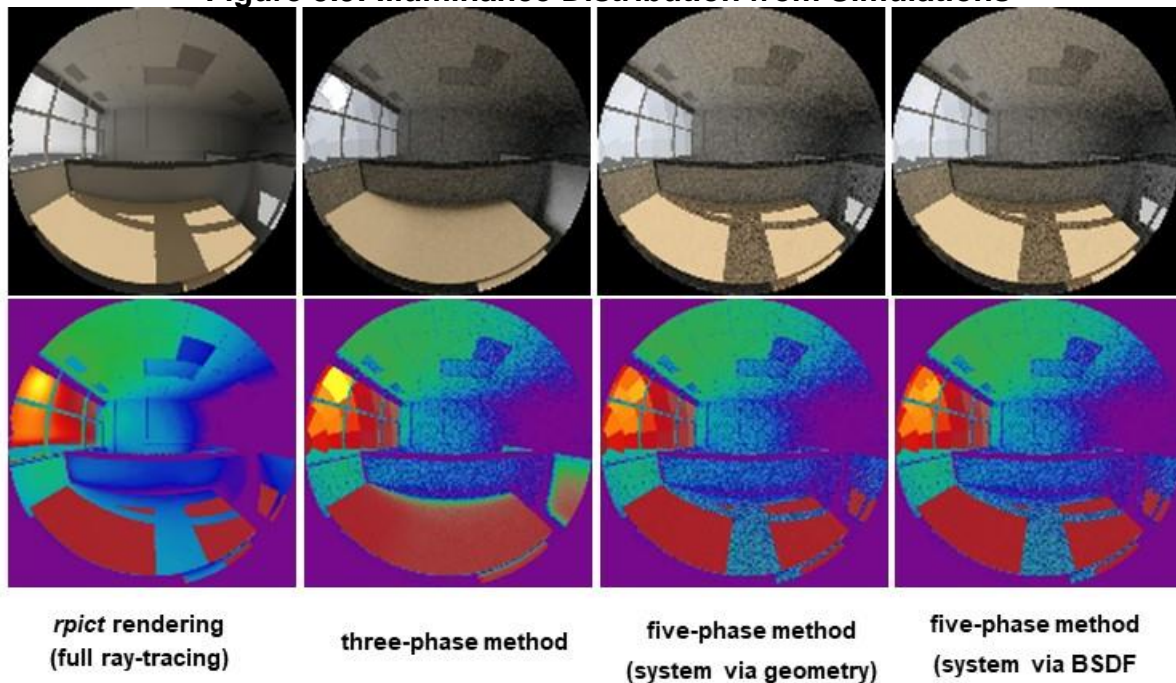
Photorealistic views (upper row) and false color luminance images (lower row) of the room interior with clear glass windows rendered using different modeling approaches, December 25, 12:50 PM. Note the absence of the shadow on the desk in the three-phase simulated image. All luminance images have the same false color scale.

Source: LBNL

5.3.1.2. Field Validation of the Four- and Six-Phase Matrix Methods for Noncoplanar Systems

Field validation of the four- and six-phase methods involved comparing simulation data to measured data in a day lit room with a noncoplanar, drop-arm fabric awning (Wang et al. 2018). Measurements were performed over a year in the LBNL Advanced Windows Testbed (Figure 5.10). The façade or "F" matrix represents the flux transfer between the window and the boundary planes encompassing the noncoplanar shading system. Different methods for defining the F-matrix (i.e., F1, F1H, F7 F-matrices) were evaluated. Once the F matrices were generated, the geometry of the exterior shading system was no longer used in the simulations. For the alternate methods (DC, three-phase, and five-phase), the awning geometry and material were included in the daylight (D) matrix (Figure 5.4). Annual simulations were then performed through matrix multiplication.

Figure 5.10: LBNL Advanced Windows Testbed with a Fabric Awning

Source: LBNL

Figure 5.11 shows the level of agreement between the field measurements and simulation results for one of the workplane illuminance sensors nearest the window. Data are given for all measurement periods (5-min interval data, all daylight hours during the summer, 8:00 a.m. to 6:00 p.m. standard time during the winter) and several simulation methods. The six-phase methods with the F7 and F1H matrix and the DC method produced similar levels of agreement with measured data (11–13 percent) because all three methods mapped all incoming flux from the sun and sky to the indoor point. The six-phase method with F1 matrix had poor agreement (34 percent error) because the F1 matrix omitted flux from the sides of the awning to the window.

Figure 5.11: Measured Versus Simulated Illuminance with Drop-Arm Awning

6PM_F7 (NMAE: 11.4%)

DC (NMAE: 11.7%)

6PM_F1H (NMAE: 13%)

6PM_F1 (NMAE: 33.6%)
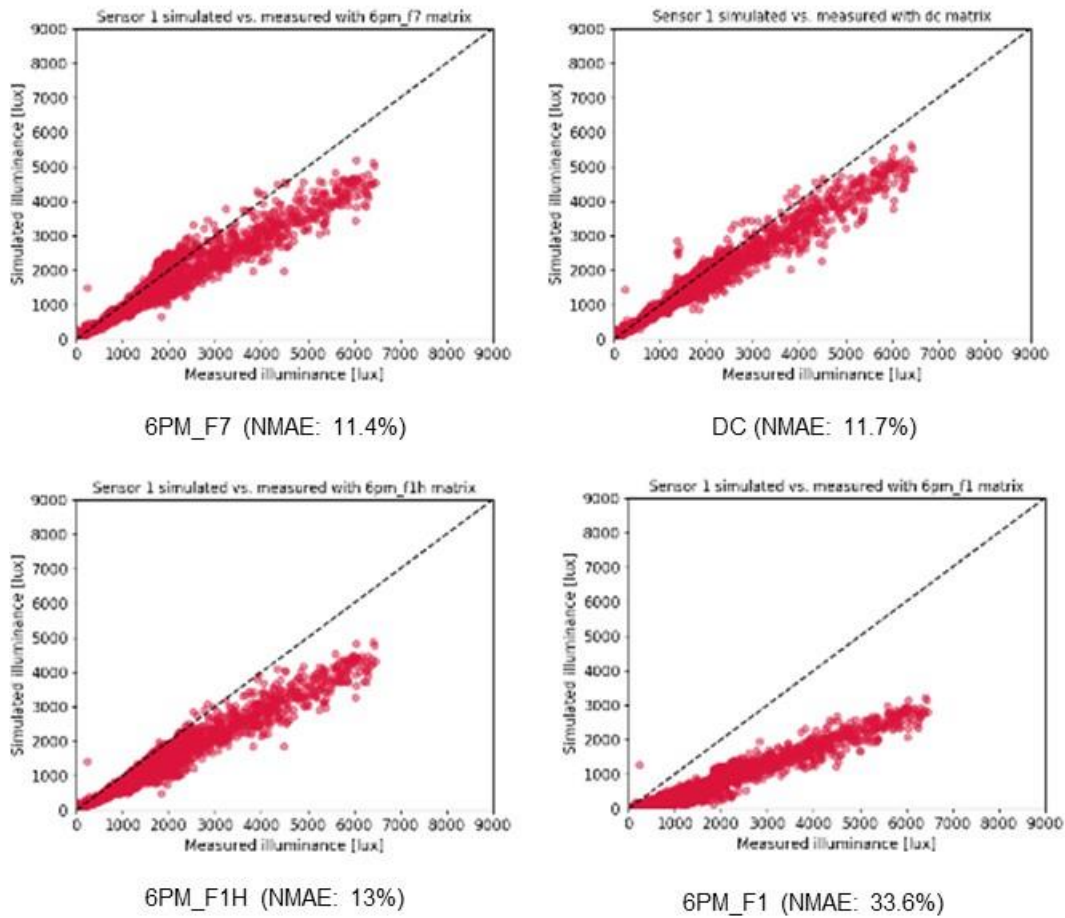
Scatter plots showing measured (x-axis) and simulated (y-axis) workplane illuminance at Sensor #1 (near the window) for the entire monitored period using different matrix-based simulation methods. Agreement is best for the upper row of plots (DC and 6PM_F7) and worse for the lower row of plots.

Source: LBNL

The workplane illuminance nearest the windows was the most challenging to predict. Overestimation of workplane illuminance (centered around the 2,000 lux illuminance level for the measured condition) occurred for all but two of the methods: the five- and six-phase methods with the F1H aperture. These overestimated simulated data were likely caused by the direct sun contribution being represented by a large solid angle. The overestimation was most significant with the three- and four-phase methods, then decreased with the five- and six-phase methods. In the case of the six-phase method with the F7 aperture, overestimation still occurred. Additional increased resolution of the sky matrix would likely improve accuracy (Wang et al. 2018).

Results showed that simulated workplane illuminance results using all methods except for the four- and six-phase methods with the F1 aperture (i.e., 4PM_F1, 6PM_F1) were comparable to the measured illuminance (Figure 5.12). For middle to rear sensors, the

normalized mean absolute error between measured and simulated results for the summer and winter periods was
6.7–15.8 percent. For the sensors nearest the window, the error was 10.3–23.6 percent. Differences between valid methods were negligible in this study.

Simulated values for the DGP index agreed well with measured values (6.4–8.6 percent error) with the exception of the four- and six-phase methods with the F1 aperture (12.0–15.2 percent error). Table 5.1 summarizes these results. The larger error for the four- and six-phase methods with F1 aperture can be explained by unaccounted flux in the F1 matrix. The small difference in error between the four- and six-phase methods with the F1H or F7 aperture was likely due to the use of a relatively opaque fabric with minimal transmission of direct sunlight.

To reiterate, the four- and six-phase methods with the F1H aperture enable efficient parametric modeling of exterior, noncoplanar shades (i.e., different materials and geometries, operable systems) through simple substitution of the F-matrix and are thus most suited for applications where the increased set-up time is outweighed by the overall reduced time needed for the annual simulations.

Figure 5.12: Illuminance Error for Noncoplanar Simulations
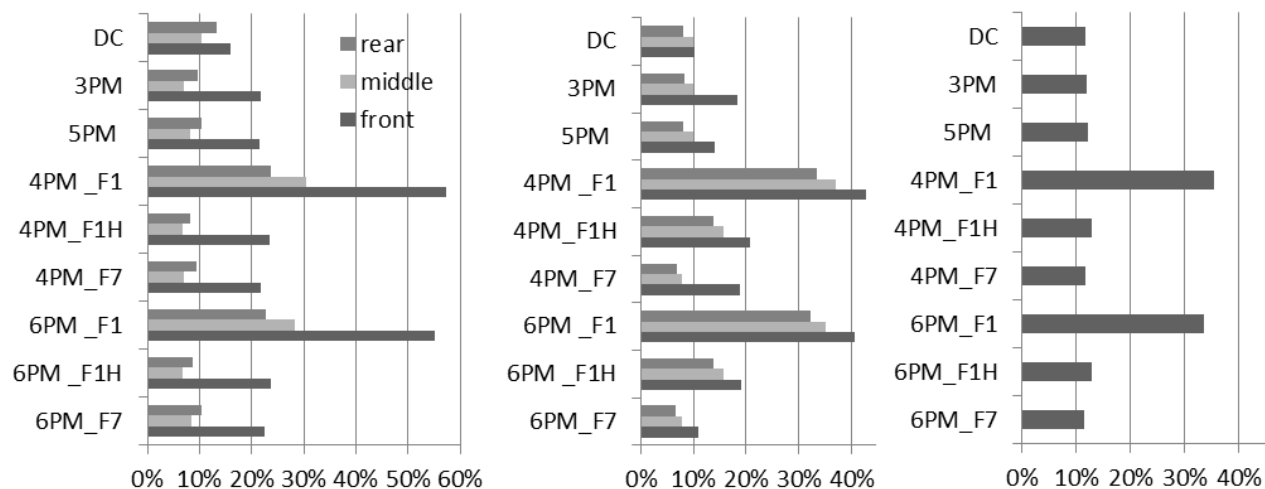
Normalized mean absolute error (NMAE) between measured and simulated workplane illuminance at the rear, middle, and front (nearest the window) of the room. Left: Summer, awning angle 50°. Middle: Winter and spring, awning angle 125°. Right: All sensors, summer and winter test periods.

Source: LBNL

Table 5.1: Daylight Glare Probability (DGP) Error for Noncoplanar Simulations

Matrix method	Overall error (%)
DC	6.5
3PM	6.8
5PM	8.2
4PM_F1	12.9
4PM_F1H	7.9
4PM_F7	6.4
6PM_F1	15.2
6PM_F1H	8.6
6PM_F7	8.0

Error between measured and simulated results.

Source: LBNL

5.3.1.3. Validation of Matrix Methods for Noncoplanar Systems in EnergyPlus

EnergyPlus uses shadow and view factors to determine the reduction of solar irradiance on the window surface due to the noncoplanar system and surrounding obstructions (e.g., nearby buildings). This validation addressed the shortwave radiation effects through optically complex, noncoplanar fenestration systems. The long-wave radiative exchange, conductive, and convective effects of the noncoplanar system will be addressed in synergistic DOE-funded research in 2019.

To improve accuracy, the project team implemented ray-tracing algorithms to determine the flux transfer between the noncoplanar system, the window, and the interior, replacing the shadow and view factors of EnergyPlus. With the "F" matrix, the ray-tracing calculation takes care of the flux transfer between the outdoors and the window, including the noncoplanar system and interreflections within the noncoplanar system. Consequently, the F matrix approach also enables the simulation of geometrically and optically complex noncoplanar systems of which many tools, including EnergyPlus, are not capable.

The project team performed an analysis comparing the native EnergyPlus-simulated results for an opaque overhang with those generated with the four-phase matrix method. Good agreement for this simple case would indicate that implementation of the matrix method in EnergyPlus was accomplished without error.

There was good agreement during the winter for a south-facing, dual-pane, low-emissivity (low-e) window with the opaque overhang, but a maximum 20 percent discrepancy was found between the two approaches on a summer day (Figure 5.13). During the summer, the sun's position during noon is at high, oblique grazing angles to the window. At these grazing angles, the resolution of the BSDF basis (Klems 145 x 145) was too low, which exacerbated the averaging effect of the Klems patches and resulted in large errors.

Use of a higher-resolution BSDF basis would significantly reduce these errors. LBNL's WINDOW tool will be updated to include this option. In general, transmitted solar radiation levels agreed well between the two approaches: a root mean square error (RMSE) of 38.7 W (5.7 percent) was calculated for the period between 8:00 a.m. and 4:00 p.m. for the year, where the window surface area was 8.2 square meters (88 ft.[2]). Figure 5.14 shows a comparison of hourly data.

Figure 5.13: Transmitted Solar Radiation for the Winter (left) and Summer (right) Solstice
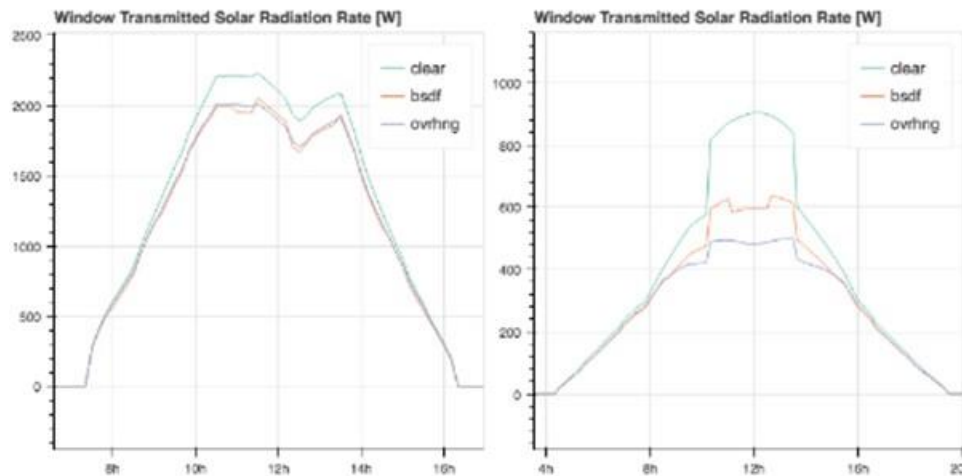
Legend – *clear*: unshaded window; *bsdf*: EnergyPlus four-phase BSDF simulation of the same opaque overhang; *ovrhng*: existing EnergyPlus simulation of an opaque overhang. Values for the bsdf and ovrhng cases should be the same, and both should be lower than the clear case.

Source: LBNL

Figure 5.14: Transmitted Solar Radiation for the Matrix Method Versus the Current EnergyPlus Method
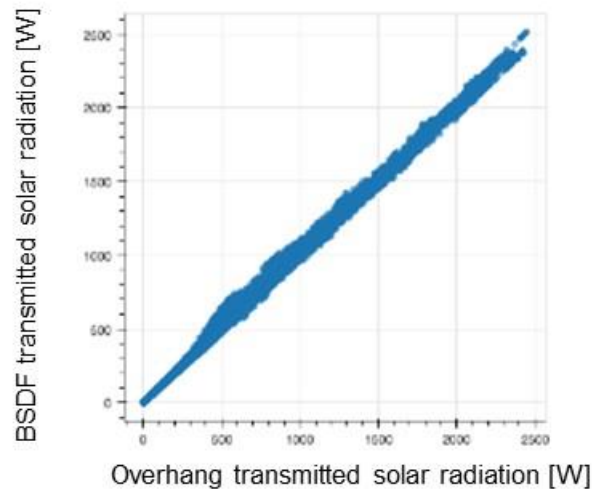
Correlation of transmitted solar radiation (W) between the existing EnergyPlus model (x-axis) and the four-phase matrix method (y-axis) from 8:00 a.m. to 4:00 p.m. over the year (15-min interval data). South-facing, double-pane, low-e window with an opaque overhang. RMSE = 38.7 W (5.7 percent).

Source: LBNL

5.3.1.4. Field Validation of the Matrix Approach for Tubular Daylighting Systems

The noncoplanar matrix methods should be applicable to skylights as well as to conventional exterior shading systems. This applicability was confirmed with a comparison to measured data from a field test of a tubular daylight device (TDD) installed in a 14 x 16 x 9 ft. core zone in the LBNL FLEXLAB facility (Figure 5.15). The project team carried out measurements over a week in February. Horizontal illuminance was measured at 1-min intervals on a 5 x 5 ft. grid. For the four-phase simulations, the BSDF data representing the TDD were generated through ray tracing (similar to generation of an F matrix) using a geometric description of the TDD provided by the manufacturer (Solatube 350DS) and BSDF data for the composite materials measured using the LBNL scanning goniophotometer and spectrophotometer.

Figure 5.15: Tubular Daylight Device in the FLEXLAB
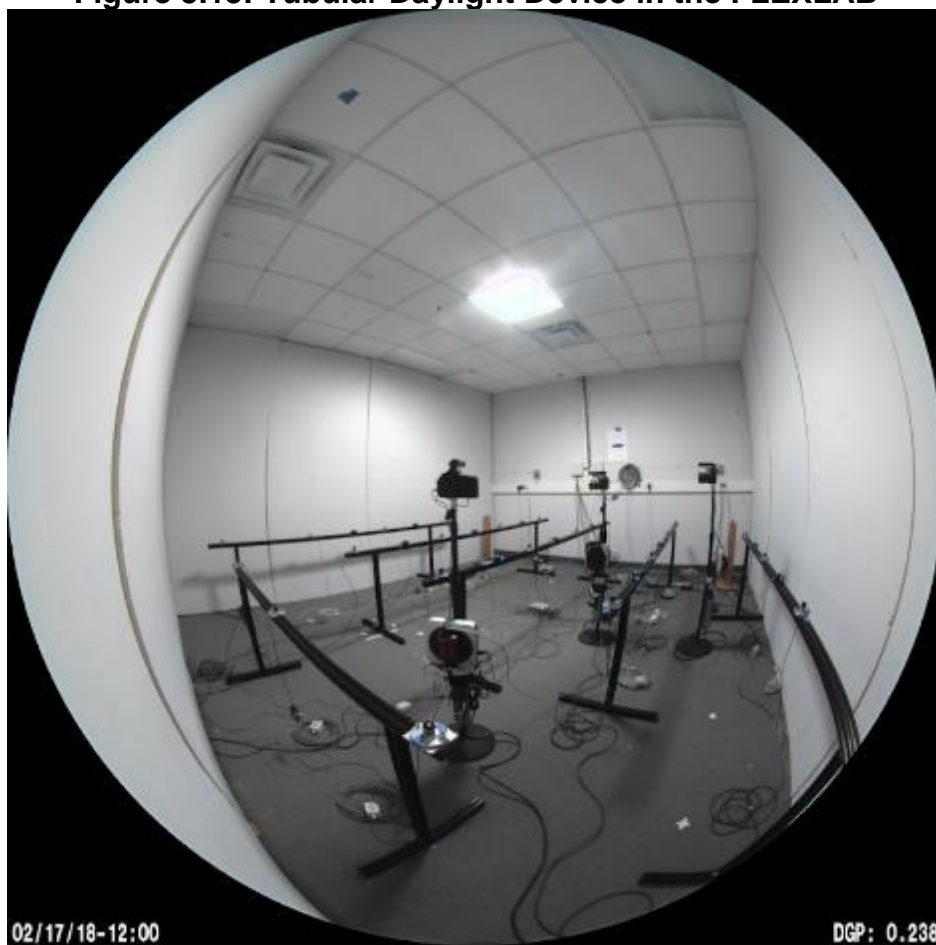
Source: LBNL

Simulated workplane illuminance agreed well with measured data, with more significant deviations occurring during unstable, dynamic sky conditions (Figure 5.16). Errors during this period were likely due in part to differences in the time stamp between the monitored sky condition, which was used as input to the simulations, and the workplane illuminance measurements. From the simulation runs, the observed RMSE across 25 workplane illuminance sensors was 19.1 percent, or 16.2 percent if outlier, noisy data were excluded. This RMSE is below the threshold 20 percent level, which is fairly standard for daylighting studies when comparing measured and simulated illuminance data. Figure 5.17a shows the scatterplot of the overall agreement between the measured and simulated workplane illuminance for all 25 sensor locations (February 17–19, 9:00–15:00). Figure 5.17b shows the same data but excludes outlier data from eight sensor locations. These results demonstrated that the matrix method is valid for daylighting systems with a significant distance (3.5 feet) between the opening and distribution apertures.

Figure 5.16: Simulated and Measured Workplane Illuminance at Two Representative Sensor Locations, Test Day February 18, 2018
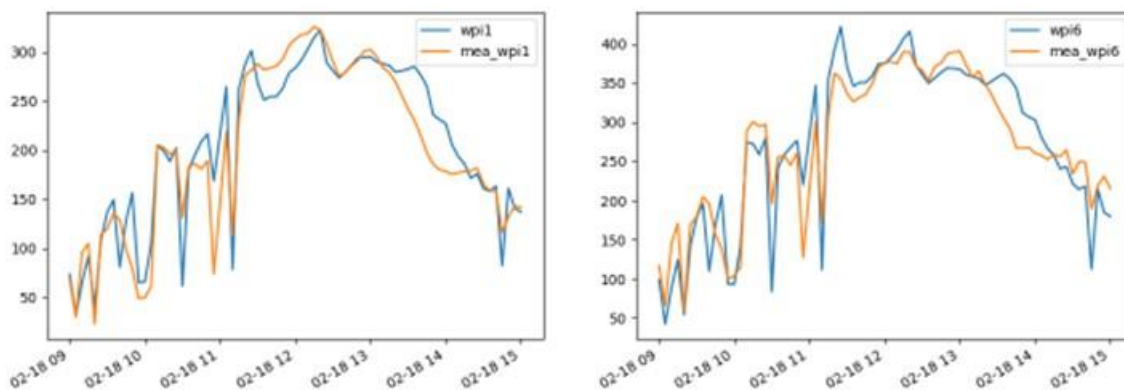
Source: LBNL

Figure 5.17: Simulated and Measured Workplane Illuminance in the FLEXLAB with a TDD
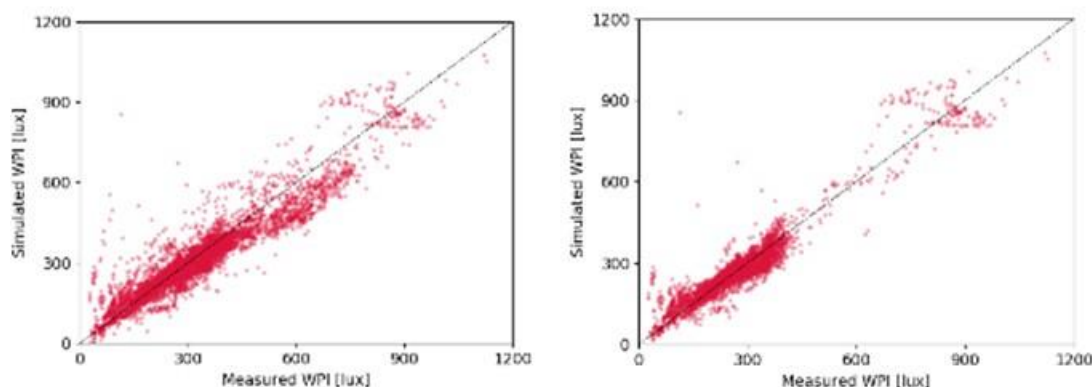
Simulated and measured workplane illuminance: (a) Left image: All monitored sensor data (RMSE 19.1 percent);
(b) Right image: Outlier data excluded from eight sensors (16.2 percent).

Source: LBNL

For conventional skylights such as diffusing plastic domes, the ability to simulate annual performance depends on being able to characterize the light-scattering properties of the skylight glazing material. For conventional diffusing plastic domes, the challenge is that the total transmittance of this material is very low, so angle-dependent measurements tend to be noisy if a standard spectrophotometer is used. LBNL will be building a new spectrophotometer facility that will enable measurement of angle-dependent properties and hemispherical transmittance of thick diffuse samples and samples with large-scale, inhomogeneous features.

5.3.2. Characterization Methods for High-Resolution BSDF Datasets

With the building industry's rapid adoption of advanced simulation tools that rely on BSDF data as input, there has been an increased demand for BSDF data for the vast array of shading and daylighting products available on the market. Several organizations have published BSDF data in the past, and there have been continued low-level activities worldwide to develop comprehensive databases for general use. In the United States, the industry-led Attachments Energy Rating Council (AERC) has been working with LBNL to define BSDF measurement standards for fabric roller shades, venetian blinds, metal screens, cellular shades, and other common shading devices. This activity has focused on generating BSDF data to evaluate heating and cooling energy use for residential applications. The European Solar-Shading Organization (ESSO) has been conducting a parallel activity.

For the commercial buildings sector, evaluation of daylighting and visual comfort performance is important to the industry. Here, current (2018) LBNL BSDF datasets provided by WINDOW and the international glazing and shading database (IGSDB) and BSDF characterization protocols developed for determining solar heat gains are likely

insufficient for daylighting. This insufficiency is due to inadequate characterization of specular transmission and reflection (e.g., peaks due to direct sunlight through shade fabrics or reflected by reflective surfaces). An LBNL study is in progress to review the various methods of generating BSDF data and determine the sensitivity of annual daylighting performance metrics to BSDF parameters (e.g., resolution of measured data, BSDF basis resolution, etc.), then validate BSDF characterization methods with field measured data. Due to the cost to measure and generate BSDF data, it will be important to develop time-efficient methods for generating accurate, high-resolution BSDF data.

As a solution, measurement standards and tools were developed to improve modeling of the specularly transmitted beam component, and evaluated using field measured data. This work will continue in collaboration with the AERC industry group and with partner research organizations through the International Energy Agency Solar Heating and Cooling Programme (IEA SHC) Task 61, Subtask C.

5.4. Technology Transfer

5.4.1. Detailed Tutorial for Radiance Matrix Methods

The research team developed a detailed tutorial to explain to users how to conduct annual daylight simulations using matrix methods (Subramaniam 2017). The tutorial provides an overview of the matrix methods, then explicit step-by-step instructions on how to create the vectors and matrices needed for the calculations using Radiance tools (Figure 5.18). It also provides case study examples and example code for the user to follow. The tutorial is designed for those who have command-line programming experience (e.g., students, advanced engineering firms) or for developers who wish to incorporate the open source models into their commercial software tools.

Figure 5.18: Explanatory Diagram From the Tutorial: Components of the Matrix Calculation
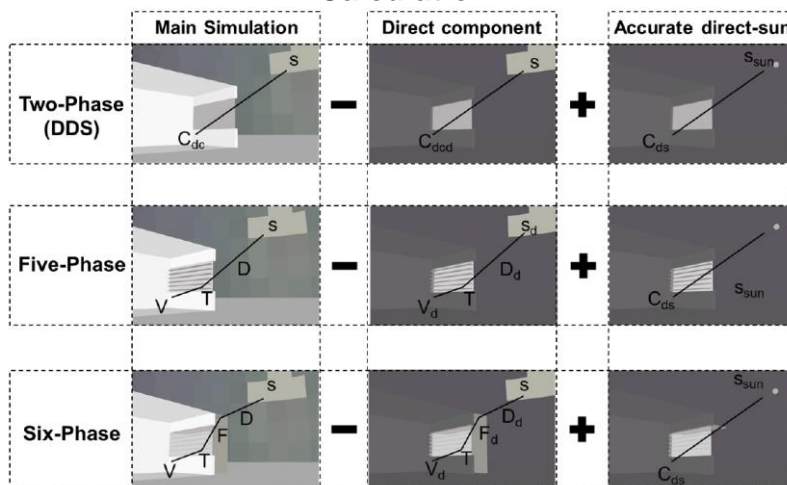
Source: LBNL

At the completion of the tutorial, the authors of Honeybee and LightStanza had incorporated the five-phase method in their open source software tool. (Most other vendors had the two- or three-phase method incorporated in their tools.) The tutorial is available on the Radiance website at https://radiance-online.org/learning/tutorials/matrix-based-methods.

5.4.2. Supporting Tools for Modeling Non-Coplanar Systems

The research team developed three tools to automate generation of the F-matrix for noncoplanar systems, simplifying the use of these systems:

- The *genmodel* enables users to input a few values to generate the code needed to describe a simple box-shaped space with one window and one rectilinear, noncoplanar shading element with a specified tilt angle. This tool is useful for vendors of awning or canopy shading systems who have no knowledge of computer-aided design (CAD) tools and enables simple comparative analysis of shading products.
- The *genfmtx* and *idfxmtx* are tools that automatically generate the F-matrix and IDF file for use in annual energy simulations.

A tutorial was developed to explain use of the above-listed tools with the LBNL WINDOW software, including an example showing use of the resultant matrices in EnergyPlus to compute window heat gains (Wang and Lee 2018).

A second script (*radmtx*) was created that automates generation of workflow for any of the multiphase matrix methods, given a set of simple inputs and specifications for accuracy. The user provides any arbitrary geometry for the building and façade, assigns the BSDFs for the various windows, and specifies climates, window orientations, level of accuracy desired, and desired output. The resultant comma-separated values (CSV) output file can be used as a scheduled input to EnergyPlus for window heat gain calculations. Operable windows can be modeled by dividing a window into zones and then assigning a BSDF file for the controlled state to each zone at each time step of the simulation. Development and testing of these scripts will be completed in 2019.

5.4.3. Modeling Annual Performance

The COMFEN tool is a simple front end user interface to EnergyPlus that enables quick analysis of a shoebox (rectilinear) space with a window. The tool was developed in a prior California Energy Commission project, then further developed under a synergistic U.S. Department of Energy project to support its use for rating and labeling shading products for the AERC program. This AERCalc tool enables users to compute an annual heating and cooling energy use rating for a wide variety of shading products that are typically used for residential applications. For the window heat balance calculation, models for convective and conductive heat flow within, through, and around the sides of the shade were updated based on the type of shade being modeled (e.g., fabric shade versus venetian blind or cellular shade), verified under laboratory conditions in

the LBNL Infrared Thermography Laboratory, and validated using the LBNL Mobile Window Thermal Test calorimeter facility (MoWiTT).

5.4.4. Standards, Rating, and Certification of Shading and Daylighting Attachments

With Title 24 2013 (California Code of Regulations Title 24, Part 6 and Part 1, Chapter 10, effective July 1, 2014) and ASHRAE 90.1 2013, daylighting controls in perimeter zones became more broadly mandated in commercial buildings (i.e., required in side lit spaces with greater than a 120 W [Title 24] or 150 W load [ASHRAE 90.1]). The U.S. Green Building Council (USGBC) Leadership in Energy and Environmental Design (LEED) Indoor Environmental Quality program also allotted points for daylighting. These requirements increased the demand for annual daylight simulation tools, such as Ladybug/Honeybee, DIVA-for-Rhino, Integrated Environmental Solutions Virtual Environment (IESVE), and a host of other software tools that use the Radiance matrix methods in core calculation engines of these tools.

In 2017, a Title 24 2019 proposal for supporting advanced daylighting measures was developed by Southern California Edison (SCE) and its consultants, Determinant and Vistar Energy. Lawrence Berkeley National Laboratory participated in technical discussions and clarified use of the BSDF data and matrix algebraic methods in support of defining credits under the Title 24 prescriptive approach. The investigation was informed in part by measured outcomes from a FLEXLAB field test that was conducted under a separate, Pacific Gas and Electric (PG&E)-funded LBNL project (Lee et al. 2016). The CASE team determined that there were insufficient BSDF test standards and data reporting standards to support the proposal. (For example, the current ASTM E2387 provides a standard for a measurement procedure but does not provide guidance on angular increments or data file structure). These gaps are being addressed in current LBNL work.

Model development and validation for WINDOW, THERM, Radiance, and EnergyPlus also were synergistic to the development of rating and certification programs (National Fenestration Rating Council [NFRC], Attachments Energy Rating Council [AERC], and U.S. Environmental Protection Agency [EPA]) for commercially available shading and daylighting products. Extensive work was conducted to support AERC's development of a residential rating and certification program for shading attachments under a synergistic DOE project. Development and validation of thermal models involving convective, conductive, and radiative heat transfer through window and shading attachments were also conducted under the DOE project. Products were rated based on annual heating and cooling energy use consumption for a prototypical home in a cold or hot climate.

For the commercial sector, work is underway at AERC to develop a comparable rating and certification program. Unlike the residential sector, commercial sector ratings need to incorporate lighting energy use, daylight, glare, thermal comfort, and view for

manual and automatically controlled shading and daylighting attachments. Work described under Chapter 6 of this report contributed to modeling operable attachments using Radiance, EnergyPlus, and Spawn of EnergyPlus software tools.

5.5. Conclusions

Matrix algebraic methods combined with BSDF input data enable time-efficient use of ray-tracing algorithms to determine annual energy and non-energy performance of optically complex fenestration systems (CFS).

Which matrix method should be used? The validation work conducted under this project has made clear the limits of applying the ray-tracing based matrix approach:

1. For metrics that do not require that the solar flux be distributed with significant spatial accuracy (e.g., window heat flow), the two-, three-, or four-phase matrix methods are sufficient.

2. For metrics that require a high degree of spatial accuracy in the determination of direct sunlight (e.g., high-intensity direct sunlight on the head versus lower-intensity sunlight across the upper body for thermal comfort), the high-resolution five- or six-phase matrix methods are required.

What resolution of BSDF input data is needed? The BSDF input data cannot be used interchangeably between the two applications listed above. BSDF data, such as those provided by WINDOW, have been derived for low-resolution matrix calculations (i.e., Klems 145 x 145 basis with angular resolution of 10°–15° apex angle) using a limited set of measured data. BSDF data with this resolution may be sufficient for the DC (two-phase), three-phase, and four-phase methods. Methods for deriving high-resolution BSDF data for metrics that require greater spatial accuracy such as glare have involved more detailed measurements. Low-cost, high-resolution methods of characterizing fenestration materials and systems are under development. In the meantime, for fenestration materials and systems that have some component of specular transmission and imprecise geometry (e.g., roller shade fabrics), it is best to not assume that the BSDF data from WINDOW are sufficient for high-resolution BSDF modeling requirements. For systems with a precise replicable geometry and a matte reflectance, such as a venetian blind, high-resolution BSDF data can be generated using the Radiance tool *genBSDF* with a geometric model and simple reflectance measurements.

What is the trade-off in labor to set up the workflow? The time needed to set up the workflow for the matrix methods can be a significant barrier, so knowledge about accuracy and speed trade-offs for the various methods can help users decide which method to use. Results from the validation studies provided some insights into the trade-offs on accuracy compared to measured data. For users of packaged software tools, many of these decisions are made by the software developer. Here, providing transparency on the underlying assumptions made by the software developer can help the end user better understand the limitations and accuracy of results. To simplify use, LBNL developed a cross-platform, command-line tool that automates the workflow for

any of the numbered phases of matrix methods. The tool consists of a Python library for each part of the workflow, and the library can be easily adapted by other software developers or advanced users. This tool will be tested by expert users then released as open source code to the Radiance community in 2019. The tool was designed to lower the simulation barrier, decrease human error, and provide a packaged workflow that can be integrated with other simulation tools. As for differences in run time between methods, the addition of matrices does increase computation time by a factor of 2–8 times, depending on the method, parameter being computed, and model complexity. A detailed investigation into run time was not conducted.

Which method should be used for which application?

- For architectural projects in the early concepts phase of design, the two-phase matrix method is likely to be the most practical for studying daylighting, solar control, and comfort impacts of core and shell designs that are evolving via rapid iterations. This is true especially for designs that are geometrically complex (e.g., curved façades, or façades with nonrepeating elements). This method has been implemented in many daylighting software tools.

- The three-, four-, five-, and six-phase methods are practical if the performance of various shading or daylighting attachment options are being studied parametrically; i.e., the BSDF matrix can be substituted for another, while the other matrices can remain without the need for recalculation. It is this feature that gives the matrix method tremendous power over pure ray-tracing or the two-phase method. Through simple substitution of the BSDF matrix using the three-or-greater phase methods, parametric analysis of shading and daylighting systems can be conducted for comprehensive studies in support of design optimization studies, energy-efficiency codes and standards, or for rating, labeling, and certification programs. Operable shading and daylighting systems also can be modeled easily.

- If accurate modeling of direct sunlight is an important factor in the simulated outcome, then the five- or six-phase method should be used to evaluate performance. Metrics such as annual sunlight exposure, visual comfort, and thermal comfort are sensitive to direct sunlight. For these methods, it is also important to use high-resolution input BSDF data.

5.6. Benefits to Ratepayers

Given improvements in accuracy and speed, matrix methods are opening new opportunities for innovative technology R&D, building design, code development, and rating and labeling programs, thereby contributing toward California and national goals of reducing building energy use and greenhouse gas emissions and opening new opportunities for the growth of new industries. New technology designs can be derived by auto-generating prototype designs, computing annual performance, and then converging on optimal designs using genetic algorithms or other optimization

algorithms. Parametric simulations can be used to identify critical design parameters on which to focus, potentially extending the depth of daylighting and improving comfort. Similar techniques can be used by the building engineering community to generate more optimal architectural designs.

New performance metrics can be developed for technology and design assessments. The Illuminating Engineering Society of North America (IESNA) Lighting Measure 83 (LM-83) metrics for daylight quality, for example, were developed by correlating human subjective response to simulated data generated using an early implementation of the matrix method. The metrics were adopted by the USGBC LEED program and have driven demand for daylight in buildings in the real estate market.

Commercially available fenestration products can now be rated more equitably, enabling product differentiation based on performance. Rating and certification programs such as that being developed by the AERC help create market demand for innovation, which in turn provide incentives for continued investment in developing energy-efficient products.

With the push to zero-net-energy buildings, accuracy improvements in loads estimation support the development of advanced HVAC and lighting systems. For multipurpose technological solutions, application of these tools could also support the development and evaluation of building-integrated photovoltaics, solar-thermal heating and cooling, and thermal energy storage strategies.

CHAPTER 6:
Dynamic, Integrated Façades

6.1. Introduction

Dynamic façade technologies such as operable shades and windows, switchable electrochromic coatings, and daylight-redirecting technologies have the potential to significantly reduce lighting and HVAC energy use in buildings through management of solar heat gains and daylight and, to a lesser extent, conductive and convective loads. Performance, however, relies on control algorithms that are able to effectively balance HVAC and lighting energy-use trade-offs in response to variable load conditions that occur with changes in weather, occupancy, and operating conditions. For example, closing a shade to reduce cooling energy use during the day may result in an increase in lighting energy use due to reductions in daylight. Given the thermal capacitance of the building or active use of thermal mass, admission or rejection of window heat gains could be timed to support preheating or precooling strategies that shift loads to periods when energy costs are lower. If one overlays variable utility rates and non-energy performance factors (e.g., visual and thermal comfort, indoor environmental quality, view, privacy), determining how "best" to control a dynamic façade can become a large optimization problem.

State-of-the-art dynamic façade controls use rule-based algorithms to manage dynamic façades in real time. Rules and threshold values can vary with climate and site-specific conditions. For many systems, there is little to no feedback on how an adjustment in one threshold value affects the performance of a codependent variable, making maintenance over the life of the installation effectively an opaque, trial-and-error process. With rule-based controls, there are no forecasting capabilities. For example, if the local summer weather pattern is foggy in the morning then clear and sunny in the afternoon, the controller may admit solar gains and daylight to offset heating and lighting requirements in the morning, and then be penalized for cooling loads in the afternoon. One could derive a set of rules to encompass load-forecasting objectives, but such solutions would likely be unique to each application, costly, and difficult to maintain.

This project investigated the energy efficiency potential and technical feasibility of using model-predictive controls (MPC) to control dynamic façade technologies more optimally based on forecasted projections of HVAC and lighting energy use, visual comfort, daylight quality, and other relevant performance parameters. Quantifying, weighing, controlling, and reporting impacts have become increasingly more pertinent as California moves toward high-performance buildings within a flexible, demand-responsive electricity market. MPC offers a potential low-cost, transparent, and adaptable alternative to rule-based controls. An MPC controller was developed,

prototyped, and tested in a full-scale outdoor testbed. Load shed and shift potential of the MPC controller were evaluated in a virtual test environment. The project team made an initial assessment of the benefits and challenges of implementing MPC dynamic façade control solutions based on the results of this study.

6.2. Project Approach

With MPC, a model of system operation, along with forecasts of disturbances, is used to predict future performance and optimize setpoint schedules or control inputs or both over a specified time horizon. The solution of the first control step is implemented, then the optimization is solved again with updated information (system state and disturbance forecasts) for the next control step. The primary advantage of MPC is that it enables optimization of many variables over a forecasted period, is modular (which makes scaling from small to large applications easier), and has the ability to adapt automatically to a changing context over the life of the installation.

Central to MPC are the model and optimization algorithms, which pose several challenges. The models must be sufficiently accurate to predict the performance of the system while being computationally efficient so they may be used within optimization algorithms. The mathematical structure of the model plays a large role in qualifying the types of optimization algorithms that can be used and to what degree of efficiency the optimization problem is solved. This includes speed and convergence to an optimal solution. In general, gradient-based optimization algorithms are more efficient than numerically based optimization algorithms (Wetter et al. 2016). However, gradient-based optimization algorithms require continuous, differentiable models. In the context of building operation, where equipment may operate only in discrete states or operating modes may change at discrete times, this continuity requirement is not always achievable.

Solving these challenges was the primary focus of this project.[2] Gradient-based optimization algorithms were used to determine the optimum control state of the dynamic façade device(s). The project team developed models for determining solar heat gains, daylight illuminance, and discomfort glare. Design analysis focused on determining how to maintain high model fidelity and achieve convergence within the defined time step. With the gradient-based algorithms, pre- and post-optimization methods needed to be developed to handle conversions between discrete and continuous states of control. Iterative testing and evaluation of the prototype relied on the MPCPy open source framework that was developed by LBNL under parallel synergistic work (Blum and Wetter 2017). The framework was based on JModelica, which enabled testing of MPC either in real time connected to a building or, for

---

2 This project did not address the broader issues of interoperability between building systems or networking and communications protocols. These issues were assumed to be addressed by standardization organizations and the building controls industry as a whole.

development and performance testing, in simulation with an emulated building model controlled by the MPC controller.

The MPC control system was prototyped, then tested and evaluated in the field. These tasks required development of a workflow framework that handled user inputs for model configuration from the facility manager and occupant, inputs from sensors and external sources of data, and conversion of the MPC code to work within the computational and memory limits of an embedded controller. The project team conducted field testing with a three-zone electrochromic window installed in the LBNL Advanced Windows Testbed. The prototype was further developed and evaluated within a virtual "emulator" environment using a model of a Title 24 2013-compliant perimeter zone in a large commercial office building.

6.3. Results

6.3.1. Conceptual Design

The objective of MPC control was to modulate solar heat gains and daylight using dynamic façade technologies to minimize time-of-use (TOU) HVAC and lighting energy cost based on forecasted weather and occupancy within comfort and daylight indoor environmental quality constraints.

The project team developed the MPC façade controller for a single, box-shaped, perimeter office zone with a vertical window (Gehbauer et al. 2017). The test case involved an electrochromic window subdivided into three horizontal control zones (top, middle, bottom), each of which was independently controlled to one of four tint states. Other types of dynamic façade elements and design configurations could be modeled using the same workflow. (The matrix methods described in Chapter 5 were used for this study.) The dynamic façade was designed to be shipped as a factory-assembled curtainwall unit or retrofit shading system with the MPC controller, sensors, power, and wireless networking and communications incorporated as a unit. Sensors included indoor and outdoor temperature sensors, an occupancy sensor, and a window-mounted sensor to acquire hemispherical luminance data. (This last sensor was developed within this project.) Weather forecast data would be acquired through the private network. For the base design, no data were required from the HVAC and lighting control systems: the dynamic façade controller operated autonomously. The team also conducted exploratory research to evaluate the load-shifting potential of dynamic façades combined with thermal mass. For this second design, the team designed the MPC controller to control the dynamic façade and the room thermostat.

To configure the base MPC façade controller before shipping the unit, the manufacturer would need to enter site-specific information using a Web-based interface. This information includes site location, simple room and window geometry, electric lighting setpoint and power-to-light dimming profile, cooling and heating efficiency, thermostat setpoints and schedule, utility rate schedule, occupant view position, and glare and

daylight thresholds. Characteristics of the building would be selected from a pull-down list of typical regional construction assemblies for the building type. Occupancy and utility rate schedules could also be selected from a predefined list. After installation, the occupant would be able to modify a subset of these settings (e.g., glare and daylight thresholds, location in the space, view position) using a Web-based interface on a computer, mobile phone, or wall-mounted touchpad. Updates to the controller, such as view position, would occur within a few minutes. If the space is reconfigured or if building equipment is upgraded, the facility manager would be able to update the system using the Web-based interface.

When activated for control, the MPC controller collects data from the sensors, obtains weather forecast data from the National Oceanic and Atmospheric Administration or other sources, then runs the optimization solver to determine how to actuate the dynamic façade. The Web-based interface logs and displays real-time status of sensors, control status of the façade zones, and value of various performance indices (estimated HVAC and lighting energy use, glare, daylight, energy cost) for troubleshooting and analysis.

A few underlying assumptions formed the basis for this conceptual design:

- A simple box model of the perimeter zone was used to predict daylight illuminance, glare, and solar heat gains in real spaces. Performance could be improved with a more detailed model (e.g., from three-dimensional computer-aided drawings of the final building), but this was assumed to increase setup costs significantly. Adaptive tuning using parameter estimation techniques could improve and maintain model accuracy over the life of the installation. Determining feasibility of adaptive tuning is the subject of future work.

- A window-mounted, hemispherical luminance sensor was assumed commercially available at low cost. A prototype sensor based on a high-end digital camera and fisheye lens was developed and tested in the Advanced Windows Testbed to support the MPC field tests. Alternatively, outdoor imaging sensors have been developed and are emerging on the commercial market (Terrestrial Light 2018; Motamed 2017).

- The base MPC façade controller ("MPC1," defined in Section 6.3.4) was assumed to operate autonomously with no data received from the HVAC or lighting controllers. For the second MPC controller ("MPC2-precool"), the coefficient of performance (COP) and heating efficiency were assumed static inputs, but the controller was designed to actuate the façade and thermostat.

Full integration of the façade, HVAC, and lighting systems with data exchanged among the networked systems was not investigated. Inclusion of more detailed HVAC models (e.g., dynamic efficiency as a function of outdoor air temperature and part load) is possible, but to provide robust control, data exchange among systems would likely be necessary (e.g., real-time data for fan and chiller power consumption, with air handling

unit [AHU] airflow and cooling coil load passed from the HVAC controller to the façade controller). Interoperable data exchange between systems would be most cost-effective if provided by system integrators (companies that integrate a wide range of control services into a single central building automation system) or by a consortium of vendors who have demonstrated turnkey interoperable control between products. These issues were also postponed for future work.

6.3.2. Implementation

The conceptual design was reduced to practice and field tested to evaluate real-time performance. The overall control system was designed as an agent-based system (Gehbauer et al. 2017). An *agent* is defined here as an independent, discrete, self-contained software component with a set of characteristics and behaviors that can function independently, but also has the ability to recognize other agents with which it interacts. Tasks within the overall control system were split into individual, autonomous operating units and optimized for a specific objective (Figure 6.1).

Figure 6.1: Overall Façade Control System Architecture
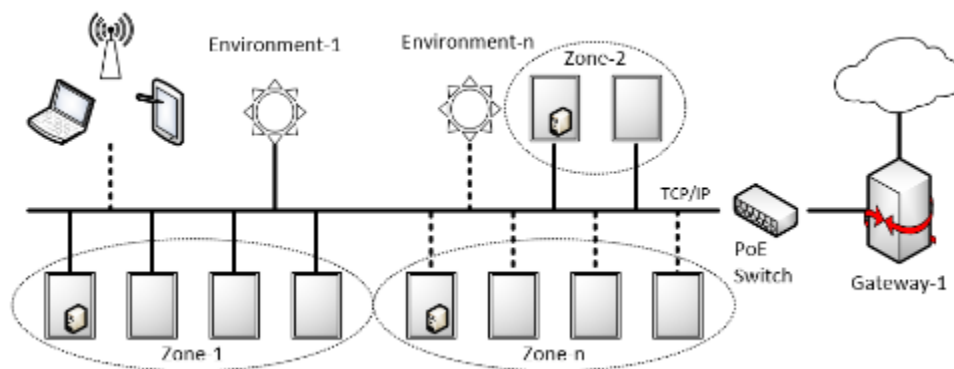
PoE: Power over Ethernet; TCP/IP: Transmission Control Protocol/Internet Protocol.

Source: LBNL

Communications within a local network were designed to be via Ethernet or Wi-Fi (IEEE 802.11) with access points for Wi-Fi-connected tablets and smartphones. Each zone controller runs several agents on the same platform. A gateway provides a single node with dual Ethernet connection to get weather data from the Internet and share the data within the private control network. Real-time environment sensing stations were built to be modular, with an accompanying sensing agent. Since each device was operated autonomously, the resulting asynchronous communication between devices was realized with a simple Hypertext Transfer Protocol (HTTP) Representational State Transfer (REST) application program interface (API). This allowed standard Web browsers to communicate with the devices, which enabled synergies with other devices for future/additional applications. Each of the hardware devices, such as a zonal controller, environment stations, and gateway, is assumed to be a low-cost, embedded controller. The Raspberry Pi 3 Model B microprocessor was used for the physical

117

prototype, providing a 1.2 gigahertz (GHz) quad-core processor, 1 gigabyte (GB) random access memory (RAM), and built-in Ethernet support for a user price of $35/unit. The total cost for the MPC controller was estimated to be $80–$105, including controller, sensor, power, and wiring, based on the retail cost for components. Volume costs are likely to be much lower.

The dynamic façade controller was field tested in the Advanced Windows Testbed (Figure 6.2) over a year through the various iterations in controller design. During this period, the controller demonstrated consistent feasibility on a laptop (Intel 2x2.3 GHz, 4 GB RAM), which was used instead of the Raspberry Pi (ARM 4x1.2 GHz; 1 GB RAM) due to compatibility issues when compiling the JModelica package on the ARM central processing unit (CPU) architecture. A cross-compilation where JModelica is compiled on a regular computer, emulating an ARM architecture, would likely solve this issue. On the laptop, the optimization solver was able to converge to an optimum solution within 10–30 seconds depending on the time of day with varying disturbances (e.g., varying solar conditions, occupancy). Extrapolating the results, a Raspberry Pi with about half of the computing power should be able to solve the problem in about double the time. In addition, the two additional CPU cores of the Raspberry Pi could be used to speed up the computation.

Figure 6.2: Three-Zone Electrochromic Window in the Advanced Windows Testbed

Photographs of the south-facing testbed chamber with automated control of the electrochromic windows during a sunny November day (left to right) in Berkeley. The upper, middle, and lower zones of the electrochromic window were tinted independently in response to commands from the controller.

Source: LBNL

6.3.3. Optimization

6.3.3.1. Convergence Time

Controls based on MPC are typically used as slow-acting supervisory controllers, as they exploit the information from many sources to make global strategic decisions. Such supervisory knowledge is especially useful when optimizing for TOU rate structures, where a single 15-minute peak defines the cost of demand charges for the entire month. Other MPC applications are those that have large time constants, such as a radiant slab or applications where control has a significant effect on the objective, or

shifting peaks from high-price periods where mass must be charged in advance. Real-time, near-instantaneous control is typically conducted by a separate controller with different objectives. The approach in this project was to use MPC control as the *real-time* controller by implementing a fast-acting optimization, ultimately resulting in more optimal operation. The challenge with this approach is the convergence time of the optimization, which increases exponentially with the number of time steps and complexity of the problem. In the initial implementation, the convergence time was greater than the desired time step for control. To avoid long, intensive optimizations, the project team developed a multistage MPC framework where the workload was separated into a supervisory *major* optimization and a *minor* optimization, which were able to operate in real-time, i.e., time steps faster than 1 minute.

Figure 6.3 shows an example for a typical day. The number of iterations and corresponding convergence time required increases for the major and minor optimization between nighttime, when conditions are relatively stable, and daytime (i.e., from 3–20 seconds and 0.5–2 seconds, or 90–400 iterations and 50–100 iterations, respectively).

Figure 6.3: Time Required for MPC Optimization
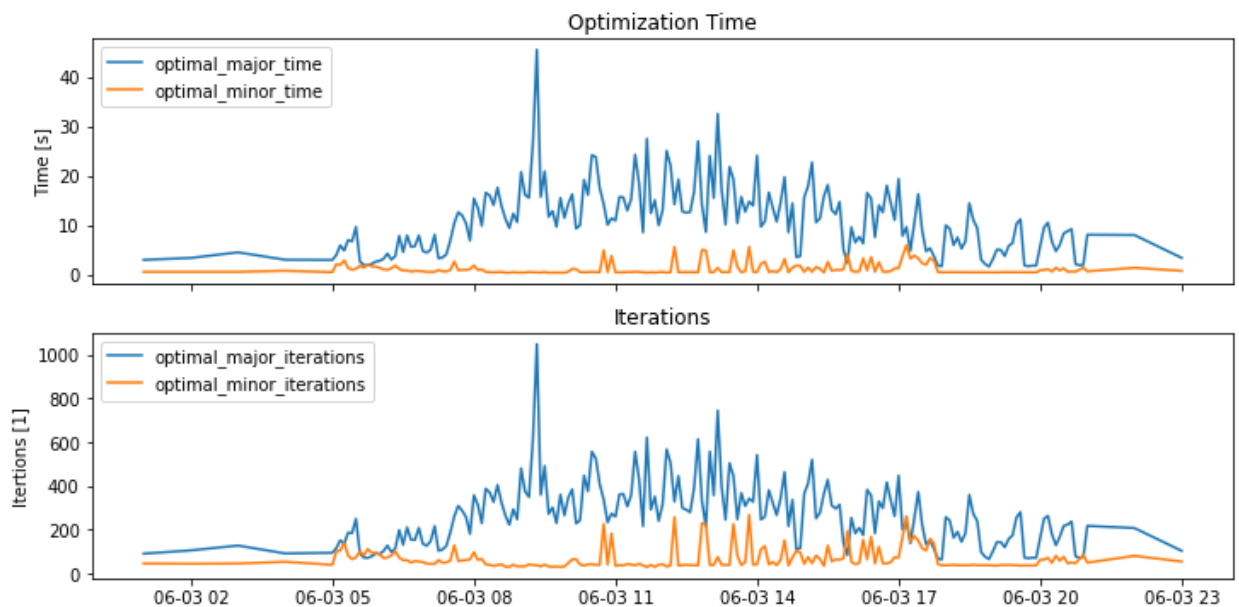
Typical convergence time and number of iterations before achieving convergence for the minor and major optimizations on a single day (June 3, 2018).

Source: LBNL

6.3.3.2. Model Accuracy

One key issue associated with the general field of model-predictive controls is poor performance due to "model mismatch." This term describes the difference in expected performance between that of the MPC controller and the actual simulated and real-

119

world, observed performance. Typically a measurement of error, i.e., root mean square error, is defined to evaluate the quality and accuracy of MPC models. However, for optimization, the evaluation of individual component model performance is confounded because the models are used in combination with other models to determine the final control state. As an example, a control objective of minimizing total energy cost using TOU rates was defined for this study, where the controller had to shift thermal loads to avoid expensive peak demand charges. Accurate projections over several hours were necessary, which then defined the requirements for the model. The project team evaluated the performance of the final model with the associated submodels and component models based on the defined objective.

Figure 6.4 shows an example of the projected and actual room air temperature produced by a precooling strategy ("MPC2-precool") that actuates the dynamic window and zone thermostat using a first-order thermal model (RC). The results of the major optimization are shown as colored lines for a 24-hour prediction horizon for each 5-min interval. The dotted lines indicate the temperature band setpoints passed to the emulator from the MPC controller. The solid black line shows the observed zone air temperature from the emulator. The setpoints can be distinguished as floating (i.e., the setpoint is at a comfort range) or actively controlled (i.e., when precooling). It can be seen that in the early morning before occupancy starts, the temperature tracks the projected temperatures. However, at 8 a.m. local time (7 a.m. on the plot, in standard time) when occupancy starts, the room air temperature rapidly rise, whereas the earlier MPC2-precool projections (colored lines) indicate coasting throughout the day without the need for mechanical cooling during peak periods. This is a strong indicator of overestimated thermal mass, as the RC model lumps all thermal mass in the concrete together with the air mass.

Figure 6.4: Projected Zone Air Temperature Using the RC Model
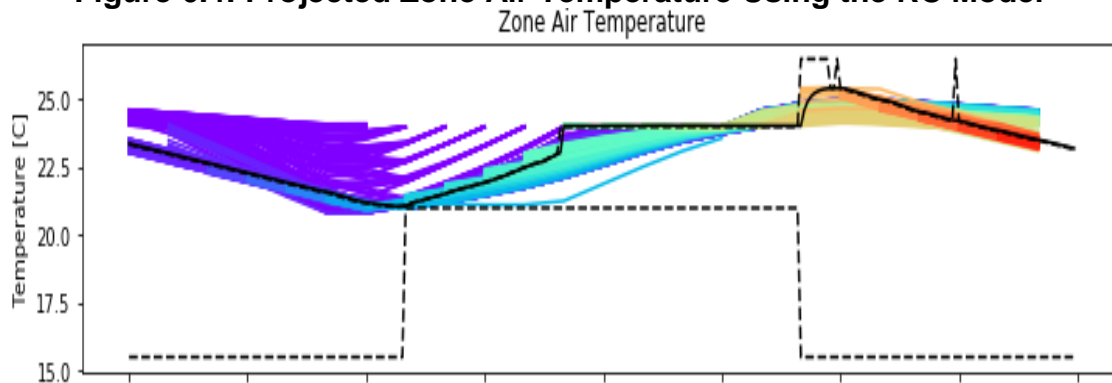
Figure 6.5: Projected Zone Air Temperature Using the R2C2 Model
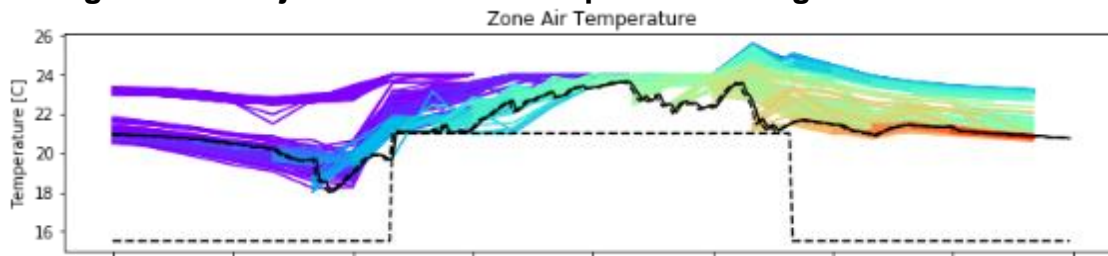
Summer period, Oakland: Example of projected room air temperature by the MPC2-precool major optimization using a first-order RC (above) and second-order R2C2 thermal model (below) versus observed temperature from the emulator, in black. The colored lines show the projected MPC2-precool results for 24 hours, for each 5-min. control time step, colored from violet in the morning to red in the evening.

Source: LBNL

Options to improve MPC control include use of higher-fidelity models and tuning the model using empirical data from the site. Higher-fidelity models specifically allow for the separation of fast and slow dynamics. In this case, using a R2C2 resistance-capacitance model (an RC model models transient heat conduction and storage in building surfaces) would allow for the separation of the *air* thermal mass, the temperature of which responds quickly to heating and cooling inputs, and *concrete* thermal mass, the temperature of which responds slowly to heating and cooling input. This model then allows for the capture of the effect seen in Figure 6.4, where at the time occupants arrive, the air temperature is likely to heat quickly compared to the slab temperature. It also accounts for the fact that, with an air-based system, charging of the concrete slab only occur can through cooling of the air to a temperature lower than the slab temperature. This cooling would require the MPC controller to cool the air significantly more during the night than what is shown in Figure 6.4. Figure 6.5 shows an example of the projected and actual room air temperature produced by MPC2-precool using an R2C2 model. The results show that the two phenomena described are predicted by the MPC controller, that the air needs to be cooled significantly during the night to charge the slab, and that the air temperature changes more quickly with heating or cooling inputs.

The R2C2 model is more difficult to calibrate manually than the RC model due to the increased number of parameters. Therefore, the R2C2 model was calibrated with a parameter estimation algorithm, implemented automatically every day at midnight using LBNL's MPCPy framework. The algorithm solves an optimization problem where the objective is to minimize the average error between modeled and measured data by adjusting the parameters of the model, subject to constraints. The air and slab temperatures of the model were set to those measured in the emulator at each midnight to prevent error from accumulating. This is reasonable because the MPC controller needs to predict only 24 hours.

6.3.3.3. Discrete and Continuous Control States

With the selection of the nonlinear optimization solver (IPOPT), it was necessary in the preoptimization stage to convert calculations of illuminance and solar heat gains for each discrete tint state into a continuous function for the optimization. This conversion introduced a small error since the computed values for the electrochromic glazings were fit with an exponential function. With other systems (e.g., venetian blinds), this relationship is likely to be less well behaved. In the postoptimization stage, however, conversion from the continuous state to the discrete state relied on predicted glare and daylight constraints, which resulted in considerably less optimal control than if continuous control of the device were an option. For example, the visible transmittance (Tvis) levels of the four tint states of the electrochromic were Tvis = 0.60, 0.10, 0.06, and 0.01. So, if the desired control state was Tvis = 0.36, then the controller would have to determine whether to control the window to discrete state Tvis = 0.60 or Tvis = 0.10, both of which result in less optimal solar control, daylight, and glare performance than the continuous optimum state (Tvis = 0.36). The manufacturer is able to increase the number of tint steps. Other electrochromic manufacturers offer products with continuous tint control (e.g., 100 stepped values).

The optimization solver included a constraint to dampen switching of the tint state for each zone of the electrochromic window when controlling to increase daylight (control to decrease comfort had no imposed delay). This is important for user satisfaction, particularly under partly cloudy conditions (and for motorized shading systems that produce noise and visual distraction when actuated). In addition, the switching speed was included as a constraint. The electrochromic window being field tested in this study can take up to 10 or more minutes to switch fully between the clear and darkest tint states if the glass surface temperature is cold. Both constraints were implemented as derivatives and were used initially in the optimization solver. The constraints were later disabled in the simulation study due to the added complexity in modeling the controller and analyzing the results.

6.3.4. Estimated Energy Cost Savings

The project team used an emulator to evaluate the energy cost savings of the model-predictive controller compared to rule-based control. A south-facing perimeter zone with the three-zone electrochromic window in a prototypical large office building was modeled to comply with the California Title 24 2016 Standard (Energy Commission 2015). The team used Radiance models to determine solar loads, daylight illuminance, and discomfort glare. Window and room heat balance calculations were conducted using models from the Modelica Buildings Library, which were validated in a separate study (Wetter et al. 2014; Nouidui et al. 2012). Simulations were performed for a clear sunny week in the summer and winter in two California climates: Oakland (moderate) and Burbank (moderate to hot). The team modeled the Pacific Gas and Electric E-19 TOU rate schedule. Hourly typical meteorological weather (TMY) data were used, where 5-minute data were derived using a linear interpolation from hourly observations.

Several control scenarios were modeled (Gehbauer et al. 2018):

- *Heuristic* control was defined by a state-of-the-art, rule-based control algorithm from a prior field study in a large office building in Sacramento (Fernandes et al. 2016). The objective of the algorithm was to reduce sky glare, preserve daylight, and minimize cooling loads due to solar heat gains based on input from an exterior vertical illuminance sensor.

- *MPC1* control was defined by model-predictive control of the electrochromic window to minimize TOU energy costs due to HVAC and lighting over a 24-hour prediction horizon. Discomfort glare and daylight quality constraints were defined. The electric lighting system was assumed to dim continuously in response to available daylight (0.8 W/ft.^{2}, 120 W full power). The HVAC system operated based on scheduled thermostat settings, which were the same used in the heuristic case. Loads were converted to energy use using a fixed coefficient of performance (COP) of 4 and no economizer.

- *MPC2* was the same as MPC1 but with added MPC control of the thermostat, enabling precooling to be implemented based on forecasted HVAC energy costs. For this case, the top surface of the concrete floor was exposed (carpet and pad were removed), and heat transfer between the air and floor surface was modeled as natural convection on a horizontal flat surface.

Example results for a week during the summer in Oakland are shown in Figure 6.6.

Figure 6.6: Total Electricity Demand Profiles with MPC Controls
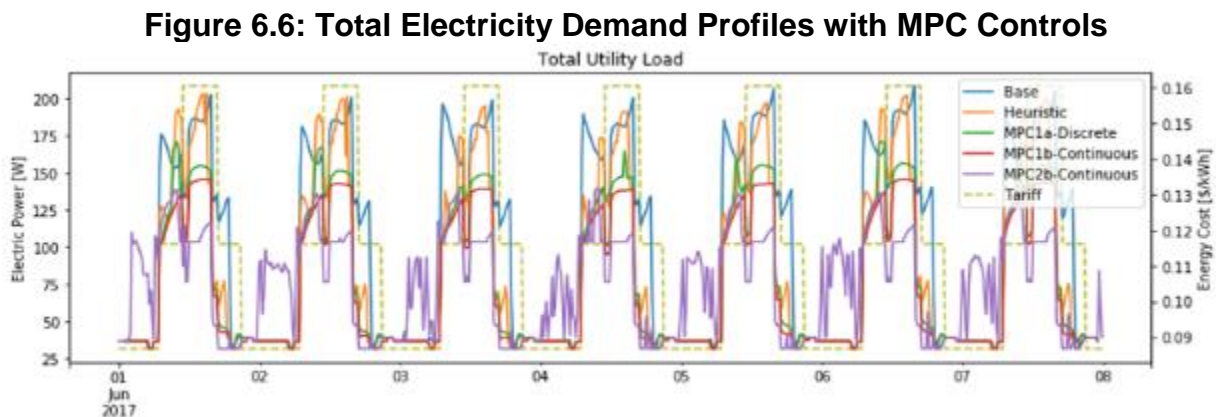
Total electricity demand versus time of day over a seven day sunny summer period for five control modes, Oakland. Energy cost is shown as a dotted line on the graph.

Source: LBNL

The total electricity use profiles demonstrate the significant load-modifying benefits of the MPC controls relative to the base case (manually-controlled indoor roller shade) and heuristic controller. MPC1 (for discrete and continuous tinting of the electrochromic windows) balanced demands for solar heat gain control and daylighting in proportion to energy cost. With MPC2, the load shift from peak afternoon to off-peak nighttime periods is quite evident. This shift was provided by the precooling in combination with

daytime solar control. Electric demand is nearly flat during the peak period between noon and 6 p.m. (delineated by the dotted energy cost line).

Compared to heuristic control, MPC1 and MPC2 strategies reduced total energy cost by 9-28 percent and coincident peak demand was reduced by up to 0.58 W/ft^2-floor or 19-43 percent on sunny summer days in Oakland. Similar percent savings were achieved for the hotter, Burbank climate.

Other control scenarios were modeled. With a modified E-19 rate schedule that shifts the peak period towards evening hours (5-10 p.m.), the electric use profiles are almost identical to those with the base E-19 rates. This is due to the non-coincident peak demand charge (highest 15 minutes of use regardless of when the peak occurs) imposed by both rate structures, which suppresses demand over the entire 24 hour period. If non-coincident demand charges are eliminated, then pre-cooling occurs in the morning hours prior to occupancy and peak demand is increased by 9 percent. If all demand charges are eliminated, then there is minimal pre-cooling and peak demand increases by 22 percent compared to MPC2 with the base E-19 rates. These scenarios demonstrate the flexibility of MPC to adapt to changes in utility rate structures that are likely to occur as California continues to adopt renewable energy.

6.4. Technology Transfer

The intended outcome of this project was to provide developers of dynamic façade systems with insights into the technical challenges and energy cost savings potential of model predictive controls, particularly given the state of the California electricity markets, which are evolving from increased statewide adoption of renewable energy sources. An MPC controller was prototyped, field tested to demonstrate feasibility, and evaluated in a virtual test environment using open source models and tools. Simulations of the MPC controller in a prototypical office zone demonstrated the load shaping potential of dynamic façade and significant energy cost savings and comfort / indoor quality benefits. MPC integration of dynamic façade and thermostat controls were shown to provide greater overall savings compared to state-of-the-art rule-based controls.

Throughout the development phase, the LBNL team engaged with technical advisory committee members and manufacturers of dynamic façade systems to solicit feedback and discuss interests in support of commercialization. Most dynamic façade manufacturers expressed interest in learning more about MPC-controlled façades.

The underlying models used in the MPC control algorithms are open source and available for all manufacturers to use for their own independent development efforts (i.e., WINDOW, Radiance, Modelica Buildings Library). The optimization solver (JModelica and IPOPT) is also available as open source software.

6.5. Conclusions

What technology was developed? This project developed a prototype, autonomous model predictive controller for a multi-zone dynamic façade system. The MPC controller used physics-derived models and a non-linear optimization solver to determine how best to balance competing solar control and daylighting requirements in real time for lowest energy cost over a 24-hour prediction horizon. Visual comfort and indoor environmental quality requirements for daylighting were set as constraints on the optimization problem. Inputs to initially configure the control system involved no more than a dozen inputs, minimizing setup costs. The MPC controller was designed to accept changes in utility rates, space geometry, building equipment operations, and occupant preferences over the life of the installation using a web-based application on a mobile device. These features increase the likelihood of occupant acceptance and satisfaction with automated control and sustained energy savings over the life of the installation. Sensor requirements were minimal, with the entire system costing an additional $80–$105, including controller, sensor, power, and wiring based on the retail cost for individual components. Costs are likely to come down with broad market adoption.

What benefits did MPC provide over rule-based controls? The MPC controller was shown to provide significant TOU energy cost savings in a south-facing, perimeter office zone during sunny summer and winter periods in Oakland and Burbank, California, compared to a state-of-the-art, rule-based control system. The MPC controller was able to achieve lower energy and demand costs (up to 28 percent) by shifting and shedding loads to periods when energy costs were lower, admit more daylight during the daytime to meet indoor environmental quality goals, and minimize glare discomfort compared to the heuristic controller. As utility rates change with the evolving California electricity markets, the MPC controller will be able to adapt and support load shift and shed objectives over the life of the installation.

Is the MPC workflow scalable? The controller prototyped in this study is scalable to the wide variety of cases where control can be limited to a single side lit perimeter zone (i.e., any size rectangular box, window size and glazing type, window orientation, climate, COP and heating efficiency, and dimmable lighting control system). Developing the initial MPC controller was challenging because there were co-dependencies between model fidelity, number of parameters included in the optimization problem, and computational speed (defined by the computational resources of the embedded controller and desired real-time control time step) that needed to be worked out. However, now that the optimization has been demonstrated to be feasible, the MPC controller can be used for the intended application without the need for further tailoring and redesign on a site-by-site basis. Alteration of the problem (e.g., from a single perimeter office to a corner office with two window orientations, or to open-plan offices with variations in window design across the façade) will require modifications to the MPC workflow, updates to the models, and re-testing for feasibility.

What are the commissioning and maintenance requirements? With rule-based controls, commissioning the system involves a trial-and-error process to minimize occupant complaints. In the case of the MPC controller, tuning the models involves minimizing the error between the predicted and actual performance metric using parameter estimation techniques, machine learning algorithms, and limited empirical data, including occupant feedback. With MPC control, the facility manager is able to visualize HVAC, lighting load, comfort, and daylight trade-offs and see the consequence of adjustments to model parameters. For the manufacturer, updates to the MPC controller over the life of the installation (15–30 years) will likely require updates to the workflow as models, tools, and solvers are improved. For these changes, staff with expertise in model predictive controls and building physics will be required. In addition, rule-based controls are also likely to require replacement within the building's lifetime, requiring a repeat of the iterative and lengthy commissioning process.

How were human factors addressed? Occupants often "interfere" with the well-intended operation of automated controls. However, lessons learned from monitored demonstrations in commercial office buildings indicate that if occupants understand the basis for the underlying control logic, automation is more likely to be acceptable (Clear 2010; Lee et al. 2013). In addition, if the control system is able to accommodate user preferences, the system is less likely to be disabled. In a prior human factors study (Clear et al. 2006), occupants were given a slider switch to set their preferred light level and indicate their sensitivity to glare; occupants found this system more satisfactory than the fully automatic system. In this study, the MPC controller was designed to accept user inputs: i.e., current location in the space, view position, preferred light level, and sensitivity to glare. The models and control thresholds can be modified to accommodate user inputs at any time over the life of the installation. If occupants are dissatisfied with the control system, it will most likely be due to inaccurate predictions of discomfort and the delayed response of the dynamic façade system (e.g., some electrochromic windows can take a long time to switch). Adaptive algorithms (based on real-time user inputs and/or data from additional sensors) will likely improve the quality of control. Further work will be needed to evaluate human factors at demonstration sites.

What are the intended applications? The MPC controller prototype in this project was designed for an office application where thermal conditions between zones are assumed to be near isothermal (i.e., no significant difference in temperature between zones). The workflow can be used to develop MPC controllers for complex building applications, but it is unclear whether complex solutions will be scalable or replicable for other building sites. Case study examples need to be developed and tested to determine how cost-effectively MPC can be applied in real-world situations.

Would data exchange with the HVAC and/or lighting system improve performance? The base MPC façade controller was assumed to operate autonomously, with no real-time energy use or control status data from the HVAC and

lighting systems. The control system incorporated occupancy-based schedules and setpoints but not the real-time operational details of the HVAC or lighting systems. The MPC2 strategy assumed MPC control of the zone thermostat and a fixed-average COP and heating efficiency of the overall HVAC system. For this case, zone air temperature data were needed to reduce model mismatch and improve control system performance No data were required from the lighting system. To improve MPC2 performance, inclusion of more detailed HVAC models (e.g., dynamic efficiency as a function of outdoor air temperature and part load) is possible. However, to provide robust control, data exchange between systems would likely be necessary; for example, real-time data for fan and chiller power consumption, with AHU airflow and cooling coil load passed from the HVAC controller to the façade controller. Interoperable data exchange between systems would be most cost-effective if provided by system integrators (companies that integrate a wide range of control services into a single central building automation system) or by a consortium of vendors who have demonstrated turnkey interoperable control among products. A supervisory, hierarchical control structure would need to be developed to incorporate explicit integrated control of the three end uses at zonal, building, and grid levels.

Next steps? Future work should address technical challenges associated with model mismatch and scaling to real-world applications. Discrepancies between projected performance from the reduced order models used in the MPC controller and actual performance (determined by the emulator) can cause degradation in MPC performance. Conversion from discrete to continuous states, then back to discrete states in the post-optimization stage, can also cause degradation in performance when non-linear optimization solvers are used. Adaptive tuning, as described for the R2C2 parameters in Section 6.3.3.2, should be investigated for the other models in the MPC controller. For discrete state control, the optimization problem should be reformulated and solved using mixed integer optimization solvers for systems with discrete (stepped) control. On the market side, discussions will need to occur between dynamic façade manufacturers, state regulators, and utility stakeholders to determine how dynamic façade technologies can be valued based on their load modifying potential.

6.6. Benefits to Ratepayers

California is making major strides toward meeting its greenhouse gas emission reduction goals, with the transformation of its electrical grid to accommodate renewable generation, aggressive promotion of building energy efficiency, and increased emphasis on moving toward electrification of end uses (e.g., residential heating). As a result of this activity, the State is faced with significant challenges of system wide resource adequacy, power quality, and grid reliability that could be addressed in part with demand responsive (DR) load-modifying strategies using controllable building technologies. Dynamic façades were shown in this project to have the ability to shift, shape, and shed loads at critical times of the day when model predictive controls were used instead of state-of-the-art heuristic controls. An autonomous MPC controller was

shown to provide significant energy cost savings. This controller could be deployed in the near term to help shape the load profile in commercial buildings during critical summer peak periods. An integrated MPC controller was shown to provide more significant energy and demand savings year round, helping California to meet its greenhouse gas emissions and demand side management goals over the long term.

GLOSSARY AND ACRONYMS

Term	Definition
AC	alternating current
A/E	architectural/engineering
AAMA	American Architectural Manufacturers Association
ABS	acrylonitrile butadiene styrene
AERC	Attachments Energy Rating Council
AHU	air handling unit
ASHRAE	American Society of Heating, Refrigerating and Air-Conditioning Engineers
ASTM	American Society for Testing and Materials
BSDF	bidirectional scattering distribution function. Angularly resolved optical reflectance and transmission characteristics of shading and daylighting materials or systems.
CA	California
CAD	computer aided design
CBECC-Com	Title 24 nonresidential compliance software
CBECS	U.S. Commercial Building Energy Consumption Survey
cfm	cubic feet per minute
CFS	complex fenestration system. Fenestration with non-specular optical transmission, including diffusion and redirection of light (e.g., venetian blinds, woven shades, ceramic frit, micro-prismatic film). Excludes conventional glass.
CO_2	carbon dioxide
COG	center-of-glass
COMFEN	Commercial Fenestration simulation tool
COMSOL	COMSOL Multiphysics finite element software
Convective heat transfer coefficient (h)	A coefficient for a quantitative characteristic of convective heat transfer between a fluid medium (a fluid) and the surface (wall) flowed over by the fluid.

Term	Definition
COP	coefficient of performance
C-PAW	California Partnership for Advanced Windows
CPU	central processing unit
DC	direct current
DC	daylight coefficient method
DDE	daylight delivery efficacy. the ratio (in units of lumen/watt) of horizontal illuminance at the workplane at the back of the room (lux) and vertical irradiance at the façade (watt/m^2). A higher DDE value indicated a better ability to deliver daylight to the interior space.
°C	degrees Celsius
°F	degrees Fahrenheit
DGI	daylight glare index
DGP	daylight glare probability. A daylight discomfort glare metric based on human subject tests.
DGPs	daylight glare probability simplified. A version of the DGP metric calculate using only vertical illuminance at the eye.
DOAS	dedicated outdoor air systems
DOE	U.S. Department of Energy
EMS	energy management system
Energy Commission	California Energy Commission
EPA	U.S. Environmental Protection Agency
EPIC	The Electric Program Investment Charge, created by the California Public Utilities Commission in December 2011, supports investments in clean energy technologies that benefit electricity ratepayers of Pacific Gas and Electric Company, Southern California Edison Company, and San Diego Gas & Electric Company.
ESSO	European Solar-Shading Organization
FLEXLAB	Facility for Low Energy Experiments in Buildings
ft	foot, feet

Term	Definition
ft2	square foot
genBSDF	A Radiance sub-program
GF	glass filled
GHG	greenhouse gas
GHz	gigahertz
GPU	graphics processing unit
GWh	gigawatt-hours
HDR	high dynamic range
Hi-R	highly insulating windows
HVAC	heating, ventilation and air conditioning
http	hypertext transfer protocol
IEA SHC	International Energy Agency Solar Heating and Cooling Programme
IESNA	Illuminating Engineering Society of North America
IGU	insulated glazing unit. A glazing unit with two or more glass panes and an airtight gap in between.
IGU	Insulating glass unit
IPOPT	A non-linear optimization solver
IR	infrared
IOU	investor-owned utility
JModelica	An extensible Modelica-based open source platform for optimization, simulation and analysis of complex dynamic systems
kWh	kilowatt-hour
LEED	Leadership in Energy and Environmental Design
LBNL	Lawrence Berkeley National Laboratory
low-e	low-emittance
LPD	lighting power density
LSG	low-solar-gain
LS4	low-solar-gain with surface 4 low-e

Term	Definition
LVER	local ventilation and energy recovery device
m	meters
Modelica	a non-proprietary, object-oriented, equation based language to conveniently model complex physical systems containing, e.g., mechanical, electrical, electronic, hydraulic, thermal, control, electric power or process-oriented subcomponent
MoWiTT	Mobile Window Thermal Test calorimeter facility
MPC	model predictive controls
NFRC	National Fenestration Rating Council
NMAE	normalized mean absolute error
NREL	National Renewable Energy Laboratory
Nusselt number (NU)	The ratio of convective to conductive heat transfer across (normal to) the boundary
overall heat transfer coefficient (U)	The coefficient for the proportionality constant between the heat flux and the thermodynamic driving force for the flow of heat
PG&E	Pacific Gas and Electric, a California utility company
PIER	Public Interest Energy Research
Prandtl Number (PR)	A dimensionless number, named after the German physicist Ludwig Prandtl, defined as the ratio of momentum diffusivity to thermal diffusivity
PV	photovoltaic
PVC	polyvinyl chloride
PVWatts	A calculator for estimating the energy production and cost of energy for grid-connected PV systems
R2C2	An MPC model with two capacitances and two resistors
R-value	The capacity of an insulating material to resist heat flow. The higher the R-value, the greater the insulating power.
R&D	research and development

Term	Definition
Radiance	A free, open-source lighting program used by engineering firms to design innovative solar control, lighting, and daylighting, to improve building energy efficiency
RH	relative humidity
RMSE	root mean square error
RSHE	rectangular solid heat exchanger
s	seconds
SCE	Southern California Edison, a California utility company
SHGC	solar heat gain coefficient
Sherwood number (Sh)	A dimensionless number that represents the ratio of the convective mass transfer to the rate of diffusive mass transport
smart grid	Smart grid is the thoughtful integration of intelligent technologies and innovative services that produce a more efficient, sustainable, economic, and secure electrical supply for California communities.
TDD	Tubular daylight device
TG	thin-glass
THERM	A computer program used to model two-dimensional heat-transfer effects in building components
TMY	typical meteorological weather
TOU	time-of-use
Tvis	visible transmittance
U-factor	overall heat transfer coefficient that describes how well a building element conducts heat or the rate of transfer of heat (in watts)
UHMW-PE	ultra-high-molecular-weight polyethylene
USGBC	U.S. Green Building Council
W	watt
WINDOW	A computer program for calculating total window thermal performance indices
WWR	wall-to-window ratio
ZNE	zero net energy

REFERENCES

Chapter 2: Highly Insulating (High-R) Windows

American Architectural Manufacturers Association (AAMA). 2008. TIR-A8: Structural Performance of Composite Thermal Barrier Framing Systems. Schaumburg, IL.

Arasteh, Dariush. 2006. Zero Energy Windows. Proceedings of the 2006 ACEEE Summer Study on Energy Efficiency in Buildings, August 2006, Pacific Grove, CA.

Arasteh, Dariush, H. Goudey, and C. Kohler. 2008. Highly Insulating Glazing Systems Using Non-Structural Center Glazing Layers. 2008 Annual ASHRAE Meeting and Proceedings, Salt Lake City, UT.

CBECC. 2016a. California Building Energy Code Compliance software for Commercial/Non-residential Buildings, Version 2016.3.0 SP2.

CBECC. 2016b. Title-24 Prototype Building Office – Medium for California Building Energy Code Compliance software for Commercial/Non-residential Buildings, Version 2016.3.0 SP2.

COMSOL. 2015. COMSOL Multiphysics Reference Manual, version 5.0. COMSOL, Inc. www.comsol.com.

Itron. 2006. California Commercial End-Use Survey. Consultant Report to the California Energy Commission. CEC-400-2006-005. March.

LBNL. 2016a. Berkeley Lab WINDOW version 7.6.04: A PC Program for Calculating Thermal and Optical Performance of Windows. Lawrence Berkeley National Laboratory.

LBNL. 2016b. THERM version 7.6.01: A PC Program for Calculating Two-Dimensional Conduction Heat-Transfer Analysis with the Finite-Element Method. Lawrence Berkeley National Laboratory.

Selkowitz, Stephen, R. Hart, and C. Curcija. 2018. Breaking the 20 Year Logjam to Better Insulating Windows. 2018 ACEEE Summer Study on Energy Efficiency in Buildings. Pacific Grove, CA.

Selkowitz, Stephen, D. Arasteh, and J. Hartmann. 1991. Thermal Insulating Glazing Unit. United States Statutory Invention Registration, H975, Nov. 5 1991.

Chapter 3: Energy-Recovery-Based Façade Ventilation Systems

ASHRAE. 2010a. "ANSI/ASHRAE/IES Standard 90.1-2010 — Energy Standard for Buildings Except Low-Rise Residential Buildings." American Society for Heating, Air-Conditioning and Refrigeration Engineers. Atlanta, Georgia.

ASHRAE. 2010b. "ANSI/ASHRAE 62.1-2010 — Ventilation for Acceptable Indoor Air Quality." American Society for Heating, Air-Conditioning and Refrigeration Engineers. Atlanta, Georgia.

ASHRAE. 2014. "ASHRAE Standard 52.2-2014 — Method of Testing General Ventilation Air-Cleaning Devices for Removal Efficiency by Particle Size." American Society for Heating, Air-Conditioning and Refrigeration Engineers. Atlanta, Georgia.

COMSOL. 2015. *COMSOL Multiphysics Reference Manual, version 5.0.* COMSOL, Inc. www.comsol.com.

Fisk, W. J., S. M. Dutton, M. J. Mendell, and W. R. Chan. 2013. *Should Title 24 Ventilation Requirements Be Amended to Include an Indoor Air Quality Procedure?* LBNL Technical Report. LBNL-6705E.

Griffith, B. T., D. Turler, H. Goudey, and D. K. Arasteh. 1998. *Experimental Techniques for Measuring Temperature and Velocity Fields to Improve the Use and Validation of Building Heat Transfer Models.* LBNL Report. LBNL-41772. December.

Lam, K. P., S. R. Lee, G. M. Dobbs, and C. Zhai. 2005. Simulation of the Effect of an Energy Recovery Ventilator on Indoor Thermal Conditions and System Performance. Ninth International IBPSA Conference. Montréal, Canada. August 15–18, 2005.

LBNL. 2016a. Berkeley Lab WINDOW version 7.6.04: A PC Program for Calculating Thermal and Optical Performance of Windows. Lawrence Berkeley National Laboratory.

LBNL. 2016b. THERM version 7.6.01: A PC Program for Calculating Two-Dimensional Conduction Heat-Transfer Analysis with the Finite-Element Method. Lawrence Berkeley National Laboratory.

NREL. 2018. PVWatts Calculator. National Renewable Energy Laboratory. https://pvwatts.nrel.gov/.

Springer, D. 2009. "Is there a downside to high-MERV filters?" *Home Energy Magazine* November 2, 2009.

Zaatari, M., A. Novoselac, and J. Siegel. 2014. "The relationship between filter pressure drop, indoor air quality, and energy consumption in rooftop HVAC units." *Building and Environment* 73:151–161.

Zhang, L. Z., and Y. Jiang. 1999. "Heat and mass transfer in a membrane-based energy recovery ventilator." J*ournal of Membrane Science* 163(1): 29–38.

Chapter 4: Daylight Redirecting Systems

Energy Commission. 2006. *California Commercial End-Use Survey.* California Energy Commission. CEC-400-2006-005. March.

EIA. 2016. Commercial Buildings Energy Consumption Survey (CBECS). Energy Information Administration. U.S. Department of Energy. https://www.eia.gov/consumption/commercial/data/2012/pdf/user_guide_public _use_aug2016.pdf Accessed October 25, 2017.

Fernandes, L. L, E. S. Lee, A. Thanachareonkit, and S. E. Selkowitz. 2018a. Annual performance of a high-efficiency daylight redirecting slat system. CEC EPC-14-066-T4.4a Task deliverable, June 1, 2018.

Fernandes, Luís L., Howdy Goudey, Ben Karcher, Ray Karam, Eleanor S. Lee, and S. E. Selkowitz. 2018b. A prototype for a high-efficiency daylight redirecting slat system. CEC EPC-14-066-T4.4d Task deliverable, June 1, 2018.

Konis, K., and E. S. Lee. 2015. "Measured daylighting potential of a static optical louver system under real sun and sky conditions." *Building and Environment* 92(2015):347–359.

McNeil, A., E. S. Lee, and J. C. Jonsson. 2017. "Daylight performance of a microstructured prismatic window film in deep open plan offices." *Building and Environment* 113(2017):280–297.

Rosenfeld, A. H., and S. E. Selkowitz. "Beam daylighting: An alternative illumination technique." *Energy and Buildings* 1(1977):43–50.

Thanachareonkit, A., E. S. Lee, and A. McNeil. 2014. "Empirical Assessment of a Prismatic Daylight-Redirecting Window Film in a Full-Scale Office Testbed." *Leukos: The Journal of the Illuminating Engineering Society of North America* 10.1(2014):19–45, LBNL-6496E.

Thanachareonkit, Anothai, Luis L. Fernandes, Joshua Mouledoux, and Eleanor S. Lee. 2018. Laboratory and computer simulation evaluation of daylight redirecting slats. CEC EPC-14-066-T4.4c Task deliverable, June 1, 2018.

Ward Larson, G., and R. Shakespeare. 1998. Rendering with Radiance: The Art and Science of Lighting Visualization. Morgan Kaufman. San Francisco.

Wienold, J., and J. Christoffersen. 2006. "Evaluation methods and development of a new glare prediction model for daylight environments with the use of CCD cameras." *Energy and Buildings* 38(2006):743–757.

Chapter 5: Daylighting and Shading Optimization Methods

Lee, E. S., S. E. Selkowitz, D. L. DiBartolomeo, J. H. Klems, R. D. Clear, K. Konis, R. Hitchcock, M. Yazdanian, R. Mitchell, and M. Konstantoglou. 2009. *High Performance Building Façade Solutions.* California Energy Commission, PIER. Project number CEC-500-06-041.

Lee, Eleanor S., Brian Coffey, Luis Fernandes, Sabine Hoffmann, Andrew McNeil, Anothai Thanachareonkit, and Gregory Ward. 2014. *High Performance Building Façade Solutions–Phase II.* Final project report. California Energy Commission. CEC 500-2014.

Lee, Eleanor S., Anothai Thanachareonkit, Samir Touzani, Spencer Dutton, Jordan Shackelford, Darryl Dickerhoff, and Stephen Selkowitz. 2016. Technology Assessments of High Performance Envelope with Optimized Lighting, Solar Control, and Daylighting, Pacific Gas and Electric Company's Emerging Technologies Program. ET Project Number: ET14PGE8571. September 2016.

Lee, E. S., D. Geisler-Moroder, and G. Ward. 2018. "Modeling the direct sun contribution in buildings using matrix algebraic approaches: Methods and validation." *Solar Energy* 160: 380–395.

McNeil, A., and E. S. Lee. 2012. "A validation of the Radiance three-phase simulation method for modeling annual daylight performance of optically complex fenestration systems." *Journal of Building Performance Simulation* 2012: 1–14.

Subramaniam, Sarith. 2017. *Daylighting Simulations with Radiance using Matrix-based Methods.* https://radiance-online.org/learning/tutorials/matrix-based-methods. Accessed October 5, 2018.

Wang, T., G. Ward, and E. S. Lee. 2018. "Efficient modeling of optically-complex, non-coplanar exterior shading: Validation of matrix algebraic methods." *Energy and Buildings* 174: 464–483.

Wang, T., and E. S. Lee. 2018. *genfmtx* and *idfxmtx* Tutorial. CEC-EPC-14-066 Task 5.3 Deliverable, Window/ CGDB/ EnergyPlus Toolkit Tutorials. January 30, 2018.

Ward, G., R. Mistrick, E. S. Lee, A. McNeil, and J. Jonsson. 2010. "Simulating the daylight performance of complex fenestration systems using bidirectional scattering distribution functions within Radiance." *Leukos, Journal of the Illuminating Engineering Society of North America* 7(4).

Chapter 6: Dynamic, Integrated Façades

Blum, D. H., and M. Wetter. 2017. MPCPy: An Open-Source Software Platform for Model Predictive Control in Buildings. Proceedings of the 15th Conference of International Building Performance Simulation (IBPSA). San Francisco, CA. Aug 7–9, 2017.

California Energy Commission (CEC). 2015. *2016 Building Energy Efficiency Standards for Residential and Nonresidential Buildings.* Publication Number: CEC-400-2015-037-CMF. June.

Clear, R. D., V. Inkarojrit, and E. S. Lee. 2006. "Subject responses to electrochromic windows." *Energy and Buildings* 38(7): 758–779.

Clear, R. D. 2010. Technical Memo: Post-occupancy evaluation of *The New York Times* Headquarters Building: An examination of causes for occupant satisfaction and dissatisfaction with the energy-efficiency measures. Lawrence Berkeley National Laboratory, Berkeley, CA 94720. https://facades.lbl.gov/newyorktimes/pdf/nyt-lbl-occu-satisfaction.pdf, accessed December 12, 2018.

Fernandes, Luis L., Eleanor S. Lee, Darryl Dickerhoff, Anothai Thanachareonkit, Taoning Wang, and Christoph Gehbauer. 2016. *Electrochromic Window Demonstration at the John E. Moss Federal Building, 650 Capitol Mall, Sacramento, California.* General Services Administration. Green Proving Ground Report. November.

Gehbauer, C., D. H. Blum, and E. S. Lee. 2017. Integrated Dynamic Facade Control with an Agent-based Architecture for Commercial Buildings. Technical deliverable "High-Performance Integrated Window and Façade Solutions for California." California Energy Commission. EPC-14-066, Task 6. July 14.

Gehbauer, C., D. H. Blum, T. Wang, and E. S. Lee. 2018. An assessment of the load-modifying potential of MPC-controlled dynamic facades within the California context. Technical deliverable "High-Performance Integrated Window and Façade Solutions for California." California Energy Commission EPC-14-066, Task 6.5, September 14, 2018.

Lee, E. S., L. L. Fernandes, B. Coffey, A. McNeil, R. Clear, T. Webster, F. Bauman, D. Dickeroff, D. Heinzerling, and T. Hoyt. 2013. *A post-occupancy monitored evaluation of the dimmable lighting, automated shading, and underfloor air distribution system in* The New York Times Building. LBNL-6023E. Lawrence Berkeley National Laboratory, Berkeley, CA 94720. http://buildings.lbl.gov/sites/all/files/lbnl-6023e.pdf.

Motamed, A. 2017. Integrated Daylighting and Artificial Lighting Control based on High Dynamic Range Vision Sensors. LESO-PB - Solar Energy and Building Physics Laboratory. PhD Thesis. Lausanne, EPFL, 10.5075/epfl-thesis-8277.

Nouidui, T. S., M. Wetter, and W. Zuo. 2012. "Validation of the window model of the Modelica Buildings Library." *Proceedings of SimBuild* 5(1): 529–536.

Terrestrial Light. 2018. Terrestrial Light Skyometer. http://terrestriallight.comconc/. Accessed October 31, 2018.

Wetter, M., W. Zuo, T. S. Nouidui, and X. Pang. 2014. "Modelica Buildings Library." *Journal of Building Performance Simulation* 7(4): 253–270.

Wetter, M., M. Bonvini, and T. S. Nouidui. 2016. "Equation-based languages – A new paradigm for building energy modeling, simulation and optimization." *Energy and Buildings* 117: 290–300.